Daniel José Rossa Gralheira
Bachelor in Biochemistry

Tyrosinase-Based Phenol Remediation

Dissertation for the obtention of the Master Degree in Biotechnology

Supervisor: Doctor João Marques Cortez,
Auxiliary Researcher, REQUIMTE
Co-supervisor: Doctor Marco Silva, Auxiliary Professor, FCT/ UNL

Jury:

President: Doctor Pedro Miguel Ribeiro Viana Batista,
Aggregate Auxiliary Professor , FCT/ UNL
Examiner(s): Doctor Maria Gabriela Machado,
Auxiliary Researcher, FCT/ UNL

FACULDADE DE CIÊNCIAS E TECNOLOGIA
UNIVERSIDADE NOVA DE LISBOA

Dezembro de 2012

Acknowledgements

This dissertation is the product of innumerous contributions that cannot be resumed to the author name on the cover.

I would like to start by emphasizing my deepest appreciation for the indisputable scientific correctness (that will surely guide me beyond this project), vision for this dissertation and the vast support of my supervisor, Dr. João Cortez.

The kind acceptance of Dr. Marco Silva to be my supervisor enhanced the significance of the undertaken task and brought an inestimable know-how on analytical methods. To this respect it is not possible to forget the guidance of Dr. Eduardo Mateus on the initial approach to gas chromatography and the kind treatment by the members of the analytical group.

The companionship of all my laboratory colleagues was of most importance to get through the most difficult days and, in special, the practical advices from Master João Luz were a valuable asset.

I also need to acknowledge Dr. José Gomes and Dr. Fábio Chalub, from Mathematics Department, for their eagerness to help solving the protein/nanoparticle ratio problem.

I am thankful for all my family, particularly to Hélder, my father; Cremilde, my mother and Ricardo, my brother. They gave me the necessary support to study in this fantastic university and, not helping in the work, they were crucial by not causing me much trouble.

T. Pernes, V. Correia, I. Camacho; you were laugh and suffering friends all the way and one could not wish for more.

Finally, I dedicated this dissertation to those who had lack of confidence in me making me push my limits forward, and, specially, to those who inspired me by enjoying all the creative process in this dissertation.

Abstract

Nanobiotechnology is an emerging area full of potentialities to explore and reshape instituted knowledge. In this work, the main goal was to design and test biological remediation systems (a total of three) taking advantage of nanotechnology features, as a step towards future progress of sense-and-shoot combined systems. This task involved the development of active bionanoconjugates (BNC) with two different tyrosinases (*Agaricus bisporus* - AbT, and *Tricoderma reesei* - TrT) to be implemented in three suggested phenol remediation systems.

AuNP-MUA (gold nanoparticles capped with11-mercapto-1-undecanoic acid) 1:5000 colloid was shown to be stable up to 100 mM ionic strength (sodium cloride) and able to form active BNCs with AbT. TrT:AuNP ratio for BNC formation is recommended as 100, supported by zeta potential and agarose gel mobility experimental data which, in turn, atone with the proposed theoretical estimation.

The incubation of 100 ppm phenol with BNC-MUA-AbT for 60 minutes achieved 50% substrate conversion (the efficiency of the systems were also investigated using ultraviolet-visible spectrophotometry (UV-Vis) complemented by standard addition method and solid-phase microextraction - gas chromatography (SPME-GC)).

Keywords: bionanoconjugates, gold nanoparticle, remediation, tyrosinase, phenol

Resumo

A nanotecnologia é uma área emergente cheia de potencialidades a explorar e capaz de redefinir o conhecimento instituído. Neste trabalho, o principal objetivo consistiu em desenhar e testar sistemas biológicos de remediação (um total de três) tirando proveito das capacidades nanotecnológicas, sendo um passo em direção ao futuro progresso de sistemas de deteção-e-eliminação. Esta tarefa envolveu o desenvolvimento de bionanoconjugados (BNC) activos com duas tirosinases diferentes (*Agaricus bisporus*- AbT, e *Tricoderma reesei*- TrT) a serem implementados nos três sistemas de remediação de fenóis sugeridos.

O coloide AuNP-MUA (nanopartículas de ouro revestidas com ácido 11-mercapto-1-undecanóico) 1:5000 foi demonstrado ser estável até 100 mM de força iónica (cloreto de sódio) e apto a formar BNCs activos com AbT. O rácio TrT:AuNP para formação de BNC é recomendado como 100, de acordo com dados experimentais de potencial zeta e mobilidade em gel de agarose, os quais, por sua vez, corroboram a estimativa teórica proposta.

Métodos analíticos para avaliar a eficiência dos sistemas foram também investigados: espectrofotometria ultravioleta-visível (UV-Vis) utilizando-se o método da adição padrão; e microextracção de fase-sólida - cromatografia gasosa (SPME-GC). A incubação de 100 ppm de fenol com BNC-MUA-AbT durante 60 minutos alcançou 50% de conversão de substrato.

Palavras-chave: bionanoconjugados, nanopartícula de ouro, remediação, tirosinase, fenol

Table of Contents

Table of Figures

Table of Tables

Symbols and notations

1x- TYR concentration enough to conjugate with 1 nM of AuNP ([AbT]= 9 mg/mmol AuNP; [TrT]= 100 nmol/nmol AuNP)

AbT- Tyrosinase from *Agaricus bisporus*

AFM- Atomic Force Microscopy

APS- Ammonium persulfate

AuNP- Gold nanoparticle

BCA- Bicinchoninic Acid

BNC- Bionanoconjugate

BSA- Bovine Sorum Albumin

CALKK- pentapetide : Cysteine, Alanine, Leucine, Lysine (2x)

CALNN- pentapetide : Cysteine, Alanine, Leucine, Asparagine (2x)

Cit- Citrate

CWX- Carbowax

DHI- Dihydroxyindole

DHICA- Dihydroxyindole-2-carboxylic acid

EPA- United States Environmental Protection Agency

EPR- Electron Paramagnetic Resonance

FID- Flame Ionization Detector

GC- Gas Chromatography

GC/MS- Gas Chromatography–Mass Spectrometry

HBTA- 5-hydroxy-1,4-benzothiazinylalanine

HPLC-UV- High-Performance Liquid Chromatography- Ultraviolet

ICP- Inductively Coupled Plasma Atomic Emission Spectroscopy

K_m- Michaelis constant

LSPR- Localized Surface Plasmon Resonance

L-DOPA- L-3,4-dihydroxyphenylalanine; IUPAC: (S)-2-amino-3-(3,4-dihydroxyphenyl) propanoic acid; common name: L-dopamine

GHB- *γ*-glutaminyl-4-hydroxybenzen

MBTH- 3-methyl-2-benzothiazolinone hydrazone

MNP- Metallic Nanoparticle

MUA- 11-mercapto-1-undecanoic acid

N- Number of electrons on an atom surface

NADH- Reduced Nicotinamide Adenine Dinucleotide

NP- Nanoparticle

PA- Polyacrylate

PDMS- Polydimethylsiloxane

PPO- Polyphenol oxidase

SDS-PAGE- Polyacrylamide gel electrophoresis in sodium dodecyl sulfate

SPR- Surface Plasmon Resonance

SPME- Solid phase microextraction

STM- Scanning Tunneling Microscope

T3Cu- Type III copper centres (T3Cu)

TrT- Tyrosinase from *Trichoderma reesei*

TYR- Tyrosinase

UV-Vis- Ultraviolet and Visible

V_0- Initial reaction rate

V_m- Maximum reaction rate

1- Introduction, ambit and objectives

1.1- Nanotechnology

The first documented mention to the nanotechnological concepts occurred in "There´s Plenty of Room at the Bottom", a talk by the Nobel laureate physicist Richard P. Feynman, during the American Physical Society annual meeting in 1959. In this talk it was given emphasis to the idea that, at nanoscale, it would occur a change in the magnitude of the physical phenomena over the matter.[1] The term "nano-technology" was first defined in a 1974 paper by Norio Taniguchi but still solely attached to the scale and dimension issues and, therefore, far from its actual conception. In the next decade, Dr. K. Eric Drexler promoted a much different idea for the term as he realized the technological significance of the nanoscale phenomena and so the term approached to its current sense.[2]

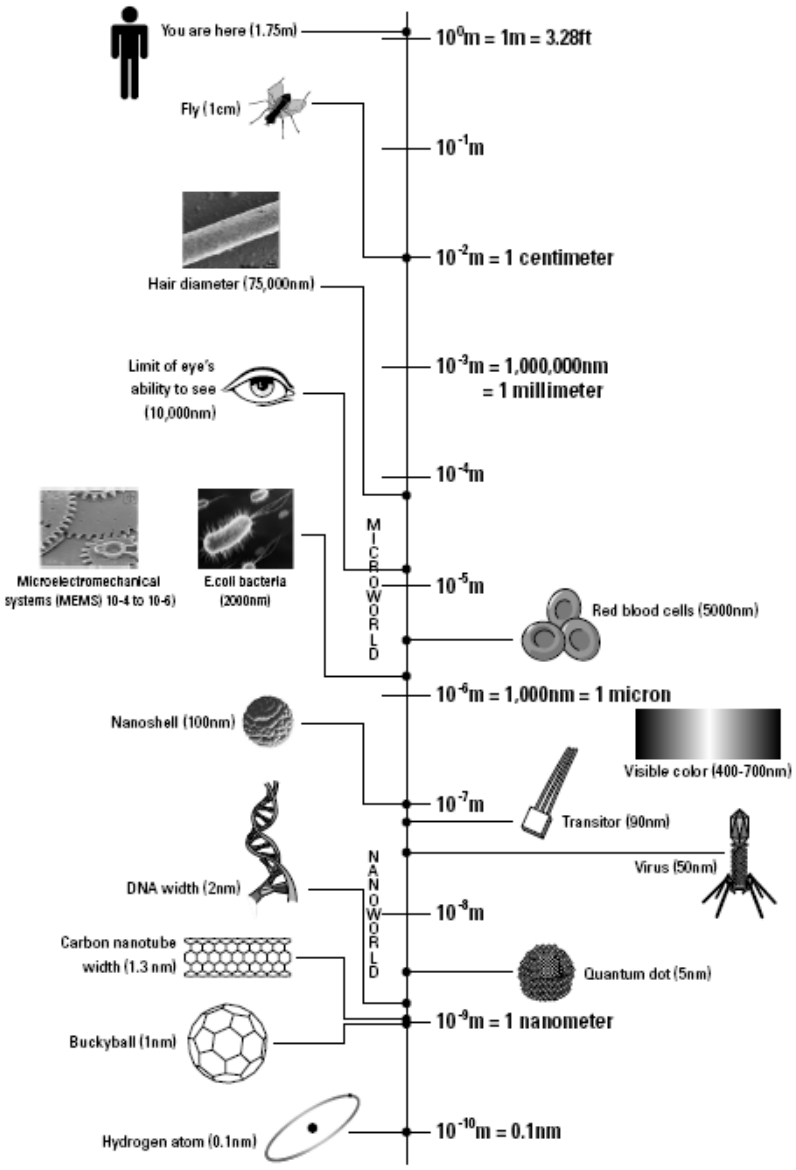

Figure 1- Comparative dimension scale from meter to nanometer.

A lack of consensus about the nanotechnology concept arose in the scientific community leading to the foundation of committees in many countries, namely the United States National Nanotechnology Initiative with the purpose to understand, create and promote systems with fundamentally new proprieties due to its nanoscale composition. This committee established that nanotechnology is the study of matter ranging from about 1-100nm –between 10^2 and 10^7 atoms[3]- (a human air measures approximately $75x10^3$ nm of thickness- Fig.1[4]). The ISO (International Organization for Standardization) technical committee for Nanotechnologies stated nanotechnology´s scope as (quoting):

1. Understanding and control of matter and processes at the nanoscale, typically, but not exclusively, below 100 nanometers in one or more dimensions where the onset of size-dependent phenomena usually enables novel applications,

2. Utilizing the properties of nanoscale materials that differ from the properties of individual atoms, molecules, and bulk matter, to create improved materials, devices, and systems that exploit these new properties.[5]

In this document, the later, will be the definition in use however, for a deeper revision on the topic, reading Michael Decker´s Newsletter "Definitions of Nanotechnology – Who needs them?"(2003) is advisable[6].

Materials with nanocomponents come from far beyond the Modern Age and have been used by the craftsmen at least since the Roman civilization (4th century). There are many examples described such as stained glass windows in European cathedrals (Fig. 2)[2, 7] owing their rich colors to nanoparticles of gold chloride and other metal oxides and chlorides, and Damascus saber blades containing carbon nanotubes and cementite nanowires (Fig. 3).[8]

In 1857 Michael Faraday started the pathway into the depth of this knowledge as he discovered colloidal "ruby" gold proving that nanoscale gold could produce solutions with different colors from the metallic one (Fig. 4).[8]

Figure 2- Detail of the South Rose Window in (1260) the Notre Dame Cathedral, Paris. © Sacred Destinations

Figure 3- A Damascus saber. (photo by Tina Fineberg for The New York Times).

Figure 4- "Ruby" gold colloid. Gold Bulletin 2007 40,4, p. 267

In the early 1980s two key developments; the birth of cluster science and the invention of the scanning tunneling microscope (STM) enabled nanoscience the first major steps. Soon, in 1986, fullerenes were discovered, in 1991 the carbon nanotubes, in 1992 the atomic force microscope was invented and in 1993 the synthesis of semiconductor nanocrystals (Quantum Dots) was started. In the present, the market outcome of nanotechnology is expressed in improved products benefiting from a new material or in manufacturing processes. Moreover, the top down approach to create smaller components has gained more tools with this science and in the other hand, the bottom up approach is getting firm soil in self-assembly processes owing to nanotecnhological phenomena comprehension.[2]

The possibility of rebuilding existing products (not mentioning the new ones) either with better performances, smaller parts and lower cost is very attractive to companies and "evolutionary nanotechonology" is predicted to run across many industries reshaping them (Fig 5)[2]. In spite of being a young field, the expectations are great and public awareness is rising due to marketing and popular culture references.[2]

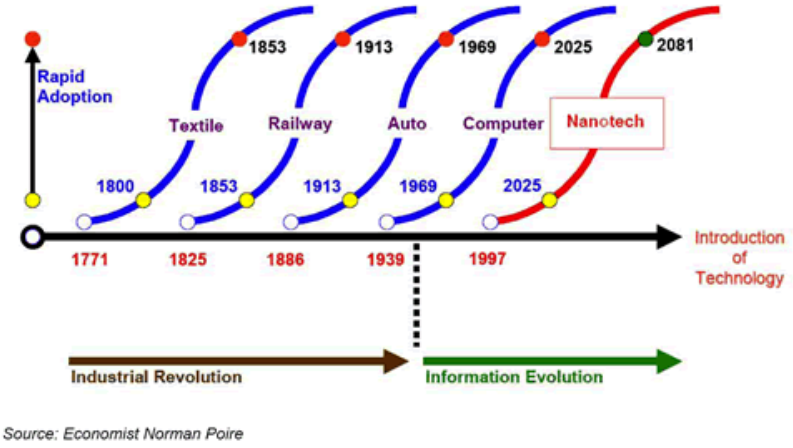

Source: Economist Norman Poire

Figure 5**-** Nanotechnology spawn is expected to drive the next industrial growth cycle.

1.1.1- Nanobiotechnology and Bionanotechnology

Classifying a work in a field of science is not critical to its integrity and do not mine its achievements but it is an important way to analyze them in the state-of-art perspective and therefore assess its impact.

Both "nanobiotechnology" and "bionanotechnology" are very recent terms crossing the same areas of expertise and many times undifferentiated. If differences can be pinpointed, the areas to which they refer to are themselves no more than fifteen years old and still in deep reshaping. On behalf of some common ground while communicating, nanobiotechnology is considered as the application of nanotechnology techniques for the development of biotechnological processes and products or, in other terms, to obtain functional nanostructures

(inorganic composites or not) from biological systems (e.g. nucleic acids, proteins and cell) and to study and develop biological processes using techniques originally designed to manipulate nanostructured materials.(Fig. 6)[9]

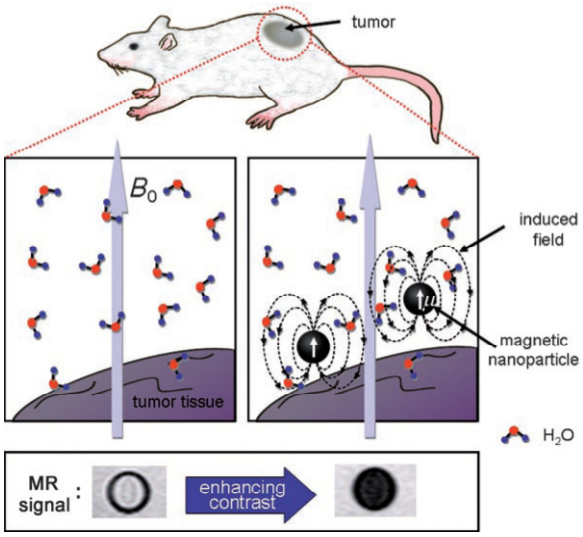

Figure 6**-** Nanobiotechnology example: magnetic resonance contrast effects of magnetic nanoparticles. Under an external field (B_0), magnetic NPs are magnetized with a magnetic moment of μ and generate an induced magnetic field which perturbs the nuclear spin relaxation processes of the water protons. This perturbation leads to magnetic resonance contrast enhancement.

This goes from the use of matrixes with nanoscale order for the controlled release of bioactive molecules or tissue engineering, to the use of nanoscale fabrication and manipulation techniques to create more sensitive and far reaching diagnosis methods which by turn can enable concepts as the “lab-on-chip” and real time nanosensors.[10]

Bionanotechnology aims to impart new properties to materials from unique characteristics present in biomolecules. This includes the use of DNA oligomers, peptide nanotubes (Fig. 7)[11], or protein fibrils for the fabrication of nanowires, interconnects and other physical elements that can be used in molecular electronics or instead metal parts for their mechanical proprieties.[10]

According to these terminologies, this dissertation can be framed as nanobiotechnology because tyrosinase enzymes (biological systems) are being conjugated with gold nanoparticles creating functional nanostructures in which the biocatalyst´s activity and specificity are being exploited.

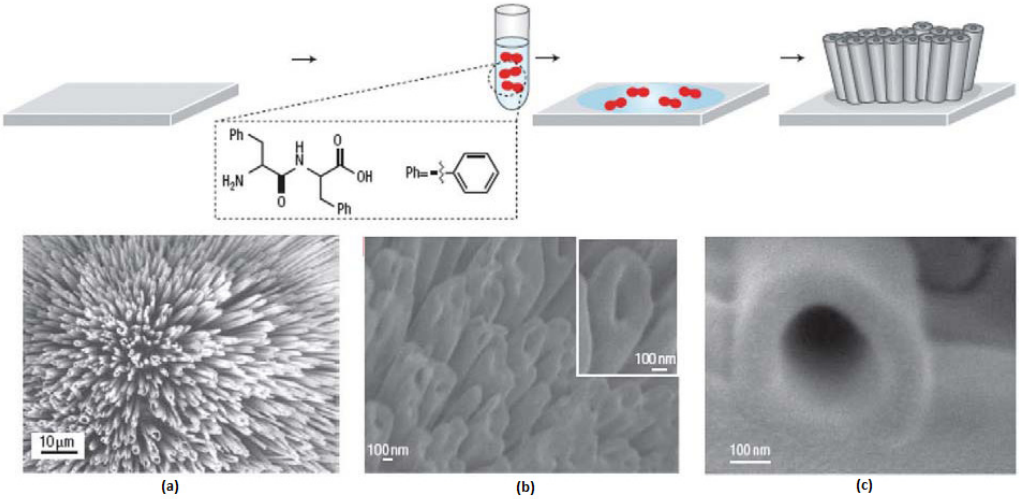

Figure 7- Proposed model for the formation of aligned peptide nanotube arrays. Images of the vertically aligned peptide nanotubes: **(a)** Scanning electron micrograph; **(b)** Cold field-emission gun high-resolution scanning electron micrograph; **(c)** High-magnification micrograph of (b).

1.1.2- Bottom-up and bottom-down approaches

It has been demonstrated that multi-dimensional superlattices of nanoparticles (NPs) exhibit different proprieties from their individual elements.[12] For example, it was reported that Ag NPs organized in a two-dimensional hexagonal network, have their plasmon peak shifted towards higher wavelengths and an increase in the bandwidth is observed because the dielectric constant of the surrounding NPs is increased.[12a] Bearing this framework in mind and the intention to any successful application, it becomes essential to find ways to secure the gathering of nanoparticles with controlled morphology in highly ordered nanostructures.

The “top-down” approaches (such as lithography and patterning) consist in eroding materials to obtain smaller ones at the cost of large material waste. The bottleneck of the “top-down” approaches is the miniaturization because operating equipment are forthcoming their scale limits and overcoming them is becoming harder and extremely expensive. To some extent, “top-down” enables nano-featuring but it is “bottom-up” that appears as the leading edge. “Bottom-up” comprises structures building from molecular components, with high yield usage of the starting materials and exploiting their natural features as possible to reduce equipment usage. “Bottom-up” approaches include scanning probe-based microscopes (e.g. Atomic Force Microscopy- AFM) and chemical synthesis (e.g. colloidal chemistry, supramolecular chemistry) but the focus of this dissertation goes to those based on self-assembly. Self-assembly can be achieved by simple methods such as evaporation-based assembly and chemical conjugation or by more advanced methods of patterned self-assembly

using lithography and microcontact printing where only the patterned areas with chemical functionalities create organized NP networks on substrates.[12a]

The term "self-assembly" has been overused as if any natural process or form of organization fits it, ranging from the non-covalent association of organic molecules in solution to the growth of semiconductor quantum-dots on solid substrate. In this dissertation the term self-assembly is considered as the autonomous organization of components into patterns or structures without human intervention being limited to processes that involve pre-existing components, being reversible, and able to control by proper design of the components.(Fig. 8)[13]

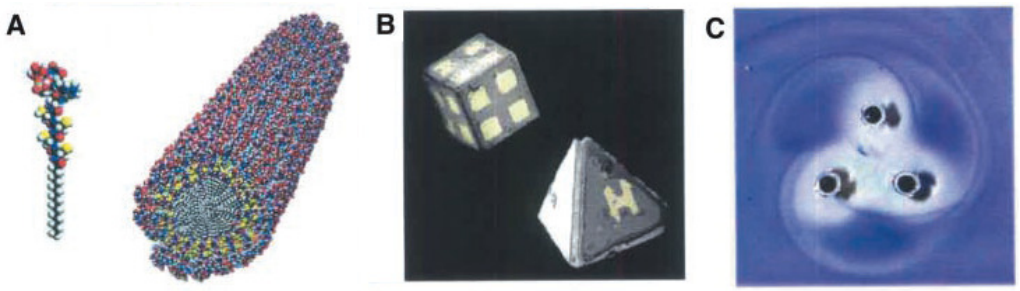

Figure 8**-** Self-assembly examples. **A-** peptide-amphiphile nanofibers. **B-** Micrometer-sized metallic polyhedral folded from planar substrates. **C-** Aggregate of three millimeter size, rotating, magnetized disks interacting with one another.

Self-assembly at molecular level involves weak interactions (van der Waals, electrostatic, hydrophobic interactions and hydrogen bonds)[14](Fig. 9)[12a], but for meso- or macroscopic elements, interactions can include gravitational attraction, external electromagnetic fields, capillary and entropic interactions which are not relevant in the case of molecules. Non-covalent binding enables favorable free-energy changes as components equilibrate between aggregated and non-aggregated states or adjust their positions relative to one another once in an aggregate so the chosen substituents of the building components are a matter of concern.[12a, 13]

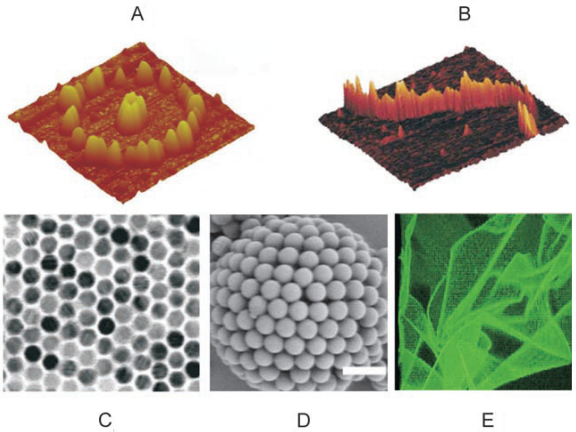

Figure 9**-** Example methods for NPs assembly on surfaces and interfaces: **A-** Cadmium sulfide NPs arranged as well defined rings in chemical lithography. **B-** DNA-templated 1D AuNPs. **C-** Shape- controlled assembly of truncated octahedral magnetite NPs. **D-** A colloidosome: NP assembly on the interface of an emulsion droplet. **E-** Cross-linked cadmium selenide NP membranes at fluid/ fluid interfaces (confocal microscope image).

The environment is crucial to the self-assembly since it can modify the interaction between the components and they need fluid phases or smooth surfaces to be mobile. Moreover, templates can reduce defects[13] and facilitate the creation of a core or scaffold that can start oriented chain reactions of the components.[14]

Putting self-assembly apart, scanning probe microscopy (SPM) methods are also very effective for particle organization at nanoscale and, therefore, suitable for "bottom-up" manufacture but they are: not suitable for large-scale assembly, very time consuming and involve a costly equipment investment. In the present, research is focussed on generating simple nanostructures and exploring surface chemistry possibilities. Self-assembled monolayers (SAMs) (Fig. 10)[12a] are fairly studied (on gold and silicon oxide surfaces) but the goal is to reach flexible and easy approaches able to create asymmetric and complex architectures from one or more types of nanostructures.

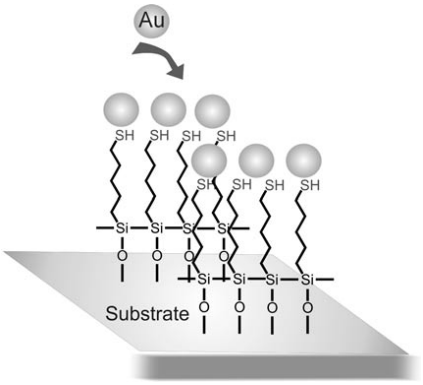

Figure 10**-** Self-assembled monolayer of thiols on a silica substrate, suitable for AuNP assembly.

1.2- Metallic nanoparticles

1.2.1- General mechanism for metallic nanoparticles formation

Finding new technologies recurring to NPs is highly dependent on the availability of synthetic methods capable of generating nearly monodisperse NPs in order to distinguish truly novel proprieties inherent to nanoscale structures from those associated with heterogeneities and polydispersity. Strictly, monodisperse particles are those indistinguishable from one another but in a more practical sense it can be used to refer do samples with standard deviations σ ≤5% in diameter.[3]

In spite of the application demands, key parameters usually also include adequate morphology, surface functionalization, size dispersion and high solubility in water.

La Mer and Dinegar (1950) showed that the production of monodisperse colloids requires a discrete nucleation event followed by a slower controlled growth on the formed nuclei

(Fig. 11A). A short nucleation burst partially relieves the supersaturation and can be accomplished by a rapid addition of reagents to the reaction vessel raising the precursor concentration above the nucleation threshold. The growth rate of all the NPs is similar, meaning their size distribution correlates to the nuclei initial size distribution. The nuclei initial size distribution is determined by the time over which the nuclei are formed.[3]

If the NPs growth during the nucleation period is smaller than the subsequent growth, NPs become more uniform over time and this phenomenon has been referred to as focusing of the size distribution. Another, yet longer, growth phase is often exhibited by NP synthesis methods, the Ostwald Ripening. While the high energy surface of the smaller NPs promotes their dissolution, larger NPs suffer material deposition. The outcome is a decreasing number of NPs with an average increasing size. Ostwald Ripening can be taken into account for the preparation of a size series of NPs: as the NPs growth goes on, periodic aliquots can be extracted from the reaction vessel, being obtained NPs with different sizes as illustrated in Figure 11[3].

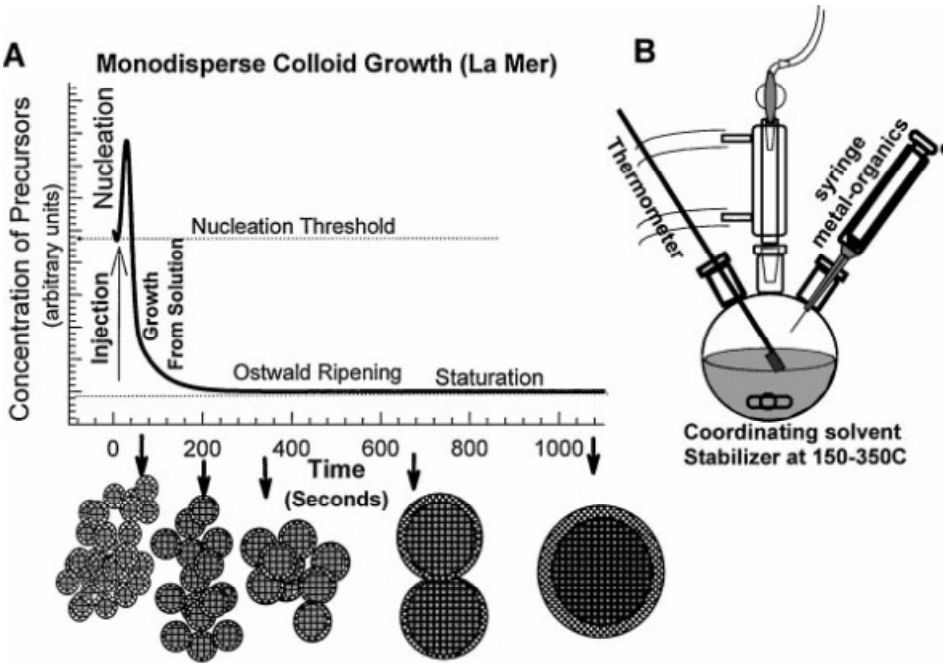

Figure 11**- (A)** Stages of monodisperse colloid growth as described by Le Mer. **(B)** Schematic apparatus employed in the synthesis of monodisperse NPs in the study of Le Mer nucleation model.

In 1951, Turkevich reviewed the subject and proposed de nucleation-growth-agglomeration mechanism of NPs formation, in conformity with La Mer findings.(Fig. 12)[12a, 15]

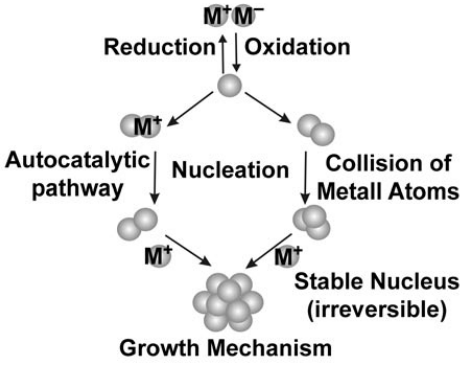

Figure 12**-** Turkevich´s nucleation-growth-agglomeration mechanism of metallic nanoparticles formation.

1.2.2- Metallic nanoparticles synthesis

Starting with M. Faraday´s (1857) chemical reduction of transition metal salts, the number of synthetics methods for the preparation of size series of monodisperse metallic colloids is surprisingly small in spite of having been studied for over a century[3, 12a]. Most of them involve the aqueous reduction of metal salts (mainly Au or Ag) in the presence of citrate anions. According to Kimling *et al*., a size dispersion of just σ < 13-16% in diameter can be achieved when AuNP´s (gold nanoparticles) diameter is inferior to 40 nm[16] but in general metallic nanoparticles (MNPs) can be obtained with distributions of 10 < σ < 15% in diameter (even so they are usually presented as monodisperse) and then narrowed to 5% through size-selective processing.[17] Other methods include the pioneering two-phase liquid-liquid reduction as described by Brust *et al.*[17] enabling the generation of stable AuNP self-assembled monolayers[18]; the inverse micelle method[19] and higher temperature reduction of metal salts in the presence of stabilizing agents to generate monodisperse transition metal NPs (e.g. Co and Ni).[3, 20] Monodisperse bimetallic NPs synthetic methods have achieved some progress and for that matter the work of Bradley and co-workers is a relevant example.[3]

AuNPs synthesis described methods are mostly based on a chemical or electrochemical reduction of a gold precursor compound in the presence of a capping agent. In the case of a chemical reduction, the reduction and the capping functions can be assured by the same agent. A capping agent is a broad term used to describe a compound that covers a nanoparticle´s surface.

Among the several described methods for the preparation of AuNPs, a frequent reducing agent arises which is citrate.[3] This is due to:

1- Citrate has a strong affinity for gold[17] leading to lower size dispersion colloids.[12a]

2- Working pH enables citrate to be negatively charged (-3 at pH 7, pka_3= 6,39[21]) conferring an ionic double layer on a NP surface which ensures strong repulsive Coulombic (electrostatic) forces to counteract the inherent Van der Waals attraction between each NP and so contributing to the colloid solution stability.[12a]

3- Negatively charged, can work as a linker by providing binding through electrostatic interactions.

4- Capping agents enabling solubility only in organic solvents, prevent interaction between the NPs and most biological targets presents in aqueous media.[19]

In general terms, the preparation of spherical size defined AuNPs is accomplished by: gold (III) salt reduction by citrate at 100 ºC; preparation in citrate at 25 ºC after UV irradiation, and particles prepared in an ascorbate solution at 25 ºC.[22]

Besides the reduction agent used, other parameters that must be considerate to ensure the size and mprphology outcome, including the reaction time and the medium temperature.

The first method, used to produce the nanoparticles utilized in this work, is known by the name of the researcher who described it, Turkevich[15], and has been modified and optimized over time.[22] This is a simple, well characterized, reproducible, size tunable and very common method for the aqueous synthesis of spherical fairly monodisperse nanoparticles with high yield (Fig. 13)[16]. Starting from a gold salt, usually $HAuCl_4$ (chloroauric acid), its oxidation from Au^{3+} (auric) to Au^0 (atomic gold) in aqueous solution is accomplished in the presence of sodium citrate (detailed protocol described in the Materials and methods chapter).[16, 22]

The proposed chemical reaction is a multi-step process[15]:

1- citrate oxidation $\mathbf{C_6H_6O_7 \rightarrow C_5H_4O_5 + CO_2 + 2H^+ + 2e^-}$
2- auric salt reduction $\mathbf{AuCl_3 + 2e^- \rightarrow AuCl + 2Cl^-}$
3- gold species dismutation and atomic gold production $\mathbf{3AuCl \rightarrow 2Au^o + AuCl_3}$

Which is represented by the global reaction:

$$\mathbf{2\,HAuCl_4 + 3C_6H_6O_7 \rightarrow 2Au_o + 3C_5H_4O_5 + 6Cl^- + 8H^+ + 3CO_2}$$

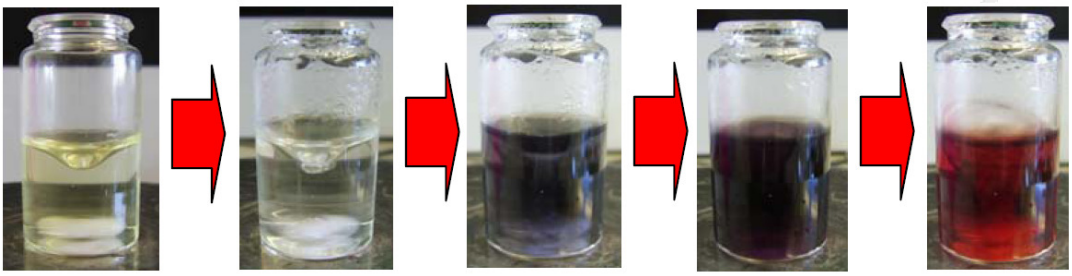

Figure 13**-** Colour changes during $HAuCl_4$ reduction by citrate at boiling temperature.

1.2.3- Capping agents

The most promising technological applications for MNPs appear to concern bioanalytical and biomedical problems thereby promoting stability, solubility in aqueous media and controllable surface chemical reactivity to key features.[23] An easy strategy to accomplish these, is by using thiol ligands with hydrophilic end groups.

As mentioned before, a capping agent is a compound that binds to a nanoparticle covering its surface. This compound is critical to avoid the NP growth beyond the nanometer range, to stabilize the colloid in the solvent and can additionally bestow a functional group useful to bind some molecule of interest later.[3] If the capping agent binds the molecule of interest to the NP, it is adding up the linker function, thus dismissing the use of another compound to play the task.

The surface derivatization of an arbitrary NP, featured by the synthesis capping agent, can be modified by ligand exchange. This may be accomplished by the exposure of the NPs to an excess of a competing capping agent. The previous capping group can them be sequestrated or the partially exchanged NPs isolated by precipitation and re-exposed to the new ligand again in successive cycles to maximize the exchange.[3, 24] This is the principle followed in this dissertation´s experimental work to generate AuNPs with MUA (11-mercapto-1-undecanoic acid) capping (Fig. 14), starting from the synthetic citrate capped AuNPs.

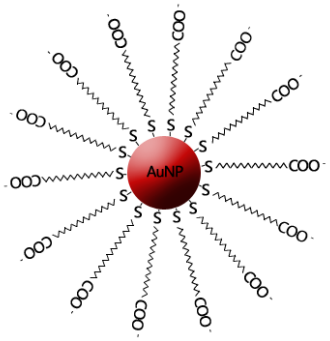

Figure 14**-** Representation of a MUA capped NP. Not at scale: MUA´s length is at least 4 times smaller than the smallest NPs prepared by common methods.

The sulphur atom from the MUA molecule competes with the citrate, establishing a stronger bond with gold (almost covalent) than the ionic one promoted by citrate. In other works, the molar stoichiometric amount of MUA to cover a 12 nm AuNP was accepted as 120 [25], but due to new data (yet to be published by our group, Luz, J. *et. al*) the ratio had to be corrected to 5000 in the course of this dissertation. Other suitable linkers are worth mentioning such as antibodies and small peptides (CALNN- Cys-Ala-Leu-Asn-Asn[23, 25], CALKK- Cys-Ala-Leu-Lys-Lys[23]).

MNPs production has to take into account that avoidance of aggregation is required to ensure their storage and some applications such as SAM production or functionalization for further use. Aggregation is usually undesirable still, it is the functional principle behind some types of bionanoprobes for rapid diagnostic.[26] MNP´s plasmonic is sensitive to the refractive index of the vicinity of the surface and as a result a color change occurs if MNP aggregates are formed. Strong aggregation can be noticed with the naked eye by a change to a blue colour, but UV-Vis (ultraviolet-visible) spectroscopy is a more appropriate method to assess its magnitude. The occurrence of this phenomenon causes the AuNPs plasmonic to become wider and to shift to higher wavelengths (Fig.15).[16]

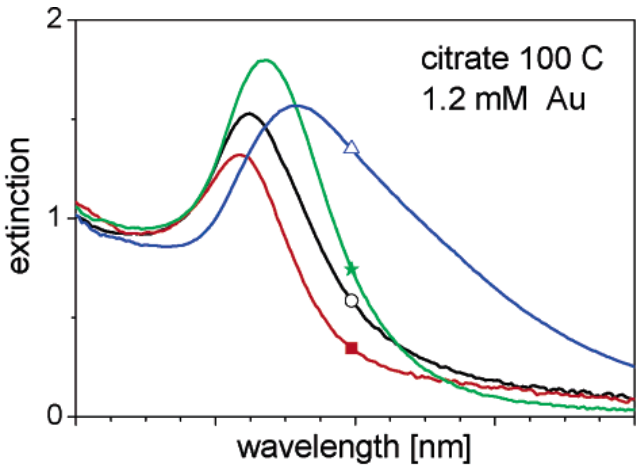

Figure 15**-** Extinction spectra of AuNPs solutions prepared by the Turkevich method with constant Au concentration, showing shifted SPR due to a successive size increase. (Size increase order: red, black, green, blue.) According to Kimling *et al.*, the diameter of the citrate prepared AuNPs is a function of the maximum wavelength of the plasmonic.

1.2.4- Proprieties of Metallic Nanoparticles

In the past fifteen years noble metal nanoparticles have been studied intensively unveiling interesting proprieties and applications, mainly for silver and gold nanoparticles.

The smallest MNPs are nearly as molecular (<1 nm, <100 atoms) while the largest ones reaches more than 20 nm (>100.000 atoms). This means a huge difference in the percentage of surface atoms in this size range: >75% to <0,5% respectively. For that reason and because van der Waals attraction forces are weaker in smaller MNPs (so they tend to aggregate slower), the smaller ones are better suited for standard chemicals and surface sensitive probes while the larger MNPs are more appropriate to physical probes which exploit the periodicity of the particle´s internal lattice.[3]

Entering the nanoscale domain, the optical proprieties of the metallic nanoparticles are remarkably different for two reasons: the energy levels gap´s become wider and superficial plasmonic resonance (or surface plasmonic resonance) become a significant phenomenon.[22, 27]

The mass, and therefore the size, enables the wider energy levels that the electrons can undergo which explains the intense red colour of the AuNPs solutions and its deviations in the UV-Vis spectrum according to diameter: the smaller the particle, the bigger the energy oscillation implying a shift of the plasmonic to smaller wavelengths.[16]

The surface plasmonic resonance (SPR) occurs when the size of the metallic nanocrystal is inferior to the incident radiation wavelength. SPR is often referred as LSPR (localized surface plasmonic resonance) as it is a localized phenomenon. SPR is originated as follows (Fig.16)[27]. The electric field of an incident electromagnetic wave induces the polarization of the free electrons relative to the ionic nuclei with much higher mass. The difference in global charge is much more intense at the crystal surface and produces the oscillation of the electrons at a certain frequency. To sum up, the free electrons in the conduction band suffer an in phase oscillation with the incident electric field.[27] This electronic collective movement excitation is called plasmon.

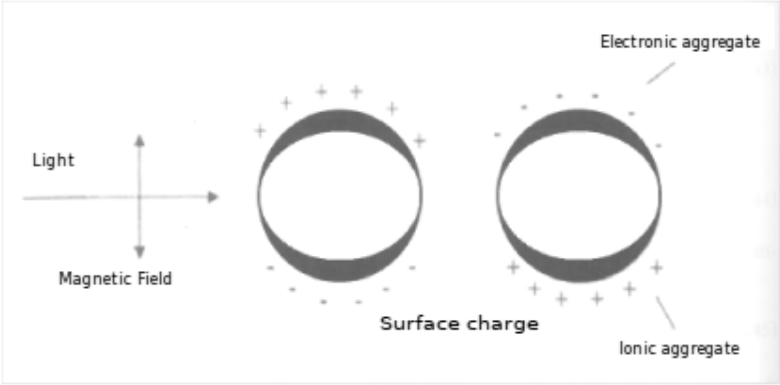

Figure 16**-** Surface plasmonic effect in a spherical nanoparticle.

SPR depends on the nearby dielectric surroundings and on the free electron density of the particle. The plasmon frequency depends on the metal dielectric function and on the shape of the nanoparticle (NP) and is responsible for the creation of an adimensional electric field with equal frequency at the particle´s surface.[27] Furthermore, small changes in the plasmonic can occur due to refraction index of the solvent.

In fact, the most prominent propriety of metallic nanoparticles is their intense and well defined Ultraviolet-Visible (UV-Vis) spectrum which reflects the size, nature and shape of the nanoparticles in solution.[22]

Besides their optical proprieties, nanoparticles are robust and have a high surface/ volume ratio which implies an elevated functionalizable area with capping agents and/ or biomolecules.[28] Moreover, for small spherical gold nanoparticles there is no experimental

evidence of associated toxicity.[29] Depending on the capping/ functionalization, applications in bioreactors[30], biosensors[12a, 30], bionanoprobes for quantification and clinic diagnostic[12a], nanoelectronics[12a], materials for affinity chromatography separation, and controlled pharmaceutics deliver can be met[22].

1.3- Bionanoconjugates

This dissertation aims to study and apply the advantages of bionanoconjugates (BNCs) in a phenol remediation system. Therefore, BNCs must be obtained, compared to the non-conjugated enzyme and, at last, incorporated in a remediation system.

Having monodisperse NPs with the desired capping will usually mean they are stable and therefore reaction controlled and limited. Their usage is thus closely linked to other molecules that can be "added" to the NP for the application sought (such as tyrosinases in this work). Besides the linkage capability, the capping agent specifies the type of interaction that will be set with the intended molecules (e.g. proteins, antibodies): it can be chosen to enable the adequate conjugation to a compound that will bestow its function to the assembly. This whole assembly of a nanoparticle linked to specified molecules is referred as nanoconjugate and as bionanoconjugate if the linked molecules are biological.

Covalent interactions (in opposition to electrostatic interactions for instance) enable greater stability of the BNCs, but that can also imply more tension and less stereoliberty of the BNC and the active biomolecule. Namely, in the case of linked proteins, conformational changes can occur deriving in denaturation, loss/ gain of substrate specificity, increase/ decrease of activity.[31] In some situations stronger binding may be desirable which tends to ensure longer lifetime of the BNC and higher specificity to a certain substrate, but in general non-covalent binding is preferable, as it interferes less with the native structure of proteins.

In this dissertation it is studied the system composed for AuNP-MUA bound to two different tyrosinases (functional molecules).[12a, 31]

1.4- Tyrosinases

1.4.1- Tyrosinases- General considerations

Tyrosinases are part of the polyphenol oxidases (PPOs) enzymatic family, and are classified as monophenol, *o*-diphenol:oxygen oxidoreductase EC 1.14.18.1.[32] These enzymes are widely distributed in nature (mammals, plants, bacteria, fungi) and play an essential role in melanin biosynthesis.(Fig.17)[33] In fact, they catalyze both the *o*-hydroxylation of monophenols (cresolase activity) and the subsequent oxidation of *o*-diphenols to *o*-quinones (catecholase

activity).[34] In aqueous solution, *o*-quinones are unstable and deteriorate over a period of minutes to hours by a combination of nucleophilic reactions and further oxygen mediated oxidations, not all of which are understood.[35]

Melanin pigments are polyphenolic polymers ubiquitous in living organisms: in mammals they are responsible for skin, eye and hair pigmentation conferring protection by absorbing UV radiation[33a, 36]; in invertebrates tyrosinase interfaces with defense reactions and sclerotization[37]; in microorganisms it has been proposed that melanin has a role in the formation of reproductive organs, spore formation, the virulence of pathogenic, and the tissue protection after damage[34a]; in plants tyrosinases assist the regulation of the oxidation-reduction potential and the wound healing system.[32b]

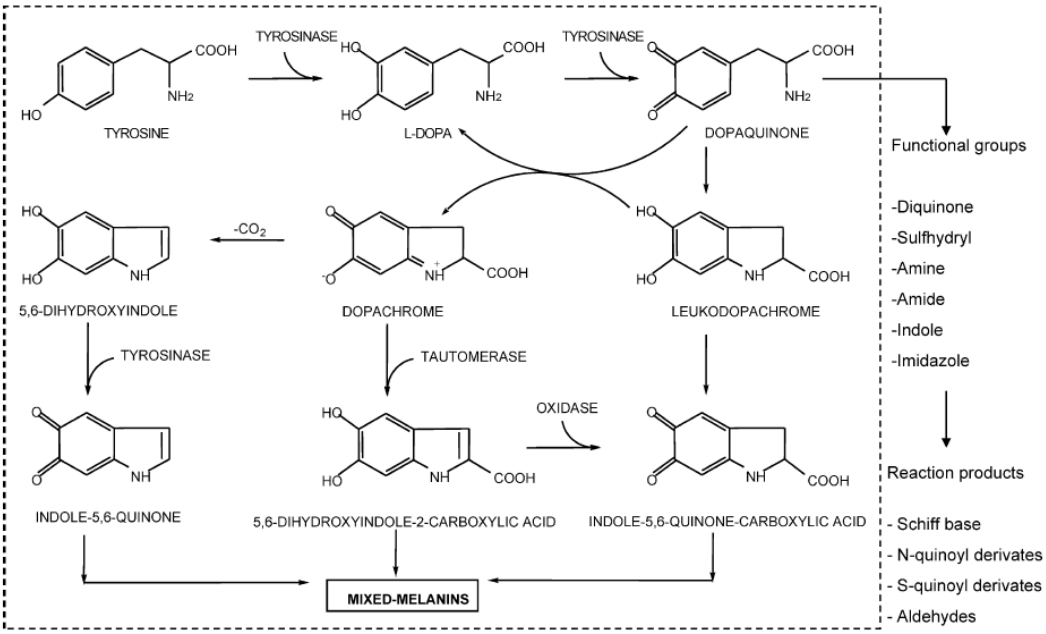

Figure 17**-** Melanin biosynthesis starting from the natural substrate, tyrosine. Dopaquinone is converted by the TYR to L-DOPA (which can also be the starting substrate) and dopachrome through auto-oxidation.
TYR- tyrosine IQ- indole-5,6-quinone; L-DOPA (L-3,4-dihydroxyphenylalanine); DHI- dihydroxyindole; DHICA- dihydroxyindole-2-carboxylic acid; ICAQ- indole-2-carboxylic acid-5,6-quinone; HBTA- 5-hydroxy-1,4-benzothiazinylalanine

The browning phenomenon in fruit and fungi that occurs after tissues injuries or harvest is also usually related to oxidative polymerization, similar to melanogenesis.[33a] This is an undesirable phenomenon in fresh fruits, beverages, vegetables and mushrooms which decreases the commercial value of the products and compels research to comprehend the role of tyrosinases in biological metabolism.[32b, 33a]

Traditionally tyrosinases have been exploited in plant-derived food products (e.g. tea, coffee, raisins and cocoa) to enhance organoleptic properties, but due to their ability to catalyze crosslinking between peptides and carbohydrates; methods for stabilizing structure in low-salt

and low-fat food and tailoring polymers in material science (grafting of silk proteins onto chitosan[38]) have been reported.[32b, 33b]

Besides PPOs, also peroxidases (EC 1.11.7.1) are known for oxidize polyphenols, however they are highly dependent on the use of hydrogen peroxide as oxygen donor and are unable to function in the presence of catalase.[32a]

Tyrosinases are cytosolic enzymes that are often partially bound to organelles or membranar structures such as: thylakoids of the chloroplasts mainly in higher plants and melanosome in mammalians.[39] Gross tyrosinase extracts such as those used in this dissertation have a fair amount of issues that should be mentioned. They contain endogenous phenolic substrates already oxidized which can inhibit protein activity or lead to enzymatic artifacts, and raise the initial absorbance when colourimetrics assays are performed. The removal of these phenols by ion exchange resins usually result in an accentuated activity decline as result of the loss of some isoforms and co-factors. Another issue is the reproducibility of the activity of PPOs extracts due to variations in the development phase in which the mushroom is harvested and due to which tissue was used.[32a]

1.4.2- Structure of Tyrosinases

From both structural and functional point of view, the most studied tyrosinases are those from *Streptomyces glausescens*[33a], *Neurospora crassa*[34b] and from *Agaricus bisporus*.[32a] *Agaricus bisporus* is a champignon mushroom and the tyrosinase extracted from this source is commercially available (the lyophilized extract can be used without further treatment) and is highly homologous with the mammalian ones. As a result, this tyrosinase has been used in almost all studies on tyrosinase inhibition and is well suited for studies on melanogenesis.[33a] Astonishingly, considering the numerous studies based on it, only recently (2011) became available the crystallography structure for this protein (Fig.18).[40]

Sequence comparison of tyrosinases has demonstrated that exists a high heterogeneity concerning length and identity, but also that all tyrosinases have highly conserved regions at the active site.[32b] Tyrosinases are characterized by Type III copper centres (T3Cu) which consist of a pair cooper ions (Fig. 19)[39, 41] within a domain containing strictly conserved aminoacid residues[33a, 42] (each copper is coordinated by three histidine residues).[32b]

These centres are common in oxidases and oxygen-transporting proteins, such as hemocyanin and due to strong antiferromagnetic coupling (spin pairing between the two Spin =1/2 ions) these proteins exhibit no EPR (Electron Paramagnetic Resonance) signal.[32b, 43]

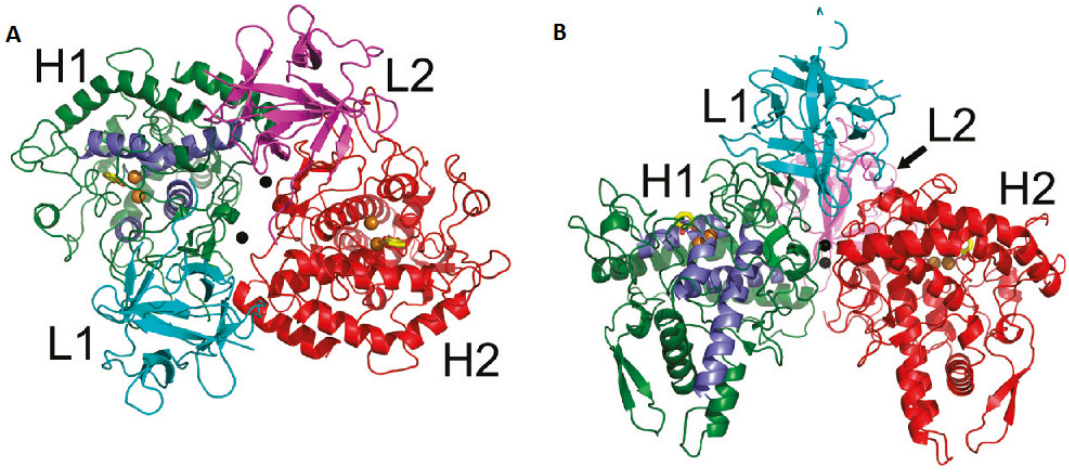

Figure 18**-** Top (A) and side (B) views of the *Agaricus bisporus* tyrosinase structure. The H_2L_2 tetramer structure was obtained by x-ray crystallography (2,6 Å resolution). H-L dimer interactions are between H1 (green) and L1 (cyan), and H2 (red) and L2 (magenta).
Brown spheres- cooper ions;
exogenous compounds: Black spheres- holmium ions; Yellow sticks- tropolone molecule in the active site

Comparative and complementary information can be obtained through the *Streptomyces castaneoglobisporus* tyrosinase structure obtained by Motoba *et al.*

The tyrosinase from *Agaricus bisporus* (AbT) usually presents as a tetrameric globular protein with a molecular mass of 120 kDa composed of two subunits of ~43 kDa (H subunit) and two subunits of ~14 kDa (L subunit).[32a, 40] This is atypical among other PPOs that only present a monomeric subunit similar to the H subunit mentioned. The monomeric tyrosinase (43 kDa) isolated from mushroom fruit bodies is active,[40] and the T3Cu centres solely appearance in the H-alike subunits regard this as the functional part, which define a tyrosinase. The function and origin of the L subunit is yet unknown.[40]

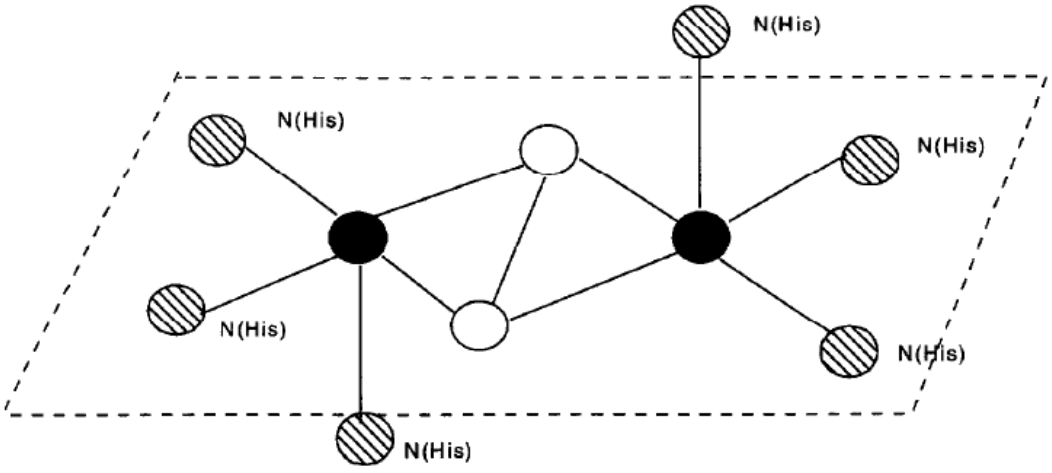

Figure 19- Type III Copper centre representation. Dioxygen (white circles) in the peroxide form bounds to both copper ions (black circles) which are in turn coordinated by nitrogen atoms (striped circles) from histidine residues. In the oxi form, Cu(I) become Cu(II).

Agaricus bisporus copper mass represents 0.2% of its total mass, present in the H subunits. Copper is strongly bound and only dialysis against strong complexing agents (such as HCN) can remove it.

Besides the AbT a recently produced and promising[32b] tyrosinase was also studied in this dissertation. The tyrosinase from *Trichoderma reesei* (TrT), was recently (2006) overexpressed under a strong promoter in the native host and it is secreted into the culture supernatant. Until now, all plant, animal and fungal tyrosinases studied had intracellular origin, so the reported TrT expression is a new achievement within this enzyme class.[44] TrT was obtained much purer than AbT (close to 100% purity)[45], available in Tris-HCl buffer pH 7.5 concentrated solutions from VTT, Finland. Its molecular mass is 43.2 kDa, but no structure is yet available and it revealed to have more activity and stability within a neutral and alkaline pH range, being greater at pH 9[44] (Fig. 20[45]).

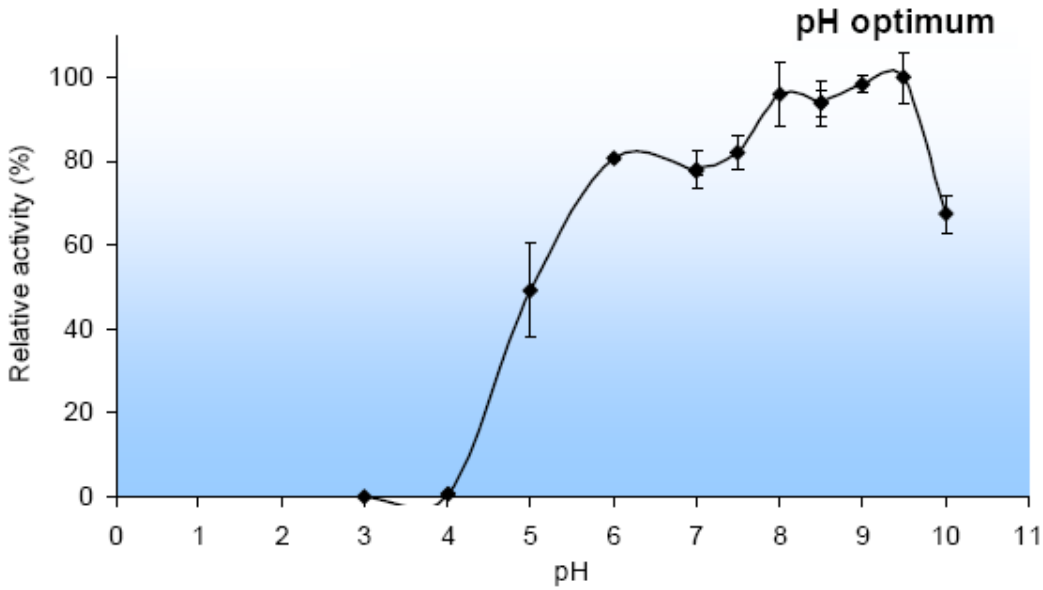

Figure 20- TrT activity on 15 mM L-dopa 300 - 400 nkat/mg (depending on the enzyme formula and preparation), Tris-HCl buffer pH 7.5.

TrT has stable activity (1h, 25ºC) at pH 7-9 and an optimum activity temperature of 30-40 ºC, so it can be easily attempted do use in any application suited for AbT. It offers the advantages of higher purity; higher activity (Fig. 21) and heterogeneous expression under a strong promoter, opposed to the disadvantages of a higher production price (the process scale-up is limited so far) and a low activity at acidic pH. The instability even at slightly acidic pH is an important operational problem considering the substrate conversion pushes the pH of the reaction system towards bellow neutral values as the reaction proceeds.

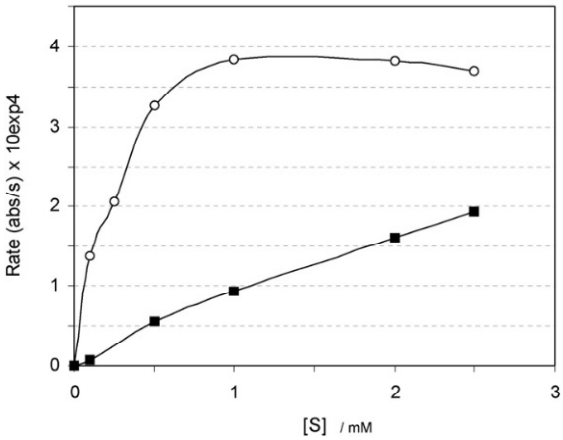

Figure 21- Reaction rate at different tyrosine concentrations for AbT (black squares) and TrT (white circles).

1.4.3- Activity of Tyrosinases

The cresolase activity is the rate-limiting reaction (can be until 40 times slower than catecholase[32a]) in melanin synthesis (Fig. 22)[46] and this makes biological sense because the outcome of the reaction can proceed the pathway spontaneously at physiological pH value.[33a]

In both cresolase and catecholase activities an oxygen atom from a dioxygen molecule is incorporated in the substrate while the other atom is reduced to water by a co-substrate (monophenol or similar molecule).[32b] There are also broad substrate specificities for both activities, but the enzyme has more affinity for L-isomers than for the corresponding D–isomers.[33a] The main endogenous substrates are L-tyrosine, *γ*-glutaminyl-4-hydroxybenzen (GHB), and aminephenol[39]. In the case of phenol as substrate it can be converted directly to *o*-quinones by an undetermined process or can be processed trough cresolase and catecholase activities.[47]

The study of tyrosinase kinetics is usually assessed by Michaelis-Menten parameters (Fig. 22). Mainly because, experimental points have shown to fit Michaelis-Menten kinetics and its parameters have proven to be very sensitive to the nature of the substituents present on the aromatic rings.[35] When cresolase activity is much slower than catecholase (as in the tyrosinases studied in this dissertation), the first reaction has a major weight in the kinetic parameters (V_{max} e K_M) and, all together, tyrosinase´s global activity can be considered a classic two-substrates reaction, with each activity following an ordered Bi Bi sequential mechanism (two substrates generating two products) according to studies in plants and bacteria.

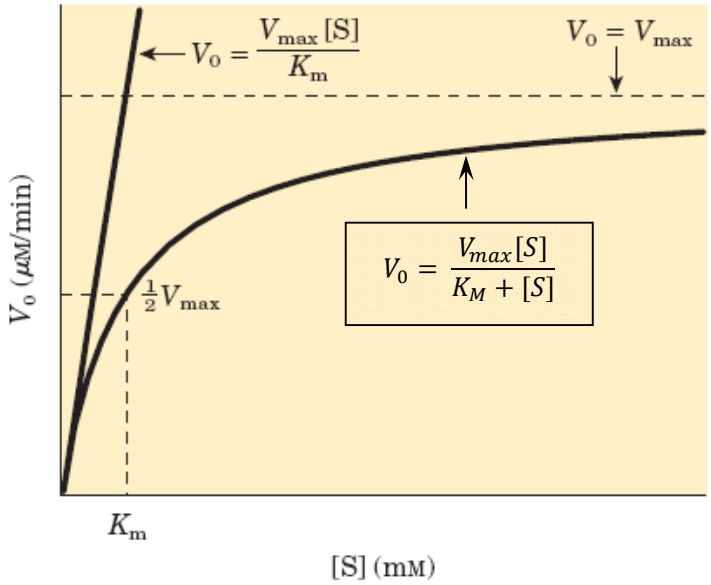

Figure 22- Typical Michaelis-Menten kinetic curve: initial velocity (V_0) vs. substrate concentration ([S]).
V_{max}- maximum reaction rate
K_m- Michaelis constant

The cresolase activity is characterized by an initial lag phase followed by a linear phase, so the observed Michaelis-Menten curve resembles a sigmoid. The lag phase can vary between one minute to two hours and is dependent on the concentration and nature of the enzyme, substrate and co-substrate concentrations[33a, 46] and oxygen. Being well suited for the free enzyme, these parameters are appropriated to compare its performance with the immobilized and conjugated forms, namely using chitosan and gold BNCs respectively. This assessment was not performed in this work, although it is a practical and moderately fast way to evaluate losses/ gains caused by immobilization and BNC.

AbT and TrT have been comparatively studied under the V_{max} and K_m parameters to a variety of substrates and it was concluded that K_m values were approximately ten times lower for AbT than for TrT (the lower the K_m, the bigger substrate affinity it suggests), while for the V_{max} parameter was found a high dependence on the substrate used.[48] However, two remarks concerning the enzyme activities must be made: for the same substrate, the enzymes do not necessarily present the same saturation concentration (condition required for a Michaelis-Menten analysis), and it is nowhere mentioned if the activities are specific, or, in other terms, if the absorbance variation per minute is divided by the total amount of enzymatic units or catalytic centres present in the solution. Lack of information regarding these, added to the high activity discrepancies (confirmed in this dissertation) in AbT label lots from Sigma-Fluka, render unclear the published results.

1.5- Bioremediation

1.5.1- Bioremediation concept

According to the United States EPA (Environmental Protection Agency), bioremediation consists in the use of living organisms to clean up oil spills or remove other pollutants from soil, water or wastewater; use of organisms such as non-harmful insects to remove agricultural pests or counteract diseases of trees, plants and garden soil.[49] This definition can be expanded beyond whole living organisms and resumed as being the application of biological processes for the treatment of hazardous chemicals present in the environment.[50] The treatment aims to transforms the hazardous compounds to an innocuous form or to degrade them to below the established concentration limit.

Bioremediation can be complemented with physical, chemical or mechanical methods but, alone, it presents the advantage of not generating toxic side products. Enzymatic bioremediation also enables enzyme *in situ* digestion by indigenous microorganisms after the treatment; enzymes can be produced at a higher scale than whole microorganisms, with enhanced stability and/or activity and at a lower cost by using recombinant-DNA technology, but it has some drawbacks such as the exposure to high stress and lack of cofactors outside a cell.

Enzymatic bioremediation can be explored simply by searching for a microorganism capable of feeding on a particular pollutant, identifying the enzyme responsible for the transformation and then improving it to sustain operating conditions.[51]

1.5.2- Phenol remediation

Aromatic compounds, including phenols and aromatic amines, are a major class of pollutants worldwide and many are classified as priority pollutants by the United States EPA[52] and the European Union[53] and subject to specific legislation. They are found in wastewaters of a large number of industries such as coal conversion, petroleum refining, resins and plastics, wood preservation, dyes, metal coating, chemicals, synthetic fibers, mining and paper pulp.[54]

Aromatic compounds are persistent and associated with toxic effects[55] and, as result, wastewaters must be treated to decrease these compounds to a level suitable for discharging. Another, sometimes unsuspected, source of these compounds is the introduction of xenobiotics through agriculture promoting the contamination of underground water and household medication which end up in the sewers. To accomplish the legislation of each country, the methods synthesized below have received the most attention.

1- Peroxidases can treat a large variety of phenolic compounds over a wide range of pH and temperature. Peroxidades (mainly from horseradish) in the presence of hydrogen peroxide originate free radicals that spontaneously react to form polymeric products of reduced solubility,

which can be removed by sedimentation after a coagulation step.[56] This approach has the prohibitive cost of the enzyme and the hydrogen peroxide as downside.[57]

2- Tyrosinases catalyze the oxidation of phenols to *o*-quinones using molecular oxygen as electron acceptor. This enzyme is widely available in nature and has a cost comparable to the peroxidases. It has been reported to have more than 50% of optimum activity at pH 5-8 with a maximum at pH 7, and instability under acidic conditions at elevated temperatures.[57]

3- Photocatalytic degradation of phenol in the presence of semiconductor oxide catalysts (ZnO and TiO_2 for instance) using high potency UV irradiation.[58] This process mineralizes organic compounds into CO_2 but it is very time consuming, lacks selectivity for aromatic compounds (much less for phenol) and many variables (e.g. scale-up and degradation yield vs. light-wavelength/potency) are yet to be studied.

4- Activated charcoal has affinity for non or weekly polar compounds and can be regenerated by heat. Its high porosity confers a wide internal surface, also meaning high absorption capacity. It is considered a cheap and undemanding method.

Lately, enzymatic methods have received most attention because they require low retention times comparing to others. Conventional methods fall short of achieving the required degree of removal of these pollutants while enzymes can target specific pollutants even if diluted are becoming cheaper and customizable (by genetic engineering), and they are less likely to be inhibited by substances toxic to living organisms performing the same remediation.[54b] A promising feature of enzymatic systems is the possibility to combine pollutant quantification with pollutant degradation. This approach is called sense-and-shoot and nanotechnology plays an essential role in it.[59] AuNPs particularly, provide a stable surface for enzymatic immobilization and can act as nanoscale electrodes interchanging electrons between the enzymes and the electrode material (Fig. 23)[60]. This is expected to increase the detection limit (especially important for endocrine disruptors[61]) owing to a bigger responsive area in the sensor; and, by modulating the current in the electrode, to improve the enzymatic activity without the need of external electron-transfer mediators.[60, 62]

Nevertheless, the use of the mentioned enzymes in a remediation system is critically unappealing due to the enzyme production costs. In this dissertation, this approach is reconsidered because the newly available TrT is produced under a strong promoter and secreted to the culture supernatant. This method, being recent, has yet an elevated scale-up potential, associated with obvious costs reduction. If a commercial application is found, scale-up studies become justifiable and phenol remediation via enzymes may become competitive. In this work some steps were taken towards the adequacy of using TrT in phenol remediation. Some remediation setups were conceived and tested using AbT, and, in a later phase of the study, it was aimed to implement TrT in the most promising ones.

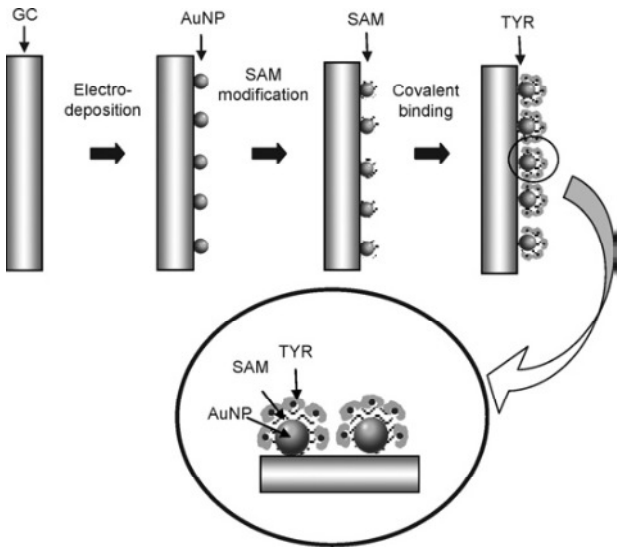

Figure 23- Glassy carbon- Gold nanoparticle-Tyrosinase (GC-AuNP-TYR) electrode approach for biosensing.

1.6- Phenol detection

1.6.1- Analytical methods

Accurate and highly sensitive detection of phenols is important to assess the quality of the available water sources and to ensure trustworthy investigation towards them.

Complex matrixes limit the analytical methods prone to be applied in practical situations. The elements of a matrix have very specific proprieties by their own but they are not necessarily known nor quantified by the operator, therefore the convenience of calling it “complex” in the situations where this happens. Not knowing sufficiently the composition of a matrix adds up the problem of the interaction within its elements because mutual inertness cannot be ensured. Assuming a global equilibrium is met; the physic-chemical processes can potentially be translated in a change of density and viscosity, and origin phases, emulsions and solid suspensions, in fluids. These factors are important for the selection of the analytical method/ necessity of a pre-treatment but, more importantly, the matrix elements themselves may mask the analytes detection.

Phenol contaminated wastewaters are complex matrixes rich in solvents and industrial sub-products and so, quantification analysis must attend to it. A simple way to contemplate the matrix influence in an analytical process is to complete it with the standard addition method. Considering now the simplest reaction mixtures obtained from TYR (tyrosinase) activity, they generate a panoply of unstable (short aqueous life-times) aromatic compounds (mainly quinones) that enter in a mutual equilibrium[41] (in Fig. 13 only the most representative and stable species are represented). If the TYR used is the impure AbT extract, the reaction mixture can

also be expected to already contain peptides, inactive proteins, cellular residues and various phenolic compounds.[32a] Because products are not stable and because an unique product cannot be singled out, the reaction rate assessment is more accurate by detecting the latent substrate.

Most available methods (gas/liquid chromatography, spectrophotometry) required demanding sample treatments and their operation is very time-consuming.[59] Advances in the technology of amperometric tyrosinase-based biosensors proved them to be very simple, highly sensitive and effective for phenol assay. Regardless of all these potential advantages, many of them still are at the "proof-of-concept" phase and it can be pointed out that the measured signal is greatly susceptible to the matrix complexity and the molecular targeting is a major concern.[60-63]

To predict the efficiency of any remediation system using tyrosinases, it is important to study their kinetic proprieties. These proprieties are commonly evaluated by four methods: colorimetry; oxygen electrode; oxygen manometer and radiochemical liberation of ^{3}H from a L-[2,6-^{3}H]monophenol used as substrate.[32a] Oxygen measurements lack precision because products are easily oxidized and recycled multiple times using molecular oxygen cost. Colorimetry is the simplest method and it is very effective if the enzymatic extract is free from other oxidizing enzymes. The TYR´s activity can be measured at 280 nm (ε_{280}= 1440 $M^{-1}cm^{-1}$)[35] because the oxidation to L-DOPA contributes the most to absorption variations in this wavelength, however many other aromatic compounds absorb in this region and so a better alternative is to follow the formation of the final reaction product (*o*-quinones). To accomplish it, an indirect way is used consisting in reading the formation of the main product of the side reactions, the dopachrome, at 475 nm (ε_{475}= 3600 $M^{-1}cm^{-1}$).[41] For environmental legislation purposes, there are standard procedures described to quantify trace (<100 ppm)[64] and ultratrace (<1 ppb)[64b] levels of phenol that often occur.[65] They typically comprehend a sample extraction step by liquid-liquid extraction or evaporation of the extract to isolate and concentrate the analyte followed by GC/MS (Gas chromatography/mass spectrometry), GC (Gas chromatography) with electron capture detection in a dual-column set-up, or HPLC-UV analysis[55, 66] The analysis using GC with sample detector is amenable as well.[67]

To favor the rate measurement exactitude, *o*-quinones can be recycled back to *o*-diphenol by an UV-absorbing reducing agent (ascorbate or NADH for instance) and the consumption of this agent monitored. Another process involves the formation of stable adducts which appearance can also be followed by colorimetry.[32a] Either way, none of these reactants could be used in this dissertation work because they would have an aggregation effect over the AuNPs/BNCs.

Another problem is the suicide inactivation of TYR by its own products, meaning activity rate measurements have to be promptly performed and that TYR cannot catalyze for long periods. To prevent this, besides the adduct formation, an alternative has gained much attention lately. Chitosan is reported to induce precipitation of reaction products arising from phenol transformation without affecting the rate of the catalyzis.[57] This is especially important for

remediation because chitosan (Fig. 24) is a natural polymer derived from chitin (via deacetylation with alkalis) know for its nontoxicity and biocompability[68] but more work needs to be done concerning its inhibition preventing role.

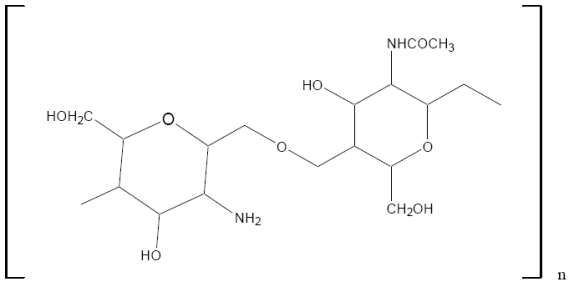

Figure 24- Molecular structure of chitosan.

Sample preparation- SPME

Brute matrixes analysis often generates interferences and incompatibilities in the analytical equipments. To avoid these problems and to seek analyte isolation and concentration, sample preparation methods are chosen according to the analytic technique to be used.

Solid-phase microextraction (SPME) is a technique developed in 1990 that suits well gas chromatography demands, mainly because it has a high concentration potential adequate for GC detectors sensitivity, facilitates the transportation of the extracted material to the chromatographer and avoids the introduction of non-soluble particles from the matrix in the GC column.[54b, 69] It is a rapid and solvent free extraction alternative technique used in environmental, food and drug abuse fields nowadays.[54b] SPME equipment is based on a silica baton with a 10 mm ending covered with a thin polymer film [e.g. polydimethilsyloxane (PDMS), polyacrylate (PA) or Carbowax (Cwx)] or with an adsorbent solid (e.g. activated charcoal).[69](Fig. 25) The sample preparation by SPME is simple, reproducible as long as the adsorbent is consistently treated the same way, and fits general purpose analysis with few adjustments. Due to all the above mentioned, SPME is appropriated for this dissertation objectives.

The baton ending is immersed in the sample and extracts, according to the partition coefficients, the compounds present. Headspace extraction is also possible depending on the fibre characteristics. After saturated, the fibre is introduced in the injector port of a GC where the analytes are thermally desorbed under a gas flow that carries them to the chromatographic column.[69]

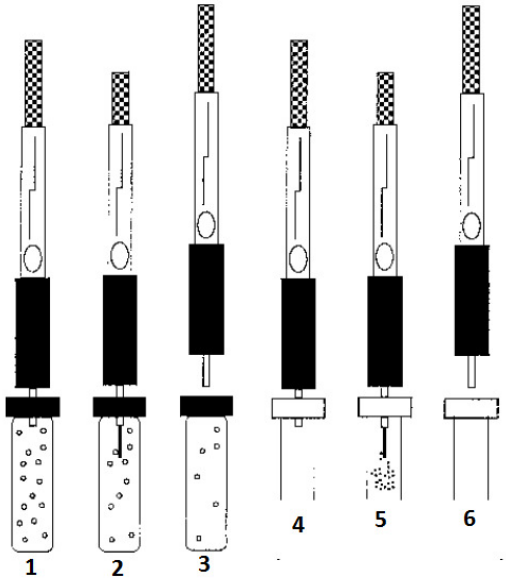

Figure 25- SPME typical sampler, extraction (1-3) and injection (4-6) stances. At 2nd and 4th frames, the extracting fiber is exposed from the needle to the sample and to the injector respectively.

In SPME the molecules in the matrix of the sample have to migrate and penetrate the coating adsorbent material which means that mass transfer and kinetic resistivity are important factors to the time required until partition equilibrium is achieved between the sample matrix and the solid-phase coating.[67, 69] To reduce migration time and promote effective adsorption impacts, matrix agitation is crucial.(Fig. 26)

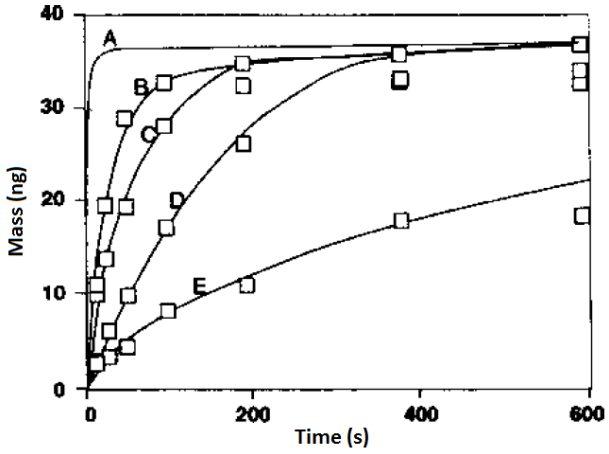

Figure 26- Aqueous benzene (1 ppm) extraction outlines under different magnetic agitation intensities. **A-** Theoretical behavior; **B-** 2500 rpm ; **C-** 1800 rpm ; **D-** 400 rpm ; **E-** no agitation

2- Material and methods

2.1- Reagents

2.1.1- General considerations

All weighting was performed using a AS220/c/2 (Radwag) scale.

All buffers and solutions involving AuNPs were prepared using ultrapure milliQ water (purity=1 at >10 MΩ/cm) obtained from Watermax W2 (Diwer).

All absorbance measurements were acquired bellow the unitary value. When the sample had higher absorbance, it was diluted and then measured, which means the Absorbance values higher than one, presented in this dissertation, are corrected ones.

The pH of all buffers was corrected with the corresponding weak acid or base of the buffer and measured using a pH-Meter BASIC20+ (Crison).

L-tyrosine and L-DOPA oxidize quickly in solution so fresh solutions were always used.

All controlled stirring and heating were done by an Agimatic-N (P-Selecta) plate.

Activity rate assays were only performed using bubbled oxygen 99,9% to confirm the labels information. All the others were performed at atmosphere conditions.

TrT is a novel and expensive enzyme, produced at VVT, Finland, and consequently our laboratory supply was limited to 900 uL. Due to this limited amount, generally, TrT assays were performed with no duplicates.

GC prepared standards were all filtered using Acrodisc Syringe Filter with 0.45 µm pore Nylon membrane (PALL).

2.2- Bionanoconjugates preparation

It was stated in the Introduction that reproducibility is a major concern regarding tyrosinase investigation. Not only for being a recommended investigation practice, but also to have comparable data and more precise conclusions, all enzyme lots used during this work were tested for protein concentration and activity.

2.2.1- Protein concentration – BCA Assays

Total protein concentration was assessed by the Bicinchoninic Acid assay (BCA). QuantiPro™ BCA Assay Kit from Sigma-Aldrich [Bicinchoninic Acid solution; copper sulphate solution; Bovine Serum Albumin (BSA) 1 mg/mL)] -(range: 0,5–30 µg/mL) was used. Bicinchoninic Acid was mixed with copper sulphate in a 50:1 ratio. For AbT, BSA in 7 different

concentrations in the 0-24 mg/mL range, while for TrT 8 different concentrations in the 0-70 mg/mL range, were used to do the calibration curve. TYR samples (triplicate) and standards (duplicate) were prepared adding 1 mL of the Bicinchoninic Acid mix to 30 µL of protein; followed by 37 ºC incubation in a muffle furnace for 30 minutes. The next step was reading the absorbance at 562 nm in spectrophotometer (Varian- Cary 50- Bio, Cary WinUV software- simple reads). A calibration curve was drawn using the data from the standards, and TYR concentration was calculated using the extrapolated linear regression.

2.2.2- Protein concentration – Activity determination

Besides the previously stated, it was noted that the Sigma criteria for Catalytic Unit differed from the international convention and thus Sigma Protocol (Appendix 1) had to be performed to confirm AbT supplier's information.

Supplier´s activity assay for TrT was performed using 100 nM of enzyme in L-DOPA 15 mM, pH 9 buffered. The assay was changed in order to use the more accessible glycine buffer [pH 9 50 mM- glycine (Sigma-Aldrich 99%, sodium hydroxide anhydrous (Sigma-Aldrich ≥98%)] and a lower L-DOPA concentration (1.82 mM) to avoid solubility problems. If the original protocol was well designed, substrate should be in a concentration that would enable Enzyme-Substrate complex stationary state for long enough to make possible an activity reading with a clear linear phase reading, and not so much that would cause inhibitory effects. By reducing the substrate concentration we hoped to obtain a shorter linear phase; a proportional, but not maximal, slope because not all TrT will bound to substrate molecules at the same time; a longer activity period and more effective percentage of L-DOPA in solution: L-DOPA decays quickly by oxidation with atmospheric oxygen and to dissolve the proposed concentration, time and heating are required which will contribute to L-DOPA loss.

The activity rate for both Tyrosinases was measured by the formation of the principal reaction product, dopachrome, at 280 nm wavelength, using a UNICAN- W2 spectrometer.

2.2.3- Gold Nanoparticles synthesis

To ensure reproducibility on the AuNP´s surface coverage studies, the Turkevich method was used. Particle characteristics (diameter and sizes) were determined according to the work of Haiss *et al.,* to guarantee a diameter close to 12 nm and a concentration of 15.6 nM.

AuNPs synthesis was made by $HAuCl_4$ 1 mM (Aldrich 99.99%) reduction by a sodium citrate solution 1% (p/v) (Sigma 99.99%). A 200 mL solution of the auric salt was heated and kept under agitation in a two-neck round bottom flask, in reflux, until ebullition. At ebullition, 50 mL of fresh sodium citrate solution is swiftly added. After the solution turned dark red, the heating was turned off and allowed to cool at room temperature.

2.2.4- AuNP capping

This work aimed to use AuNPs covered with MUA as this capping results in stable AuNP colloidal solutions and was found to bind proteins in a stable manner.[25] The previously accepted AuNP:MUA ratio was 1:120 but it was reviewed to 1:5000 during this work (yet to be published by our group). Capping with MUA was made by adding AuNP to a MUA solution in order to obtain always 3 nM AuNP-MUA solutions. These solutions were then ultracentrifudged at 20817G (centrifuge 5819R- Eppendorf) for 60 minutes at 4 ºC. The pellet was isolated and then ressuspended in milliQ water.

The efficiency of the capping was tested adding AuNP (3 nM) to a phosphate buffer saline solution (Sigma-Aldrich) in which MUA at 5000x AuNP molar concentration was already dissolved.

The aggregation salt assay was performed with NaCl (Panreac 99.9%) at 9 different concentrations (ranging from 0 to 500 mM in order to evaluate the stability of the newly produced AuNP-MUA). A UNICAN- W2 spectrometer was used to measure Absorbance at 520 and 600 mm. The ratio Abs520/600 was used as an indicator of aggregation.[25]

2.2.5- AuNP bioconjugation

AuNP conjugation with TYR was accomplished overnight at 4ºC simply by adding the proper ratio of enzyme to AuNP in solution. TrT conjugation directly at pH 9 originated aggregation of the BNCs so they had to be prepared in phosphate buffer pH 7 10 mM and then reinstated to pH 9 50 mM using a stronger glycine buffer.

The optimal conjugation rate used so far in our group depended on the stock activity and had now to be restudied in terms of total protein mass in purchased stocks. This work was accomplished by a colleague (Master João Luz) and the article publishing this work is yet to be submitted.

To verify the concentration of TrT needed to obtain an effective coverage of the AuNPs, agarose gel electrophoresis and zeta potential assays were performed. Zeta potential measurements were also employed to validate the overnight conjugation period. In this case BNC were prepared at 7 different days and then took all together to the working equipment.

For electrophoresis, an agarose gel 0.5% was prepared by dissolving agarose in 45 mL TAE pH 8 buffer 1/8x by heating the mixture until ebullition. This solution was deposited, while still hot, in the electrophoresis support and allowed to polymerize. After gelification, the gel was let at 4 ºC to homogenize. Samples were prepared by ultracentrifugation at 18514 G during 60 minutes, followed by15 uL glycerol 87% (Panreac) addition. Electrophoresis occurred in a TAE electrolyte bath (Enduro) at 150 V for 30 minutes

Zeta potential measurements were collected at 25 ºC, after an equilibration time of 300 seconds in the disposable reading cells (Malvern, UK), using a Zetasizer Nano Series (Malvern Instruments), with a 3 mW He-Ne laser in a fixed dispersion angle of 17º. Each data point is the

result of 3 measurements with 100 repetitions each in General Purpose mode. Eight different TrT concentration were used for AuNP incubation (1 nM AuNP : 0-500 nM TrT).

2.3- TYR activity as ionic strength function

The activity rate of the tyrosinases was studied at different ionic strengths. It was noted that TrT stock suddenly lost all activity when this task was being carried on and so neither this nor further studies could be made. For AbT, activity was studied under seven pH 7 phosphate buffer solutions concentrations ranging from 10 to 100 mM. The same was done to AuNP-AbT and to AuNP-MUA-AbT. To render comparison of the results possible, free AbT was prepared the day before and letft overnight at 4 ºC as processed for the BNCs. Dopachrome formation was followed at 280 nm wavelength, using a UNICAN- W2 spectrometer.

2.4- Chitosan preparation

Preparation of chitosan is not a common practice in our laboratory group and the synthesis parameters had to be refined. Three methods updated from the literature were tested:

Method I

Chitosan, 90% deacetylation, from crab shells (Sigma-Aldrich) was dissolved in acetic acid 0.5% (wt) to 6 mg/mL concentration. The solutions were placed of dishes and allowed to dry by solvent evaporation. After drying, the material was washed either with NaOH 10 mM or phosphate buffer pH 7 50 mM, and rinsed with distilled water.

Method II

Chitosan (6 mg/mL) was dissolved in acetic acid 0.5% (wt). The solution was added dropwise to a NaOH solution (2 M) with stirring. The thus formed beads were rinsed with distilled water twice and stored in humid state or filtered to dry. Beads can also be entrapped in an agarose 1% matrix prepared in phosphate buffer 50 mM. Agarose was deployed in a mold, waited to cool for a minute and then the chitosan beads were spread in it.

Method III

Chitosan (6 mg/mL) dissolved in acetic acid 0.5% (wt). The stirred solution was heated to 60 ºC in a water bath and agarose (0.5%) was added. The total amount solution was 20 mL in order to fully cover a petri dish. The composite solution was plated and immediately stored at 4 ºC until jellify (20 minutes were enough). The solid was rinsed twice with distilled water.

2.5- Phenol detection

2.5.1- UV-Vis phenol spectra

A first approach to the remediation system analysis by spectrophotometry was made by simply comparing the initial UV-Vis spectrum of phenol 60 ppm (Sigma-Aldrich Bioxtra >99.5% GC) in phosphate buffer pH 7 50 mM with the spectrum of a similar sample incubated with AbT for 10 minutes.

Phenol calibration lines before and after incubation with tyrosinase were done using 11 different phenol concentrations (0-200 ppm). UV-Vis spectra of all samples were acquired (after proper dilution to avoid absorbance values superior to 1) and absorbances at 2 wavelengths were selected to plot against the phenol concentration: 270 and 275 nm. The same procedure was applied to similar samples only different by being incubated with AbT in a concentration enough to conjugate with 1 nM of AuNP ([AbT]= 9 mg /mM AuNP designated as 1x from now on).

2.5.2- Standard addition – UV-Vis

A total 4.1 mL of reaction volume, 20 ppm phenol, phosphate buffer pH 7 50 mM with AbT 1x was prepared and incubated for 10 minutes. The reaction volume was then ultracentrifuged at 18514 G for 18 minutes using Amicon© Ultra4 (PALL) centrifugal filter Units-30 kDa cut-off to stop the reaction. The filtrated volume was diluted until a total of 8 mL in milliQ water. From that volume 945 uL were pipetted to 6 eppendorfs. Phenol was added from concentrations from 0 to 80 ppm and absorbance readings at 270 nm were taken.

2.5.3- Gas Chromatography

The phenol adsorption curve involved the preparation of a 10 ppm phenol solution distributed among enough aliquots to perform the adsorption, in gradually increasing times, under agitation, with the PDMS fiber and column injection. Eppendorf tubes (2 mL) were used to ensure total fiber immersion with a 3 mm long magnetic bar and rotations per minute set to 1100. It was used a TraceGC 2000 series (Thermo Finnigan) chromatographer with a FID (Flame Ionization Detector). The injection of the samples in the polar phase column (DBwax, 50 m x 0.32 mm; 0.50 µm film thickness) was splitless for 30 seconds ($T_{detector}$= 250 ºC; $T_{injector}$= 250 ºC); the carrier gas was H_2 (flow= 1.2 mL/min). The heating program used was: initial temperature of 50 ºC hold for 30 seconds, heating ramp at 6 ºC/min until 170 ºC, heating ramp at 10 ºC/min until 200 ºC, 5 minutes hold at 200 ºC. All areas were calculated using X-calibur

software. When possible, an automatic fit was requested, if not, a manual fit was employed. (Baseline window=500, area noise factor=1, peak noise factor=10)

The calibration curve for phenol was performed in triplicate using hexan-1-ol (≥99% Sigma-Aldrich) as internal standard.

Phenol reaction samples had to be efficiently inactivated before the fiber immersion and, to ensure this, strong acid addition was tried but quickly abandoned in favor of ultracentrifugation at 20817 G for 18 minutes using Amicon© Ultra4 (PALL) centrifugal filter Units of 30 kDa cut-off. Maximum velocity was used to rapidly concentrate BNC/free enzyme at the bottom of the tubes and 18 minutes were required to filter enough volume to use in GC.

2.6- Bioremediation systems

At the beginning of this dissertation three remediation systems were idealized: batch remediation followed by ultracentrifugation to isolate the catalyte from the remediated effluent, an immobilized petri dish batch system, and “plug-flow” using and adapted regular syringe.

Because of its simplicity, the ultrafiltration system was the one in which efforts were concentrated.

2.6.1- Ultracentrifugation recovery batch system

This system was evaluated by testing the effects of centrifugation upon BNC-MUA-AbT incubated with tyrosine and phenol. BNC were subject to different cycles of centrifugation (Fig. 27; Amicon Ultra-4 centrifugal unit 100 kDa cut-off(Millipore)], and between each one they were incubated with phenol for an hour or just left resting (for assays identified as “tyrosine”). After centrifugation (1699 G for 4 minutes), activity rate was measured by the Sigma protocol.

Figure 27- After 1 hour reaction, the BNC were ultracentrifuge, and recovered in the filter to be ressuspended and reused.

2.6.2- Immobilized petri dish batch system

Optical microscope slides existing in the laboratory were cut in approximately 26 mmx26 mm squares. 0.2 mL of chitosan (6 mg/mL in 0.5% acetic acid) were laid in the centre of each square. Given the high viscosity and the volume used, no overflow occurs. The slide was then rinsed with phosphate buffer pH 7 50 mM and milliQ water. To each square, 100 uL of free enzyme 1x and BNC-cit/MUA-AbT 1 nM in phosphate buffer pH 7 10 mM were deposited. Two other squares had no deposition and were left blank. All squares were then covered with 400 uL of chitosan equal to the previews one. Less than this volume is not enough to ensure full coverage, and therefore, entrapment. Rising with phosphate buffer pH 7 10 mM was repeated. All slides were stored at 4 ºC so that the hydrogel could gain consistency and fuse the bottom and top gels. A petri dish for each slide (Fig. 28) was set with 12 mL (volume needed for full submersion of the gel) of equivalent reaction mix purposed by Sigma in their activity protocol assay (phosphate buffer pH 7 18 mM, 0.3 mM tyrosine). The activity reaction started by depositing each square in the tyrosine solution. One of the black squares was left as a chitosan control and the other was used in a batch in which free enzyme was pipetted directly into the reaction solution. Stirring was effective at 500 rpm using a 2.5 cm long magnet centered in the dish. At regular time between 0 and 30 minutes, an aliquot from the reaction volume was taken and absorbance at 280 nm measured. After the reading it would be replaced in the reaction. Duplicates were made.

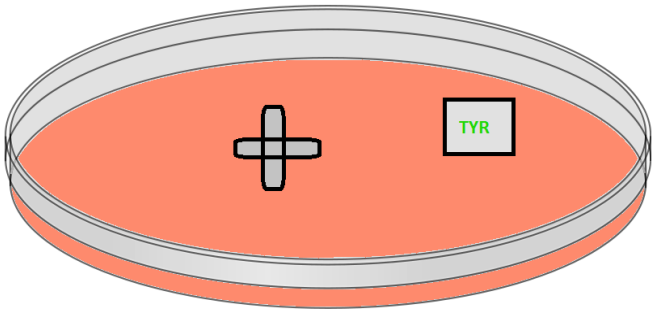

Figure 28- Petri dish containing a glass square with immobilized BNC/TYR immersed in a tyrosine solution, under agitation.

2.6.3- Plug-flow syringe

An operative module was designed using 25 mL syringe (Braun Injekt) parts. No needles take part in this setup. The emboli was retrieved from a syringe and cut according to Figure 29 (B). The cross section was cut to facilitate the confluence of the fluxes from each of the four paths and the concave plate was filled with holes. This part was inserted in another syringe as seen in Figure 29 (A).

In spite of not being tested, we propose this setup as an alternative that could be put to work by laying a tyrosinase containing gel (chitosan and/ or agarose) and them to push the substrate through, recovering the product in a vessel at the ending.

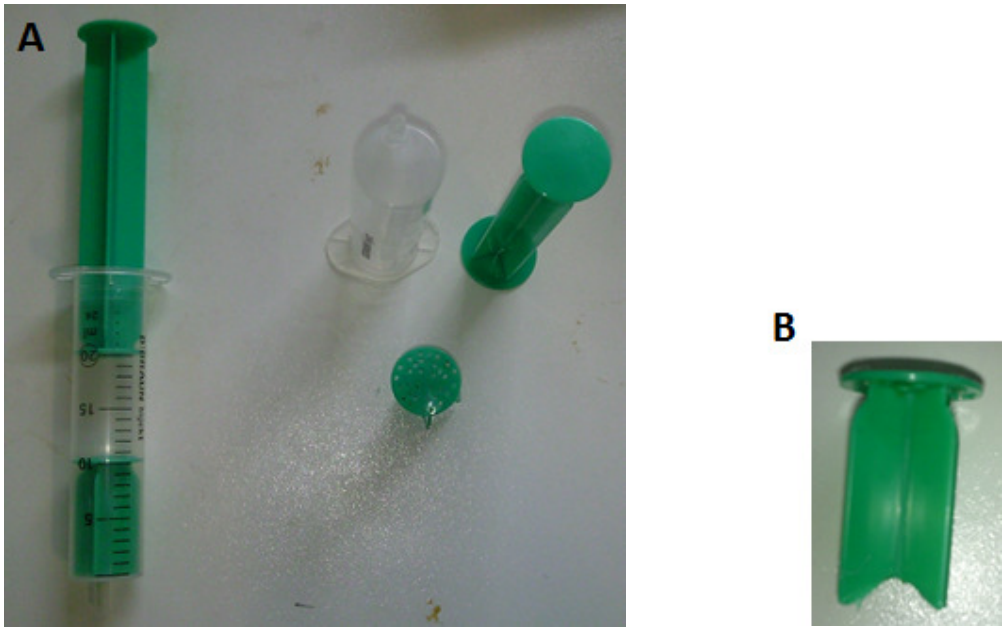

Figure 29- **A-** Assembled plug-flow module and its three different parts. **B-** Shaped emboli with perfurations on top.

3- Results and discussion

3.1- Bionanoconjugates preparation

Bioconjugation ratio is highly dependent on the nature and total amount of proteins in the solution. Previous work solely based on the expected activity[25], lack to acknowledge that impure extracts such as AbT have many variable impurities and that even when inactive TYR can be occupying AuNPs surface. Because of this, conjugation ratios already reported have to be questioned. Since that is not the main subject of this work, but it depends on an effective bionanoconjugation, a serious detour had to be made, by using a theoretical estimation model, zeta potential and electrophoresis to assess BNC proper conjugation ratio.

3.1.1- Protein concentration – BCA Assays

Three AbT commercial lots used during this dissertation were tested (Appendix II). The results are shown in Table 1. The three lots are consistent between each other and it can be concluded that, on average, only 62% of the solid extract sold commercially is proteic. This means that 62% of the weight consists in peptides and unspecified proteins from which an undetermined part was actually active AbT. Therefore, for this commercial extract, conjugation studies should be based on the total amount of protein.

Table 1- Protein content (wt/wt) in 3 commercial AbT (Sigma-Aldrich) lots.

Lot number	[Prot] (mg/mg extract)	
1	0.621	
2	0.576	
3	0.661	
Total	0.619±0.043	**62%**

The BCA assay was also used to test the commercial TrT solution (VVT, Finland). (Appendix II)

BCA assays performed on TrT often resulted in high standard deviations among replicates. This can indicate low homogeneity of the TrT aliquots or the occurrence of a precipitation process. According to Table 2, the lot has very high protein content and due to its production process (INTRODUCTION: 1.4.2- Structure of Tyrosinases), it can be expected a great TrT purity.

Table 2- Protein content (µg /mL) in the commercial TrT (VVT) lot.

Lot number	[Prot] µg/mL	
1	553	**92%**

For both tyrosinases, BCA assays could be also complemented with ICP- AES (Inductively Coupled Plasma Atomic Emission Spectroscopy) for copper atoms. Quantification of cooper would be valuable information for the precise quantification because each catalytic unit contains 2 cooper atoms.

3.1.2- Protein concentration – Activity determination

Sigma provided a total of three protocols to study AbT activity. All three were considered, but two of them were dependent on ascorbic acid (incompatible with AuNP testing) and presented less precision, so they were excluded for this work. In the remaining of the three, it was noted that the definition of catalytic unit in Sigma Activity protocol (Appendix I) was different from the recommended by the Nomenclature Committee of the International Union of Biochemistry.[70] Due to this and high variability in the activity results being obtained experimentally (face to the expected ones), all TYR lots were tested when purchased (Appendix III) according to the method declared by Sigma to acquire the lots labeled data (Appendix I).
The variations found between lots (Table 3) argue against the approach of developing AuNP conjugation according to enzyme activity: not only it appears as a highly variable parameter (function of lot and time), but, it is easily understandable that inactive TYR and unspecified proteins (see BCA assays data) can still bind to the AuNPs. These simple tests point out how misleading investigation can be when based on manufacture´s information, especially considering many reports on this area that take suppliers data for certain.

Table 3- Commercial AbT activity (U /mL). Total represents the results comparatively to labeled data.

Lot number	Act (U/mL)	TOTAL
1	10033	234%
2	16193	378%
3	3820	106%

TrT activity was also tested (Appendix III) using testing information from the supplier (VVT, Finland). Due to some changes undertaken to perform the testing conditions of the supplier (described in Matherial and methods), the activity variation found cannot be considered significant. (Table 4)

AbT activity intensity relative to the substrate L-Tyrosinase typically achieved with 200 µg of solid extract can be attained with less that 2 µL of the purchased TrT aliquot. This suggests that TrT was extremely pure and concentrated besides the intrinsic higher activity than AbT. (Fig. 21)

Table 4- Commercial TrT activity (nkatal). Total represents the results comparatively to labeled data.

Lot number	Act (nkatal)	
1	5530	**90%**

3.1.3- Capping agent- MUA

The reported MUA ratio for a complete Turkevich AuNP (as described) capping was 1 AuNP : 120 MUA (in molar).[25] During this work, the ratio was found to be incorrect and a new one was proposed by a colleague- 1:5000. The viability of this dissertation depended on the use of AuNP-MUA prepared adequately and, therefore, reproducible synthesis had to be ensured.

Moreover, the first activity tests using bionanoconjugates obtained from these 1:5000 AuNP:MUA were unsuccessful. Since bionanoconjugates activities with MUA capping had been reported[25], no suspicion has fallen upon the new ratio of 1:5000. However, since thiols are known to be tyrosinase inhibitors, a way to ensure the coverage while dismissing the leftover MUA in solution had to be found. The way was achieved by ultracentrifugation of the AuNP-MUA 1:5000. The pellet was isolated and then resuspended in milliQ water. UV-Vis spectra were made to search for AuNP aggregation evidence or method variation between batches, but no aggregation was found.(Fig. 30)

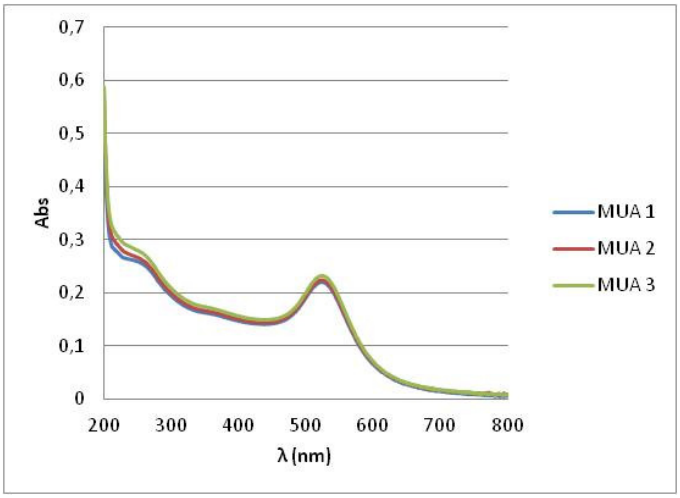

Figure 30- AuNP MUA 1:5000 produced by the new proposed method. Diluted 1:101 from the recovered pellets. NP concentration estimated between 130-137±4 nM; diameter: 11,74±0,04 nm.

The MUA conjugation with the AuNPs was also performed in a saline solution. MUA was dissolved in PBS solution prior to the AuNP addition enabling a visual comparison between the capping kinetics competing against the aggregation kinetics. (Fig. 31)

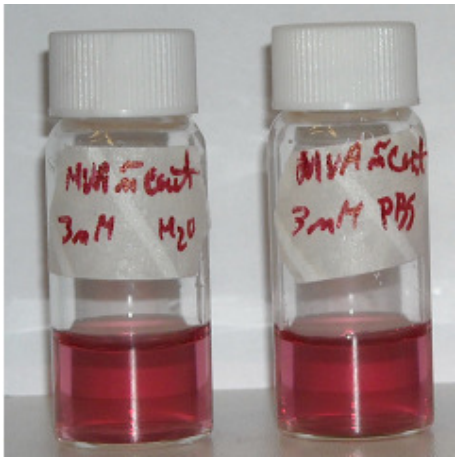

Figure 31– AuNP-MUA 1:5000 3 nM non ultracentrifuged. In order: non-centrifuged NP in water, and phosphate buffer saline.

This data suggests that MUA capping kinetics is faster than aggregation kinetics of AuNPs while in ionic strengths corresponding up to 139 mM.

The aggregation study with sodium chloride, showed a typical plasmonic behavior for AuNP. (Fig. 32)

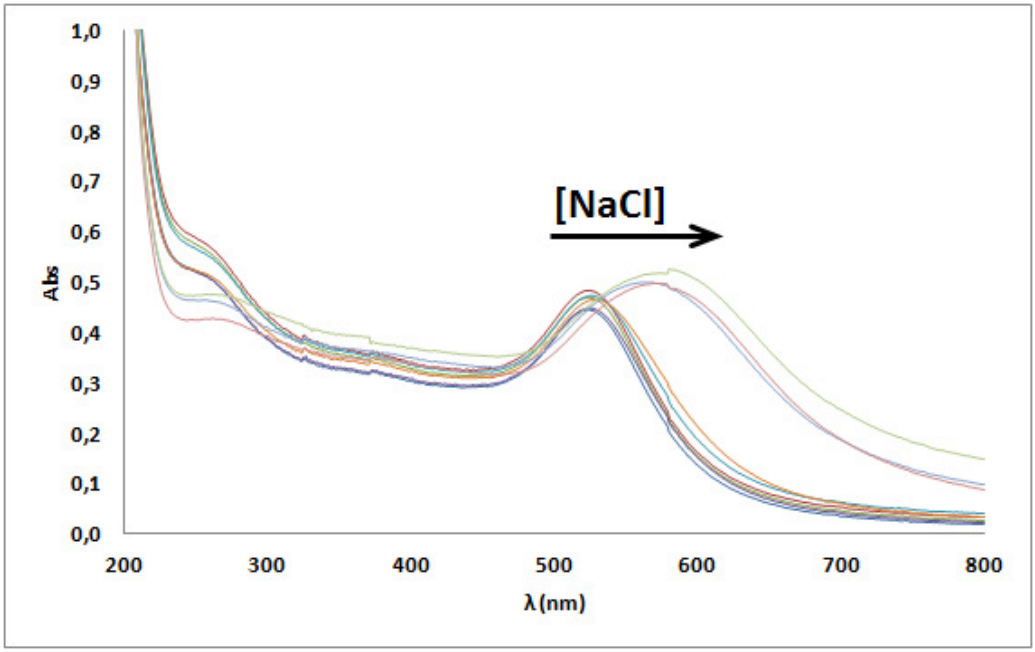

Figure 32–UV-Vis spectra for ultracentrifuged AuNP-MUA 1:5000.

Aggregation status can be evaluated by the Abs600nm/Abs 520nm ratio. (Fig. 33)

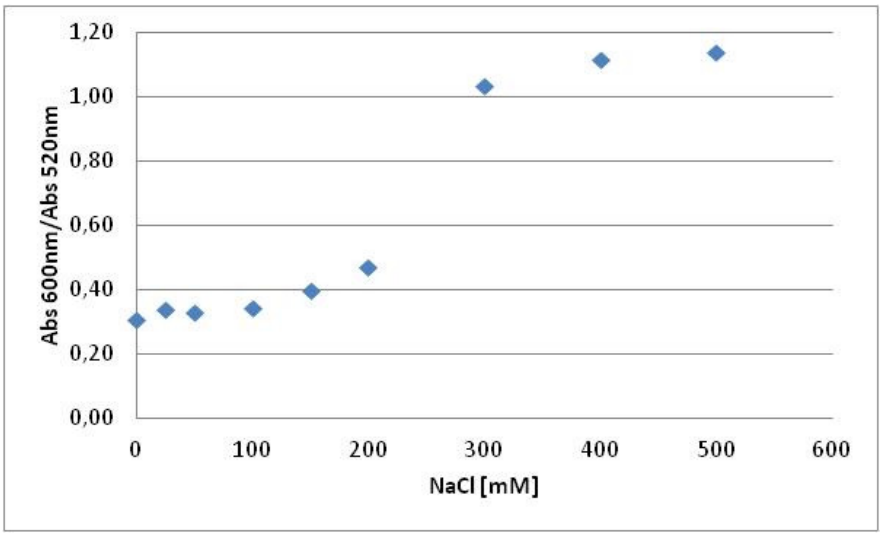

Figure 33– Abs600 nm/Abs 520 nm ratio for ultracentrifuged AuNP-MUA 1:5000.

A ratio of near 0.35 was maintained up to 100 mM of NaCl whereas an inflection starts indicating that aggregation was initiating for NaCl concentration. Regarding this data, ultracentrifudge AuNP-MUA 1:5000 samples showed stability seems to be stable until an ionic strength corresponding to 100 mM NaCl.

3.1.5- Enzyme conjugation ratio

After preparing suitable AuNP-MUA the next step was their conjugation with TYR. Surprisingly, no theoretical model was found in the literature to estimate the number of (bio)molecules a NP can contain around it in a monolayer. Since a tool like this was missing in our investigation group and validation criterion was needed to criticize experimental data acquired in this work, a method is thereby proposed as follows.

Knowing the diameter of the spherical AuNP with the capping, the surface area can be calculated. If the conjugated protein is globular, the problem can be resumed to the following: how many spheres (approximate) can fit around a single spherical NP?

Firstly the diameter of the covering spheres must be known. AbT structure was published only very recently, while for TrT none is yet available. Considering this as a recurring difficulty, it is needed a way to estimate the diameter of unfamiliar proteins is necessary. Considering globular proteins[32a], the problem is fairly easy to solve. From the literature it was possible to collect and correlate diameter and molecular weight of a known protein. Applying a tenth base logarithm, a good correlation was found.(Fig. 34)

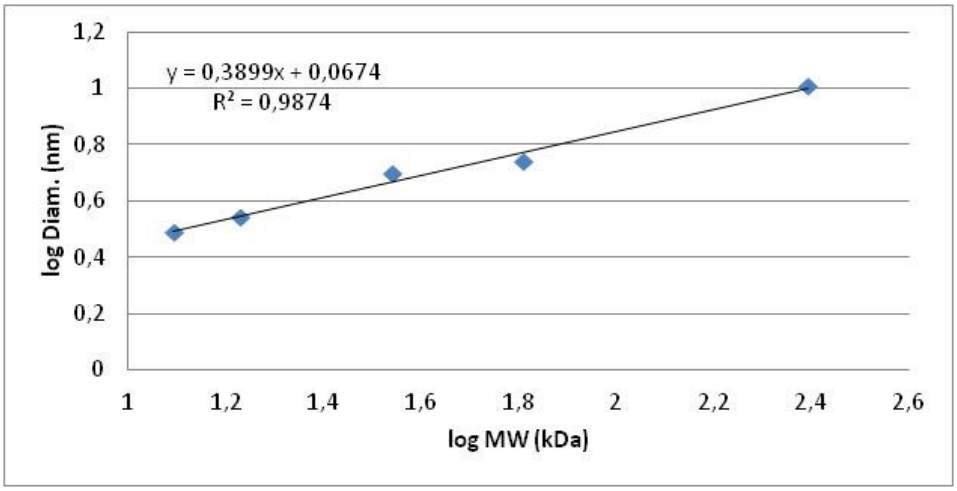

Figure 34**–** Correlation between experimental globular protein diameters and molecular weight. Data from (from least to most heavy): cytochrome C; myoglobin; insulin hexamer; hemoglobin; catalase.

Using this correlation a diameter of 7.6 nm was estimated for AbT and 5.1 nm for TrT. Meanwhile, an online tool (http://www.calctool.org/CALC/prof/bio/protein_size) was found which accomplished this same purpose using the same principle used by us: correlation between empirical results of several model proteins and enzymes. Now the estimated diameter was 6.9nm for AbT and 4.9 nm for TrT. Since the online tool must be based on a more extensive database it was decided to use its estimates.

Our propose uses the Thomson´s Model. It has long been applied to describe electrons arrangement and energy states around atoms. It is based on the principle that the electrons on the surface of an atom rearrange according to the most stable configuration. That implies electron maximum mutual distance because they all are negatively charged. Proteins have a characteristic isoelectric point and that determines if their global charge is positive or negative. Either way, since all are equally charged they tend to repulse each other.

For the bionanoconjugation purpose, the optimal coverage can be considered achieved when a NP has a single compact monolayer, meaning they are so close that they are in touch and the angle between two proteins is minimum.

Solutions to the Thomson´s Problem are presented in form of tables presenting the configurations of smallest known energy for N electrons. Given a N number of electrons, the symmetry was predicted so that the angle between them is maximized. Taking a protein in consideration, the process can be though in reverse: given the smallest angle separating each enzyme, what is the corresponding N number of proteins. The smallest angle is exactly the one made by two protein centres and the core of the NP, and it can be estimated using the circular arc (Fig. 35).

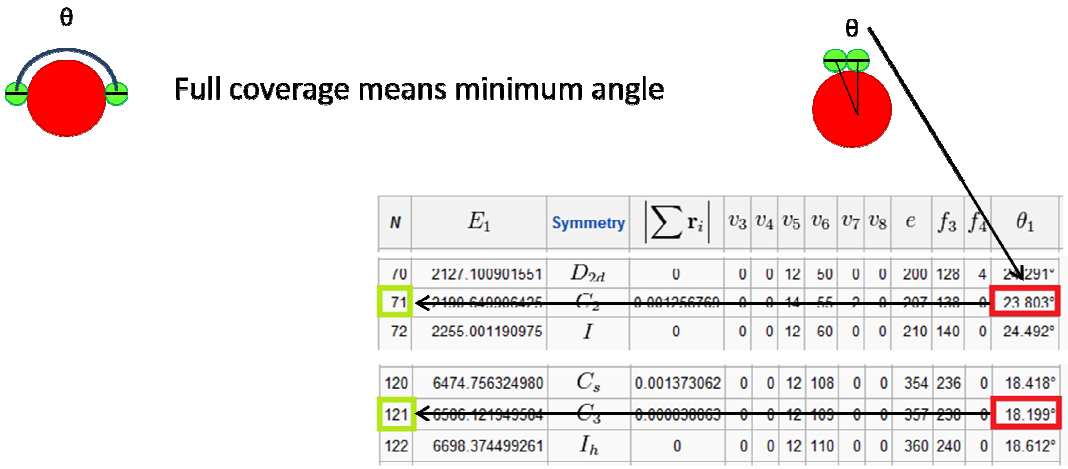

N	E_1	Symmetry	$\left\|\sum \mathbf{r}_i\right\|$	v_3	v_4	v_5	v_6	v_7	v_8	e	f_3	f_4	θ_1
70	2127.100901551	D_{2d}	0	0	0	12	50	0	0	200	128	4	24.291°
71	2190.649006425	C_2	0.001256769	0	0	14	55	2	0	207	138	0	23.803°
72	2255.001190975	I	0	0	0	12	60	0	0	210	140	0	24.492°
120	6474.756324980	C_s	0.001373062	0	0	12	108	0	0	354	236	0	18.418°
121	6566.121949584	C_3	0.000030063	0	0	12	109	0	0	357	238	0	18.199°
122	6698.374499261	I_h	0	0	0	12	110	0	0	360	240	0	18.612°

Figure 35– Thomson´s Model approach to estimate AuNP maximum protein coverage. The minimum angle (red frame) is calculated and then tables for Thomson´s problem are used to find the maximum N (number of surface elements)

Using the described process, we estimate that each 12 nm AuNP can be covered with 71 AbT or 121 TrT to form a full monolayer. From a practical point o view, it was expected much more agreement using TrT because it is more pure and AbT has other forms in solution than just the native tetrameric form.

Agarose gel electrophoresis

The electroforetic mobility of the BNC depends on the size and charge of the complexed particle. The less conjugated is a particle, the more negative charge it will be exposed and more extensive will be the migration from the negative (starting point) to the positive pole. When the NP is completely covered, it is achieved the maximum neutralization of the NP negative charge and superior TrT concentrations should not cause the BNC to migrate even slower.

The observed smearing is due to the photo just being taken one day later. Since the gel was left in the running buffer to prevent hydration, the bands lost resolution.(Fig. 36)

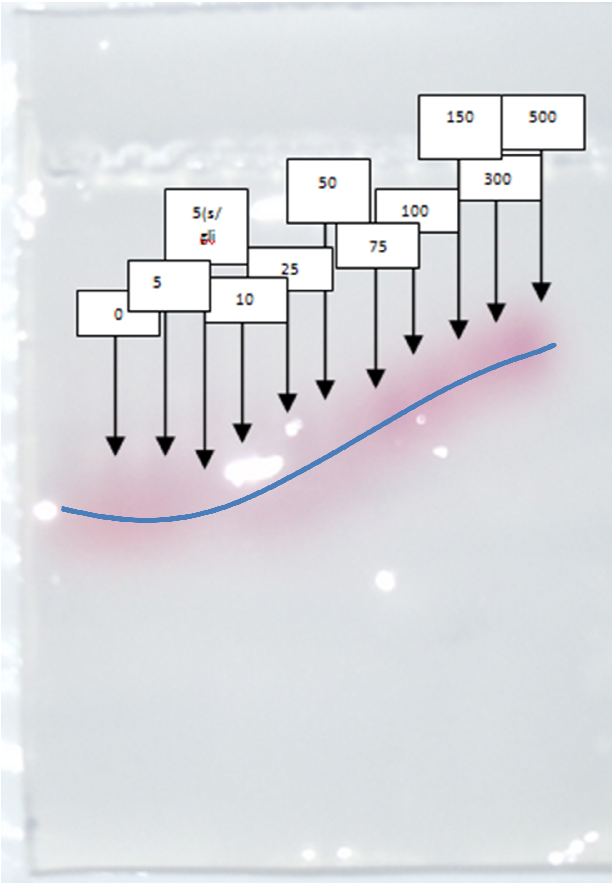

Figure 36– Agarose gel electrophoresis of AuNP-MUA incubated with progressively higher TrT concentrations. Values indicated are in nanomolar. Third sample was deposited without glycine.

To better perceive the results from this gel, a graphic of relative mobility was made as follows. (Fig. 37) Mobility has a linear behavior until about 100 nM Trt: 1 nM AuNP indicating that the tyrosinase monolayer is being formed. To higher enzyme concentrations, the surface is apparently full and the shielding effect upon the AuNPs is at his maximum and mobility suffers no more reductions.

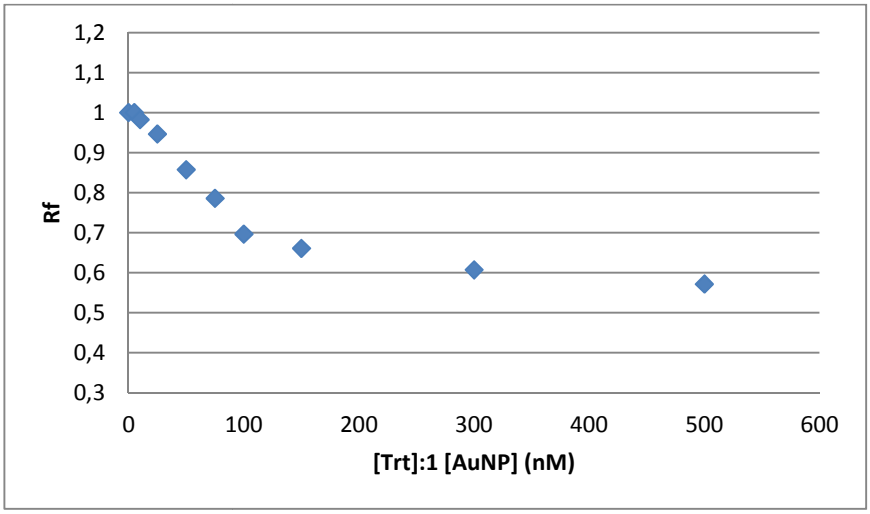

Figure 37– Relative mobility (Rf) for each BNC (TrT) band in the agarose electrophoresis gel.

Zeta potential

Zeta potential measurements were also made to study the BNC solution population and to find a correlation between zeta potential and conjugation ratio. A correspondence between agarose mobility and zeta potential results were expected since both methods are a result of the electroforetic mobility of the species in the solution (study showing the correlation between both methods is yet to be published by our group).

Zeta potential readings can the acquired through General or Mononodal modes. Mononodal only delivers one mean value to the whole solution. During the readings in General mode, samples are subject to a higher current for a fair amount of time and there is the possibility of the enzyme to unbind, nevertheless, the Mononodal mode revealed to be insufficient to follow the BNC zeta potential population peak. Hydrogen potential for the samples was in the range 9.10-9.14 and 8.91-8.96, respectively before and after the zeta potential measurements, indicating the solution remained stable during testing.

There are three main populations expected to exist in a BNC solution: unconjugated AuNPs; free enzyme and BCNs. Figure 38, complemented by Table 5, illustrate the three expected peaks: (from more to less negative) AuNP (-43 mV), BNC (-27 mV), free enzyme (-0.8 mV).

Table 5- Zeta potential data (General Purpose method) for a BNC sample with suboptimal TrT concentration (1:50).

			Mean (mV)	Area (%)	Width (mV)
Zeta Potential (mV):	-48,5	Peak 1:	-51,6	51,6	12,0
Zeta Deviation (mV):	38,3	Peak 2:	-26,2	28,5	5,95
Conductivity (mS/cm):	1,06	Peak 3:	-10,4	15,3	5,19

Result quality : See result quality report

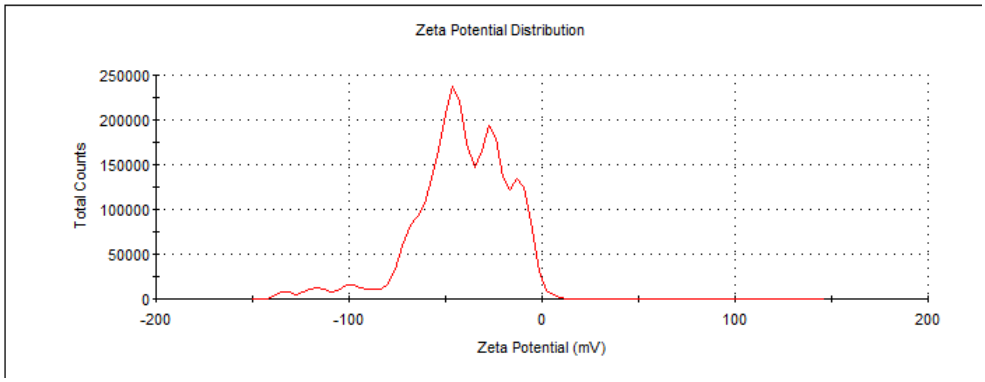

Figure 38– Zeta Potential profile (General Purpose method) for a BNC sample with suboptimal TrT concentration (1:50).

AuNPs are characterized by a negative zeta potential, which is the superficial charge at the hydration sphere. Increasing TrT concentration, more enzymes will be shielding the AuNP charge and it is expected a shift of the BNC peak to more positive zeta potential values, while the surrounding peaks disappear. Figure 39 expresses the results obtained for the BNC peak.

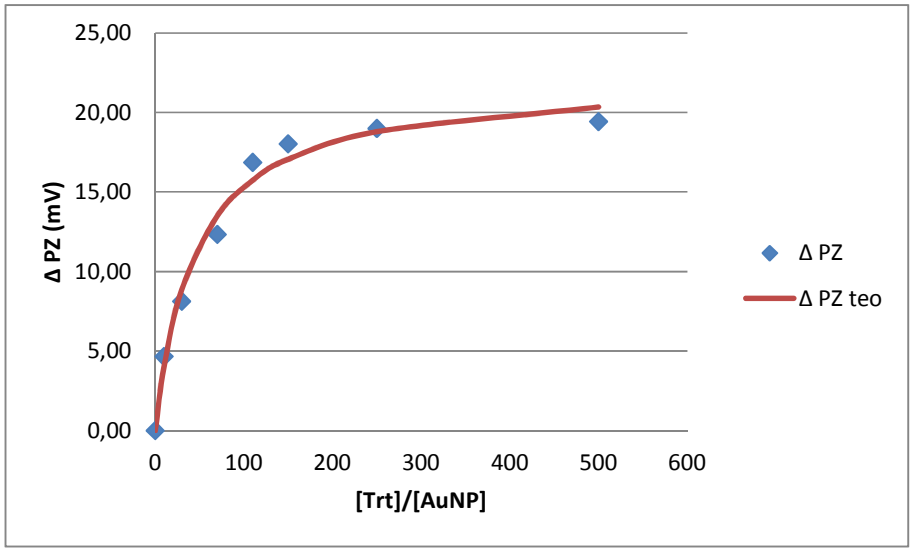

Figure 39– Zeta Potencial variation for TrT conjugation with AuNP. Conjugation at pH 7 followed by a change to pH 9. The red line corresponds to the theoretical adjustment of the data.

A good fit for a Langmuir like curve [$\Delta\zeta = (\Delta\zeta Max \,.\, KL \,.\, R) / (1 + KL \,.\, R)$] was obtained and the parameters K_L-Constant for the ligation of the protein (0.0223) and ΔζMax- Zeta potential maximum variation (22.12) were extracted. R is the variable [TrT].

The above graphic shows the formation of a plateau starting close to the experimental point [Trt]=110 nM. To achieve a more objective conclusion in pinpointing the maximum surface coverage, two criteria can be enounced, both by admitting the existence of two distinct regions: the first region attributed to the BNC population increase and the second attributed to a plateau where few or none BNC is being formed. The transition between both regions is progressive and can be interpreted as the change of the order of the reaction as new equilibriums are created by the use of different concentration of reagents. Considering the limits, the first region is described in the form of $\Delta\zeta = mx$ (first order reaction) and the second by $\Delta\zeta = \Delta\zeta Max$ (blue lines in Fig. 40). This kind of conceptualization can be used to avoid taking conclusions from the intermediate curved zone. In this work, it was chosen to intersect two lines extrapolated from the experimental points in each region (green lines in Fig. 40). From this criterion, 120 nM of TrT is indicated to be the maximum coverage, but there is a clear need for more points to define the lines. Nevertheless, this result is in accordance with the predicted by the Thomson´s Model and agarose migration assay.

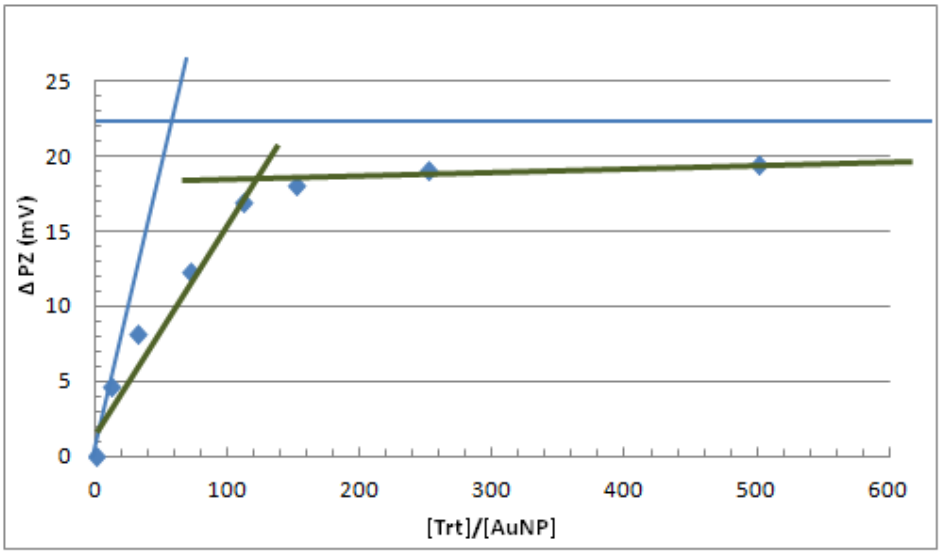

Figure 40– Zeta Potential variation for TrT conjugation with AuNP. Blue lines: Δζ = mx; Δζ = ΔζMax. Green lines: extrapolated lines from plateau and BNC growing zone.

The conjugation time was a doubt also present in this work since in the conjugation of AuNP with other proteins overnight was found to be insufficient. For AbT, overnight is an adequate conjugation time (not published by the group). For TrT, the potential zeta results are not sufficient to discredit the use of the overnight period because, the BNC peak is stable for several days. After that the BNCs might have started to precipitate or the enzyme floculating approaching the BNC peak behavior to the enzymatic one.(Fig. 41)

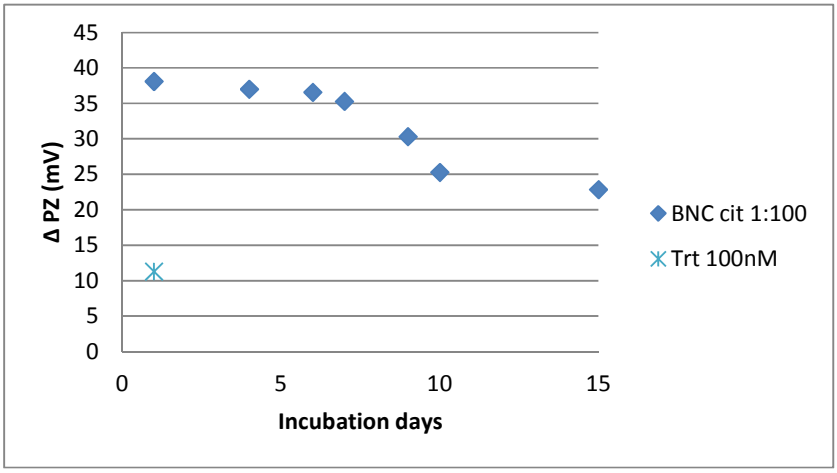

Figure 41– Zeta Potential peak shift for BNC peak as function of passing days since conjugation with 100 nM TrT was started.

Previous work in the laboratory group, indicated the ideal conjugation ratio for TrT has 100 nM/ 1 nM AuNP. The evidence collected here thought the electrophoresis and potential zeta support it. In conclusion, this was the optimal rate found to apply TrT BNC. A greater TrT

concentration would leave more free enzyme in solution that could be lost in the application (TrT is expensive), mask the BNC performance or even start the formation of a second covering layer which would block the enzyme beneath; so, for that matter, even a suboptimal ratio is advisable.

As for AbT conjugation ratio, results yet to be published from a laboratory colleague, suggest that the optimal coverage ratio AuNP- AbT is 9 mg : 1 mM AuNP. This results are concordant (surprisingly due to the impurity of the AbT extract) with the theoretical estimation described in this dissertation (8.52 mg:1 mM AuNP) so it was the ratio used to follow the work.

3.2- TYR activity as ionic strength function

While working with BNCs it is extremely important to bear in mind that they are very sensitive to aggregation factors. Ionic strength is one of the most problematic and since it has to be controlled, it was essential to know if it would have any effect on the enzyme activity. Obtained results are resumed in figure 42.

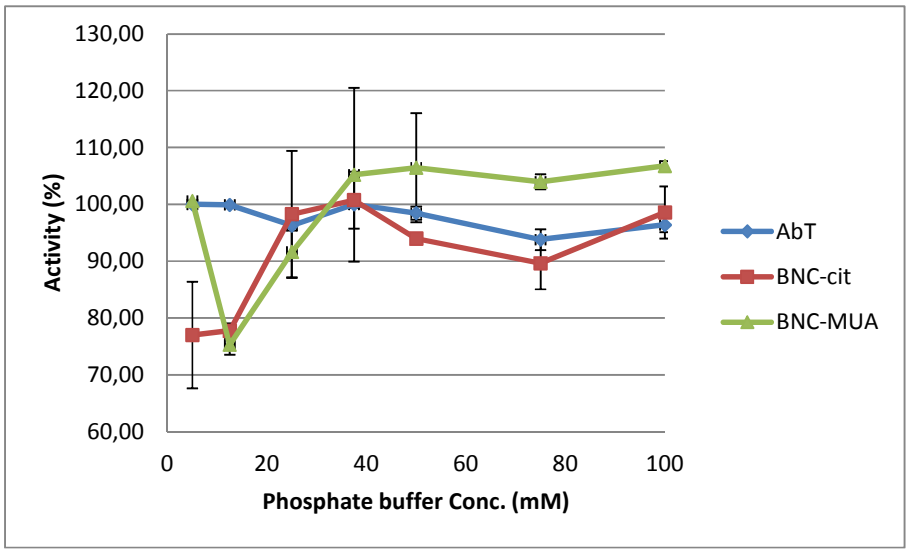

Figure 42– AbT and TrT activity rates at different ionic strengths. (100%= max act)

Sigma activity assay is performed at 18 mM phosphate buffer, equivalent to 78 mM ionic strength. In the tested range, for free enzyme, this parameter seems not to influence AbT activity significantly. A design fault occurred with this assay: all BNC were prepared in the respective buffers resulting in visible aggregation starting from 25 mM buffer samples. All BNC should have been prepared at 10 mM buffer concentration and just the added a stronger buffer, by this way avoiding aggregation effects.

Nevertheless, some conclusions can be stated: aggregation at the tested range does not cause an abrupt decay of the activity; BNC (citrate capping) behave similarly to the free enzyme and no correlation to the buffer concentration could be instated; BNC (MUA capping) also have an activity level comparable to the free enzyme but the general slight increase verified should not be dismissed.

This experience together with AuNP-MUA greater stability makes BNC-MUA the better choice to explore in a remediation system. Moreover, even if the effluents being treated cause some aggregation, it is now proved that catalysis will not be especially affected.

3.3- Chitosan preparation

Two of the three remediation systems proposed in this dissertation were dependent on the use of a support permeable material to hold the enzyme. Chitosan and agarose are hydrogels commonly used in laboratory, extensively studied and their low price encouraged their use, however chitosan hydrogels/dry films preparation presented as a much more difficult task than predicted. The main conclusions are now described.

Chitosan concentrations were tested within the 2-10 mg/mL range. The higher concentrations of 8 and 10 mg/mL are too viscous to be pipetable: 2 mg/mL solutions took much time to dry and generated fragile hydrogels. Intermediate concentrations of 4 and 6 mg/mL were viscous enough to generate resistant hydrogels and thick dry films. The 6 mg/mL was preferred in this study because its drying times were shorter.

To produce a dry film (Fig. 43) by evaporation of the solvent (acetic acid) the required time was superior to a full week even at a hotte. Besides time consuming, dry films cannot be used to trap enzymes and difficult mass transfers in the enzyme vicinity. Due to these, dry films approach was considered to be only viable to be applied in a remediation batch system in which the physical limits are covered by the films or in which the undergoing treatment solution is being circulated through those kinds of films to retain *o*-quinones as described in the literature.[71]

Rinsing with phosphate buffer stronger than 10 mM and especially with NaOH solutions originated white crystals in the produced dry films. Realizing this implies that all rinsing in gels-to-be-dried should be made with distilled water or phosphate buffer as strong as 10 mM. If enzyme entrapment is possible this becomes even more important.

Drying of the beads obtained by Method II (described in Material and methods) resulted in beads fusion to a unique paste, while the storage of them in humid state enabled one week storage at 4 ºC and successful consecutive resuspensions. AuNP-MUA added to the liquid agitated chitosan solution equally originated beads soft pink coloured indicating that none or little aggregation occurred (Fig. 44). Efforts to enclose BNCs were unsuccessful because even with only 0.5% acetic acid the solution pH was bellow to 1.

Chitosan-agarose composite hydrogels were unable to be produced in spite all trying to reproduce described conditions in the literature.[72] Changes to cooling conditions, in acid acetic concentration, and rinsing agent were carried out but none of them was successful.

Chitosan beads entrapped in agarose by Method III (Fig. 45) resulted in well defined and dispersed beads, close to the agarose matrix surface. This means that the method should only be applied to thin matrixes.

In spite all this effort, chitosan application in phenol remediation was not possible in this dissertation due to lack of time.

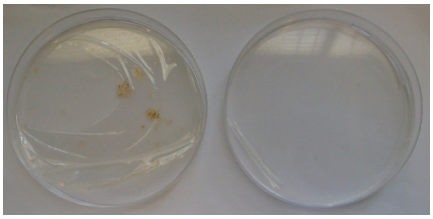

Figure 43– Chitosan (6 mg/mL) dry films. (Brown residue is a contamination)

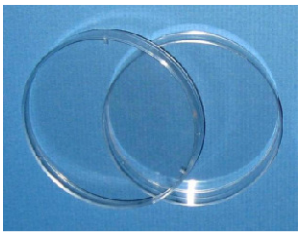

Figure 44– AuNP-MUA 1 nM entrapped within chitosan beads (6 mg/mL in acetic acid).

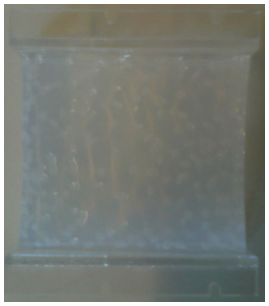

Figure 45 – Chitosan (6 mg/mL) beads entrapped in an agarose matrix (0.5%).

3.4- Phenol detection

3.4.1- UV-Vis phenol spectra

A preliminary analyses of the remediation system was simply made by incubating the AbT with phenol 60 ppm for 10 minutes.(Fig. 46)

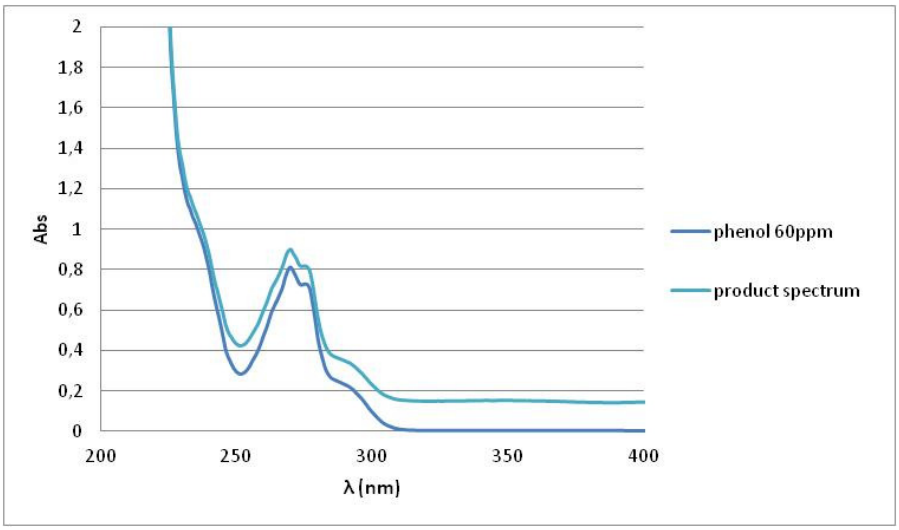

Figure 46– UV-Vis spectra of 60 ppm at pH 7 (phosphate buffer 50 mM), before (dark blue) and after (light blue) incubation with AbT for 10 minutes.

The system spectra show high absorbance in the 250-300 nm region. Either way, the phenol quantification method (intensively employed in most phenol bioremediation papers) uses an absorbance calibration line has shown in Figure 47.

Calibration lines are a good way to evaluate samples free of contaminants and phenol offers two wavelengths to perform it, from which 275 nm enables more sensitivity.

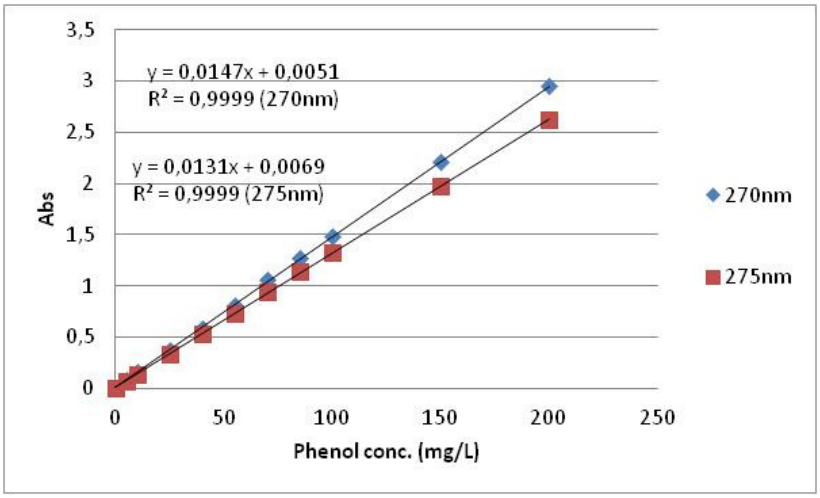

Figure 47– Phenol calibration lines using phenol characteristic peak wavelengths. (1 mg/L ≈ 1 ppm phenol)

The application of the same calibration lines to reaction mixtures with the same phenol concentration range as used in figure 47 did not prove to be so accurate.(Fig.48)

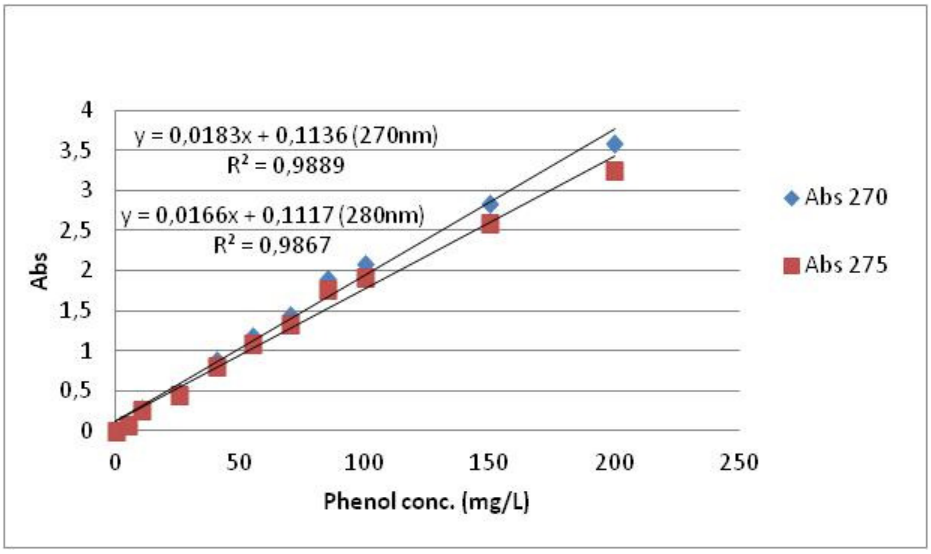

Figure 48– Phenol absorbance at characteristic peak wavelengths after AbT addition (10 minutes of reaction). (1 mg/L ≈ 1 ppm phenol)

Comparing figures 47 and 48 (Abs 270 overlaid in Fig. 49), data correlation has decreased and it can be conclude that the method provides no more than a roughly estimate for phenol concentration and tends to increase its estimation error as the reaction goes on, mainly because tyrosinase activity generates many aromatic compounds with high absorbance near 280 nm (dopachrome to name one).

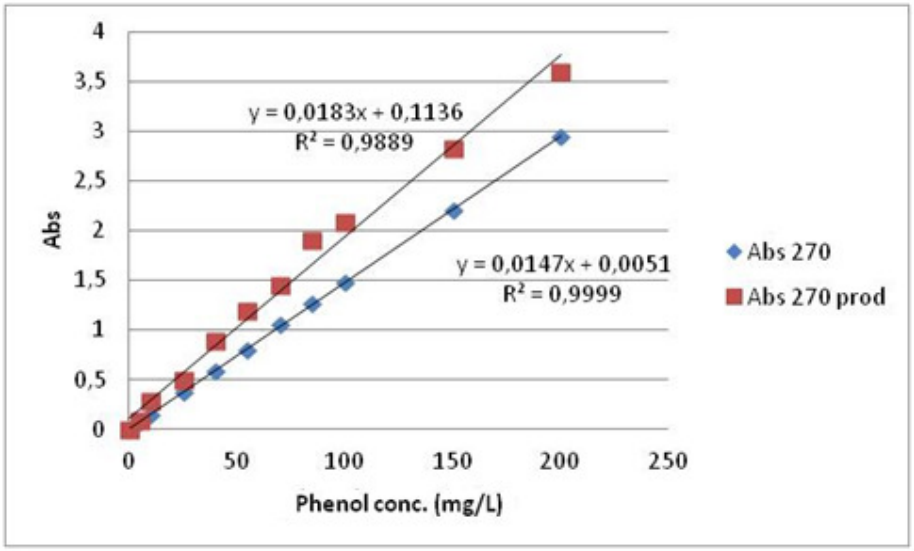

Figure 49– Calibration line for phenol standards (0minutes reaction) and the same concentrations after 10 minutes incubation with AbT.

3.4.2- Standard addition – UV-Vis

This method was used to verify its viability when using TYR treated samples. Only a simple test was carried out but it showed that the reaction occurred and the remaining substrate could be measured even under 10 ppm amounts. The estimated phenol concentration present in the aliquots used in the standard addition method, if no reaction had taken place, should be 9 ppm. However, the intersection of the linear regression (Fig. 50) with the ordinate axis estimated the present phenol as 6.4 ppm, indicating that it was consumed by AbT.

Replicate samples should be tested in parallel using both this method and GC to cross results and better access each method performance. Nevertheless, this is a proved solid method for samples with complex matrixes, as long as the reaction is effectively stopped because its takes some time to analyze. The centrifugation period is very significant considering the reaction time period which can induce a significant error, still, centrifugation is a clean and efficient method for reaction halting. Sigma activity tests regarding the filtrate revealed no activity, indicating no active enzyme was being released to the filtrate.

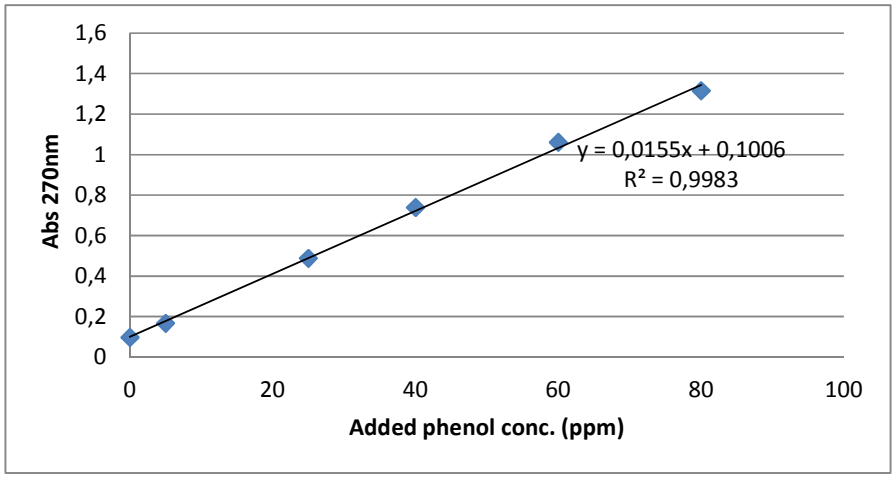

Figure 50– Standard addition method applied for a 20 ppm phenol solution incubated with AbT 1x.

2.4.3- Gas Chromatography

Before initiate GC phenol quantification, a study to determine the optimum fiber exposition time period to the sample was performed. A curve was obtained, where for the same phenol concentrations, different exposition time periods were assayed (Fig. 51). (Appendix V)

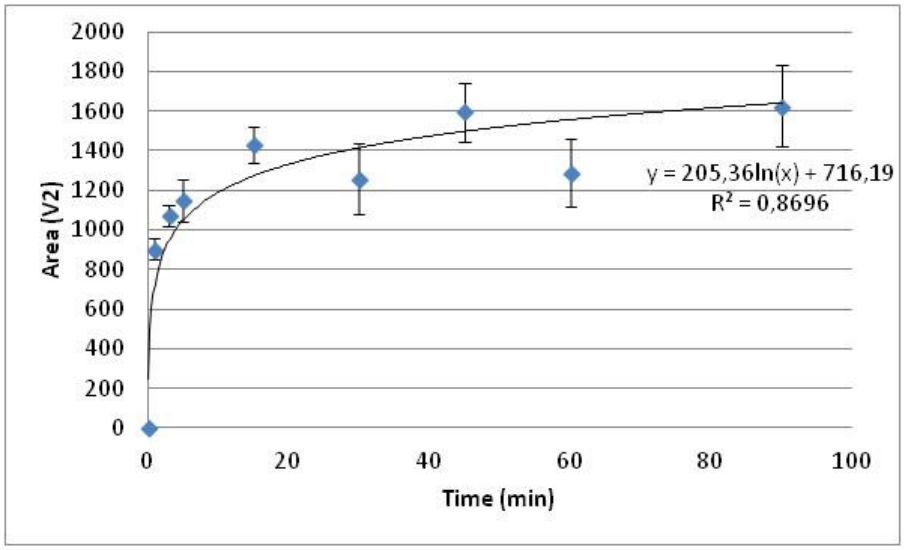

Figure 51– Phenol adsorption curve obtained after representing the exposition time vs phenol area.

The results suggest that phenol maximum absorption by the PDMS fiber reaches equilibrium close to 40 minutes of immersion and, therefore, samples and concentration calibration standards were all injected in the column after 40 minutes immersion of the fiber. A calibration curve was obtained using 40 minutes of immersion (Fig. 52).

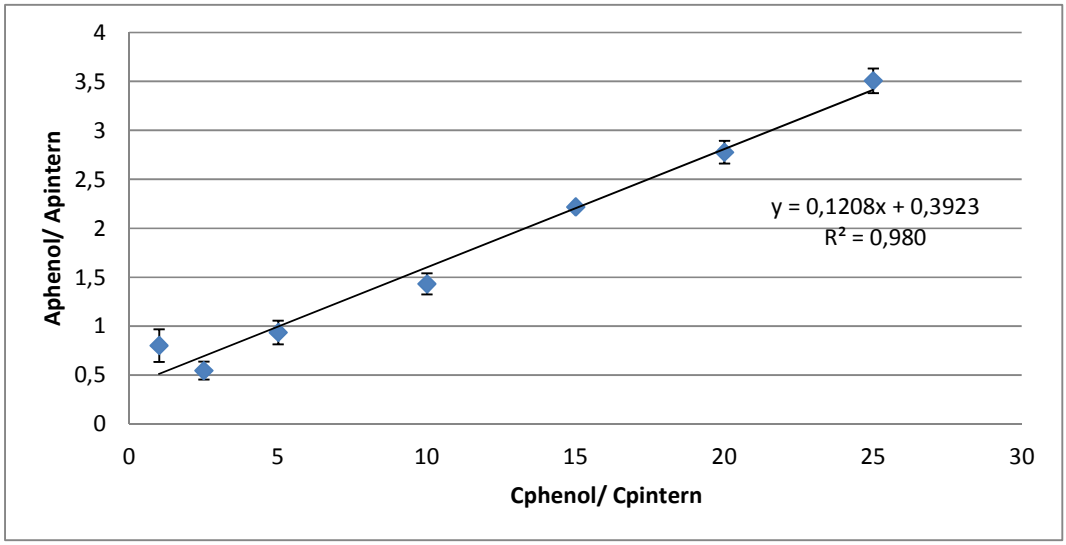

Figure 52– Calibration line for phenol concentration using hexan-1-ol as internal standard.

For a matter of availability in the laboratory, hexan-1-ol was used has internal standard (hexan-1-ol GC peak in Appendix V). An internal standard is a compound that is inert to the analyte, mixed with the samples before adsorption, with known concentration and that suffers all treatments along with the sample to analyze. This way, operational errors are discarded.

While testing real samples with dispersed enzyme in the solution (9 mg AbT:1 mmol AuNP-MUA), the reaction has to be stopped before the exposition of the sample to the fiber during 40 minutes for adsorption.

Two incubation experiences were made and the results are as follow. (Fig. 53) In the first data set, the 20 minutes incubation period point has an undetermined error because the starting, and therefore maximum, phenol concentration is 100 ppm. Few conclusions can be made from these sets of data because replicates are needed and a wider time range should be tested to understand the reaction rate profile. The data suggests that, after 60 minutes of incubation, at least 50% of phenol conversion is achieved. Then again, the disparity between sets indicates the already mentioned high variability in AbT activity.

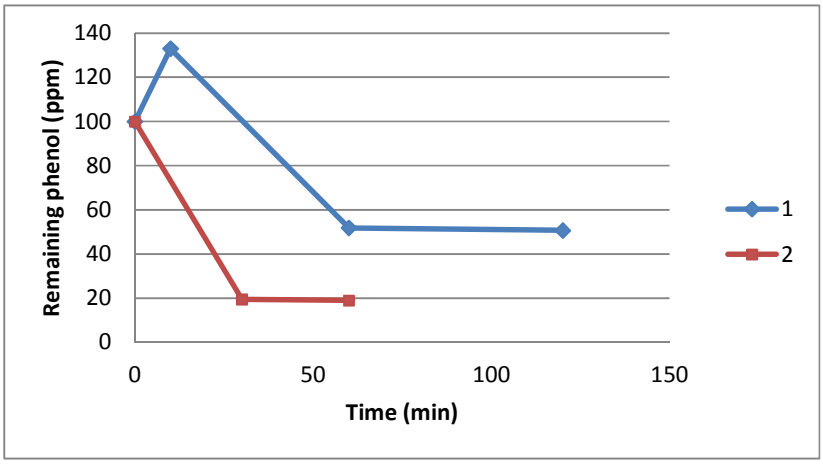

Figure 53– Phenol remaining in two sets of experiments, after incubation of 100 ppm phenol pH 7 solutions with AbT.

3.5- Remediation systems

3.5.1- Ultracentrifugation recovery batch system

This remediation system was intended to enable the reuse of the enzyme with reasonable activity retained for, at, least, 3 cycles long. In this dissertation we proposed and tested a simple design but much more room for improvement remains.

The major obstacle to the viability of this system is the recuperation of the enzyme by centrifugation. As can be observed in the Figure 54, it is notorious the accentuate decrease in activity caused by centrifugation. Since it happened also when no incubation with phenol existed, then the effect can be credited to the centrifugation process.

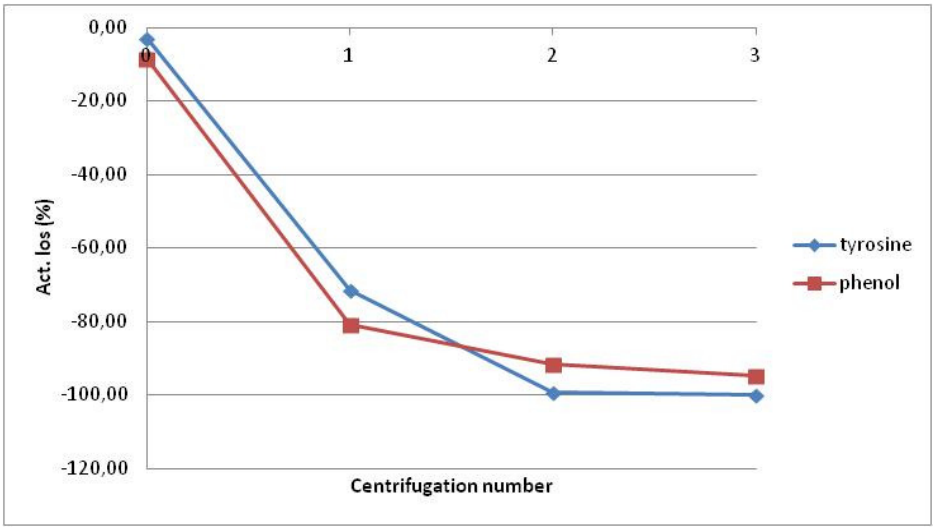

Figure 54– Ultracentrifugation recovery batch system activity performance.

Using 1699 G/ 4 min to test the system proved to be too much for the BNC-MUA to withstand occurring washing-out of the AbT. This issue was addressed by trying to optimize the rotation velocity in function of the filtered volume and retained activity (Appendix IV- Fig. 71, 72). Preliminary results indicate that a reduced centrifugation force could lead to lower loss of activity with additional cycles. Unfortunately, this could not be applied to this system due to lack of time.

Another factor that casted its attention was the duration of the phase lag by the Sigma activity protocol. As can be seen in Figure 55, initial incubation with phenol seems to have the effect of promoting the activation of the enzyme. Lag phase time is a subjective parameter but in this study it was calculated by intercepting a line that defines the plateau at the beginning of the reaction with the line that can be drawn from the maximum velocity region of the reaction.

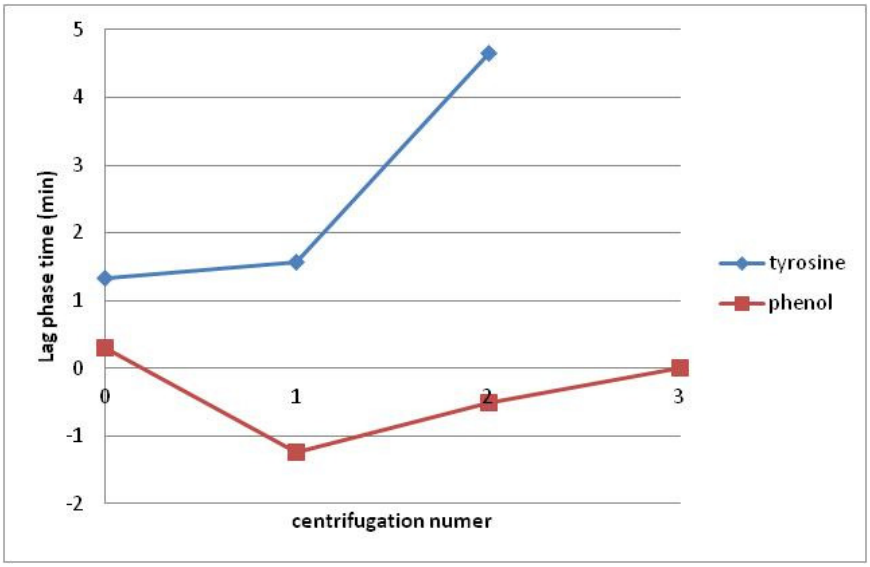

Figure 55– Lag phase time calculated for centrifuged samples at 1699 G.

Then again, replicates to atone these findings are required. It can be added that the same study should be completed by usind different centrifugation forces and the effects over catecholase activity also tested by using, for instance, L-DOPA. In this way (confirmed the existence of the activation effect) it could be atributed to the cresolase and/ or to the catecholase activities.

The filtered volume from the tyrosine set of points was also tested fo the activity rate. (Fig. 56)

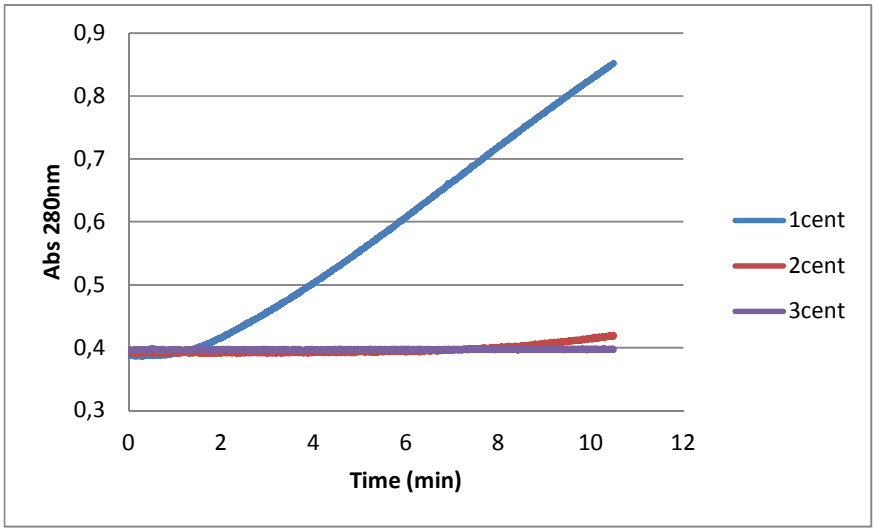

Figure 56– Reaction profile of filtered BNC-MUA at 1699 G.

Comparing the filtered and non-filtered activities at the first centrifugation, the reaction rate of the filtered was twice (202%) as the other, which implyes that most conjugated enzyme was lost in the first centrifugation. The sum of the activities from both fration (filetered and non-filtered) was 88% of the BNC-MUA activity recorded before a centrifugation step.

3.5.2- Immobilized petri dish batch system

Absorbance readings from the petri dish system revealed reduced activity for the immobilized enzyme when comparing to the free enzyme form. (Fig. 57)

Despite the significant differences, it must be considered that little enzyme quantity was employed when accounting for the 12 mL of reaction used: all reactions in this dissertation were performed with the same amount of enzyme usually in 1mL of total reaction volume.

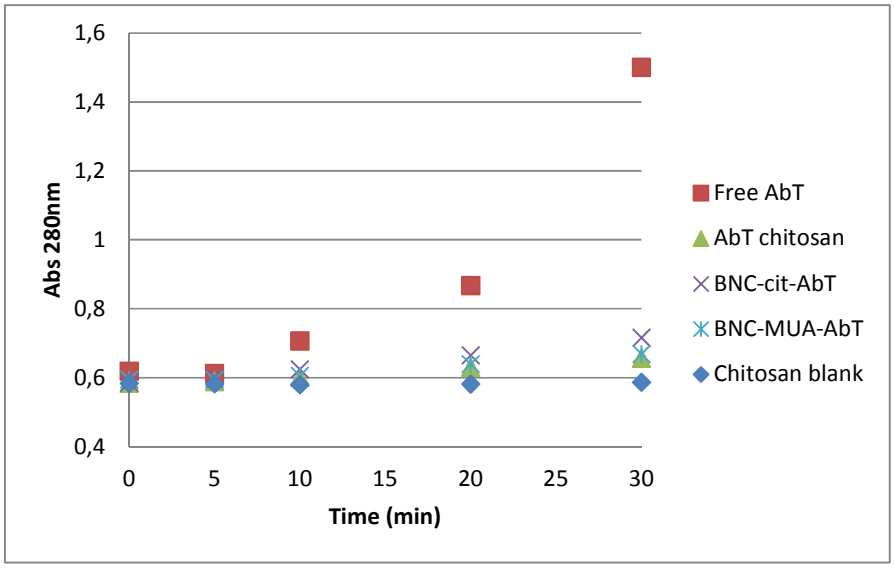

Figure 57 **–** Chitosan immobilized petri dish batch system reaction progress.

Visually, it was noticeable the colour change of the tyrosine solution from colourless to red-brown, except for the chitosan blank. Even so, it can be seen some increase in Abs_{280nm} (Fig. 58) and that can be attributed to the already reported chitosan oxidation capacity for mono and di-phenols. BNC-cit-AbT demonstrates an activity rate superior to BNC-MUA-AbT and AbT immobilized but the overall conclusion is that conjugation with AuNP seems not to interfere with the enzyme in an entrapment scenario. Testing of this system with phenol substrate in the future should consider a previous optimization of the protocol here proposed.

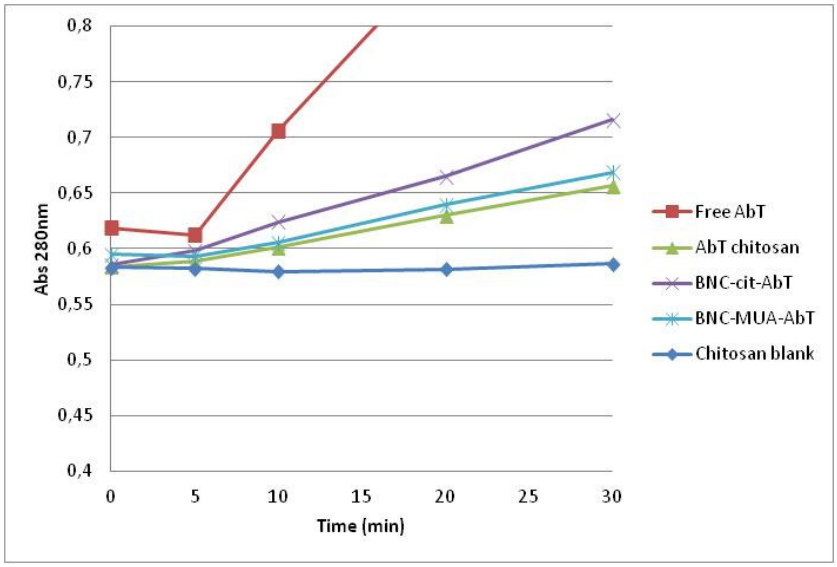

Figure 58**–** Chitosan immobilized petri dish batch system reaction progress. (magnification)

4- Conclusion

At the beginning of this dissertation´s work it was recognized the ambition in it and large quantity of work that needed to be executed. Right at the initial steps, it suffered major detours from the initial outline, which caused a dispersion of the investigation focus and lack of duplicates and triplicates to support the final results.

The BNC-TYR conjugates that were supposed to be an acquired knowledge needed a critical review right at the beginning as the viability of this dissertation depended on the use of AuNP-MUA prepared adequately. Otherwise, any advance made using faulty BNC would translate into findings with little meaning. For this matter, this work demonstrated that AuNP-MUA 1:5000 ultracentrifuged colloid was stable up to 100 mM ionic strength (NaCl) and able to form active BNC with AbT. It also shed some light upon the BNC-cit-TrT coverage, which we recommend as 100 mM per nanomolar of AuNP, supported by experimental data and also by the proposed theoretical methodology based on the Thomson´s Model. In spite of some guidelines being acquired, much more work need to be done to characterize the new AuNP-MUA 1:5000 and BNC-TrT conjugates.

Another difficulty in this work was the sudden loss of activity from TrT which caused the interruption of its study. The systems developed with AbT could be tested in TrT and so an important goal was missed. It was verified that the reaction solutions incubated with both TYRs tend to pH 7 and so keeping TrT at its optimal pH 9 would be a matter of the greatest importance.

The variability activity and fairly fixed amount of total protein found in AbT lot samples was very relevant to justify the use of mass to calculate AuNP´s enzyme coverage instead of an amount ruled by activity. Furthermore, activity of 200 µg AbT extract provided an equivalent activity to less than 2 uL of pure TrT. Considering that the price of 1 mL of TrT (500 activity equivalent assays) was enough to buy close to 80 mg of AbT (only 400 activity equivalent assays) TrT turned out to not be so expensive as seemed at first glance.

The analytical methods constituted also a concern right from the start. Much literature in phenol remediation supports its facts solely in UV-Vis spectra as quantification method. Knowing that many aromatic compounds are being formed and that they are unstable, these data has to be considered unreliable and so an effort has to be done concerning phenol quantification in complex matrixes. SPME-GC appear as alternative methods and should be directly compared and counterproof with the classical UV-vis method. Nevertheless, by SPME-GC, it was found that 100 ppm phenol incubated with BNC-MUA-AbT for 60 minutes, achieve, at least, 50% substrate conversion.

All 3 remediation methods designs conceived were of great simplicity, cheap and prompt to be applied in distinct situations. They could be combined with the agarose/ chitosan hydrogels to enhance their longevity, contaminant loading, and enzyme saving. Some promising results (despite few optimizations) were achieved and nothing seemed to invalidate them as viable approaches to use in other remediation systems, especially incorporating sense-and-shoot capabilities. The plug-flow syringing system has only received some design attention because a continuous method is only worth pursuing when the remediation agent (tyrosinase in this case) has proven stability and efficiency. Moreover, the increased difficulty to guarantee constant conditions was an extra and undesirable complexity while the reaction elements were still in a characterization phase.

As a more personally remark, seeing the initial ambition reduced to many, little conclusive and disperse results is disappointing. Dealing with this is also an important part of scientific investigation (if not the most important) and I am decided to include that as an unwanted achieved goal.

5-Bibliography

1. Feynman, R., *There's plenty of room at the bottom*. Engineering and Science: 1958; Vol. 23, p 22-36.
2. History and Future of Nanotechnology. http://www.nanotechnologyresearchfoundation.org/nanohistory.html (accessed May 5, 2012).
3. Murray, C. B.; Kagan, C. R.; Bawendi, M. G., Synthesis and characterization of monodisperse nanocrystals and close-packed nanocrystal assemblies. *Annu Rev Mater Sci* **2000,** *30*, 545-610.
4. Richard Booker, E. B., *Nanotechnology for Dummies*. Wiley Publishing, Inc.: Indianapolis, 2005; p 11, 222-241.
5. Holland, S., 2005 Nanotechnologies. *ISO TC 229*.
6. Decker, M., Definitions of Nanotechnology – Who needs them? **2003**.
7. Destinations, S. http://www.sacred-destinations.com (accessed July 20, 2012).
8. Initiative, N. N. Nanotechnology Timeline. http://nano.gov/timeline (accessed May 5, 2012).
9. Jun, Y.-W.; Lee, J.-H.; Cheon, J., Chemical design of nanoparticle probes for high-performance magnetic resonance imaging. *Angew Chem Int Edit* **2008,** *47* (28), 5122-5135.
10. Plenty of Room for Biology At The Bottom- An Introduction to Bionanotechnology. *Imperial College Press* (1), 1-2.
11. Shane Scanlon, A. A., Self-assembling peptide nanotubes. *Nanotoday* **2008,** *3* (34).
12. (a) Kinge, S.; Crego-Calama, M.; Reinhoudt, D. N., Self-Assembling Nanoparticles at Surfaces and Interfaces. *Chemphyschem* **2008,** *9* (1), 20-42; (b) Petit, C.; Taleb, A.; Pileni, M. P., Cobalt nanosized particles organized in a 2D superlattice: Synthesis, characterization, and magnetic properties. *J Phys Chem B* **1999,** *103* (11), 1805-1810.
13. George M. Whitesides, B. G., Self-Assembly at All Scales. *Science* **2002,** *295* (2418).
14. Sahu, S.; Majee, S. K.; Pal, A. J., Layer-by-layer assembly of capped CdSe nanoparticles: Electrical bistability and memory phenomenon. *Appl Phys Lett* **2007,** *91* (14).
15. Turkevich J., S. P., Hillier J., A study of the nucleation and growth process in the synthesis of colloidal gold. **1951**.
16. Kurniawan, F. New Analytical Applications of Gold Nanoparticles. Regensburg, 2008.
17. Brust M, W. M., Bethell D, Schiffrin DJ, Whyman R., Synthesis of thiol-derivatised gold nanoparticles in a two-phase liquid-liquid system. *J Chem Soc Chem Commun* **1994,** (2), 801-802.
18. Floriana Vitale, I. F., Chiara Battocchio, Emanuela Piscopiello, Leander Tapfer, Maria V Russo, Giovanni Polzonetti and Cinzia Giannini Mono- and bi-functional arenethiols as surfactants for gold nanoparticles: synthesis and characterization. *Nanoscale Research Letters* **2011,** *6* (103).
19. Aashok K Ganguli, S. V. V., Tokeer Ahmad, Synthesis of nanocrystalline materials through reverse micelles: A versatile methodology for synthesis of complex metal oxides. *Bull. Mater. Sci.* **2008,** *31* (3), 415-419.
20. Sun, S. H.; Murray, C. B., Synthesis of monodisperse cobalt nanocrystals and their assembly into magnetic superlattices (invited). *J Appl Phys* **1999,** *85* (8), 4325-4330.
21. ZirChrom Separations, I. Data for Biochemical Research. (accessed January 11, 2012).
22. Kimling, J.; Maier, M.; Okenve, B.; Kotaidis, V.; Ballot, H.; Plech, A., Turkevich Method for Gold Nanoparticle Synthesis Revisited. *The Journal of Physical Chemistry B* **2006,** *110* (32), 15700-15707.
23. Levy, R.; Thanh, N. T. K.; Doty, R. C.; Hussain, I.; Nichols, R. J.; Schiffrin, D. J.; Brust, M.; Fernig, D. G., Rational and combinatorial design of peptide capping Ligands for gold nanoparticles. *J Am Chem Soc* **2004,** *126* (32), 10076-10084.
24. Murray, C. B.; Kagan, C. R.; Bawendi, M. G., Self-Organization of CdSE Nanocrystallites Into 3-Dimensional Quantum-Dot Superlatices. *Science* **1995,** *270* (5240), 1335-1338.
25. Cortez, J.; Vorobieva, E.; Gralheira, D.; Osorio, I.; Soares, L.; Vale, N.; Pereira, E.; Gomes, P.; Franco, R., Bionanoconjugates of tyrosinase and peptide-derivatised gold nanoparticles for biosensing of phenolic compounds. *Journal of Nanoparticle Research* **2011,** *13* (3), 1101-1113.

26. P. Baptista, G. D., D. Henriques, E. Pereira, R. Franco, *Journal of Biotechnology* **2005,** *119* (2), 111-117.
27. Lobo, R. F. M., *Nanotecnologia e Nanofísica (Conceitos de Nanociência Moderna)*. Escolar Editora: Lisboa, 2009; p 122-123.
28. Kumaresh S. Soppimatha, T. M. A., Anandrao R. Kulkarnia,; Rudzinski, b. W. E., Biodegradable polymeric nanoparticles as drug delivery devices. *J Control Release* **2001,** (70), 1-20.
29. Levy, R., Shaheen, U., Cesbron, Y., Sée, V., Gold nanoparticles delivery in mammalian live cells: a critical review. *Nano Reviews* **2010**.
30. Hedenmo, M.; Narvaez, A.; Dominguez, E.; Katakis, I., Improved mediated tyrosinase amperometric enzyme electrodes. *J Electroanal Chem* **1997,** *425* (1-2), 1-11.
31. C. A. Mirkin, R. L. L., R. C. Mucic, J. J. Storhoff, *Nat Biotechnol* **1996,** *382* (607).
32. (a) Jolivet, S.; Arpin, N.; Wichers, H. J.; Pellon, G., Agaricus bisporus browning: a review. *Mycol Res* **1998,** *102*, 1459-1483; (b) Selinheimo, E.; NiEidhin, D.; Steffensen, C.; Nielsen, J.; Lomascolo, A.; Halaouli, S.; Record, E.; O'Beirne, D.; Buchert, J.; Kruus, K., Comparison of the characteristics of fungal and plant tyrosinases. *Journal of Biotechnology* **2007,** *130* (4), 471-480.
33. (a) Chang, T. S., An Updated Review of Tyrosinase Inhibitors. *Int J Mol Sci* **2009,** *10* (6), 2440-2475; (b) Mattinen, M. L.; Lantto, R.; Selinheimo, E.; Kruus, K.; Buchert, J., Oxidation of peptides and proteins by Trichoderma reesei and Agaricus bisporus tyrosinases. *Journal of Biotechnology* **2008,** *133* (3), 395-402.
34. (a) Lerch, K., Neurospora Tyrosinase - Structural, Spectroscopic and Catalytic Properties. *Mol Cell Biochem* **1983,** *52* (2), 125-138; (b) Lerch, K., Amino-Acid-Sequence of Tyrosinase from Neurospora-Crassa. *Experientia* **1978,** *34* (7), 914-914.
35. Duckwort.Hw; Coleman, J. E., Physicochemical and Kinetic Properties of Mushroom Tyrosinase. *J Biol Chem* **1970,** *245* (7), 1613-&.
36. Hearing, V. J.; Tsukamoto, K., Enzymatic Control of Pigmentation in Mammals. *Faseb J* **1991,** *5* (14), 2902-2909.
37. Sugumaran, H., Comparative biochemistry of eumelanogenesis and the protective roles of phenoloxidase and melanin in insects. *Pigm Cell Res* **2002,** *15* (1), 2-9.
38. Freddi, G.; Anghileri, A.; Sampaio, S.; Buchert, J.; Monti, P.; Taddei, P., Tyrosinase-catalyzed modification of Bombyx mori silk fibroin: Grafting of chitosan under heterogeneous reaction conditions. *Journal of Biotechnology* **2006,** *125* (2), 281-294.
39. VanGelder, C. W. G.; Flurkey, W. H.; Wichers, H. J., Sequence and structural features of plant and fungal tyrosinases. *Phytochemistry* **1997,** *45* (7), 1309-1323.
40. Ismaya, W. T.; Rozeboom, H. J.; Weijn, A.; Mes, J. J.; Fusetti, F.; Wichers, H. J.; Dijkstra, B. W., Crystal Structure of Agaricus bisporus Mushroom Tyrosinase: Identity of the Tetramer Subunits and Interaction with Tropolone. *Biochemistry-Us* **2011,** *50* (24), 5477-5486.
41. Decker, H.; Schwelkardt, T.; Nillius, D.; Salzbrunn, U.; Jaenicke, E.; Tuczek, F., Similar enzyme activation and catalysis in hemocyanins and tyrosinases. *Gene* **2007,** *398* (1-2), 183-191.
42. Klabunde, T.; Eicken, C.; Sacchettini, J. C.; Krebs, B., Crystal structure of a plant catechol oxidase containing a dicopper center. *Nat Struct Biol* **1998,** *5* (12), 1084-1090.
43. Lewis, E. A.; Tolman, W. B., Reactivity of dioxygen-copper systems. *Chem Rev* **2004,** *104* (2), 1047-1076.
44. Selinheimo, E.; Saloheimo, M.; Ahola, E.; Westerholm-Parvinen, A.; Kalkkinen, N.; Buchert, J.; Kruus, K., Production and characterization of a secreted, C-terminally processed tyrosinase from the filamentous fungus Trichoderma reesei. *Febs J* **2006,** *273* (18), 4322-4335.
45. TrTyr_PRDS - (Trichoderma reesei - Product Data Sheet). (supplier), V., Ed. Finland, 2012.
46. L. D. Nelson, M. M. C., *Lehninger´s Principles of Biochemistry*. 4ª ed.; Sarvier: 2004.
47. Sayre, L. M.; Nadkarni, D. V., Direct Conversion of Phenols to O-Quinones by Copper(I) Dioxygen - Questions Regarding the Monophenolase Activity of Tyrosinase Mimics. *J Am Chem Soc* **1994,** *116* (7), 3157-3158.
48. Selinheimo, E.; Gasparetti, C.; Mattinen, M. L.; Steffensen, C. L.; Buchert, J.; Kruus, K., Comparison of substrate specificity of tyrosinases from Trichoderma reesei and Agaricus bisporus. *Enzyme Microb Tech* **2009,** *44* (1), 1-10.
49. United States Environmental Protection Agency. RCRA Glossary of Terms. URL: http://nlquery.epa.gov/epasearch/epasearch?result_template=epafiles_default.xsl&action=filters

earch&filter=&typeofsearch=epa&querytext=bioremediation&submit=Go (acessed: September15, 2012).
50. Gianfreda, L.; Rao, M. A., Potential of extra cellular enzymes in remediation of polluted soils: a review. *Enzyme Microb Tech* **2004,** *35* (4), 339-354.
51. Alcalde, M.; Ferrer, M.; Plou, F. J.; Ballesteros, A., Environmental biocatalysis: from remediation with enzymes to novel green processes. *Trends Biotechnol* **2006,** *24* (6), 281-287.
52. *Code of Federal Regulations Appendix A to Part 423 - 126 Priority Pollutants*. United States Environmental Protection Agency: 30 de Dezembro de 2005.
53. Directive 2008/105/EC of the European Parliament and of the Council of 16 December 2008. *Official Journal of the European Union* **2008,** *348* (84), 12-13.
54. (a) Karam, J., Nicell, J.A., Potential application of enzymes in waste treatment. *J. Chem. Technol* **1997,** *69*, 141-153; (b) Lourenco, E. L. B.; Ferreira, A.; Pinto, E.; Yonamine, M.; Farsky, S. H. P., On-fiber derivatization of SPME extracts of phenol, hydroquinone and catechol with GC-MS detection. *Chromatographia* **2006,** *63* (3-4), 175-179.
55. An Vermeulen, K. W., Joeri Vercammen, Evaluation of a dedicated gas chromatography–mass spectrometry method for the analysis of phenols in water. *J Chromatogr A* **2004,** (1071), 41-46.
56. Nicell, J. A., Bewtra, J.K., Biswas, N., Taylor, K.E., Enzyme catalyzed polymerization and precipitation of aromatic compounds from aqueous solution. *Can. J. Civil Eng* **1993,** *20* (5), 725-735.
57. Ikehata, K.; Nicell, J. A., Characterization of tyrosinase for the treatment of aqueous phenols. *Bioresource Technol* **2000,** *74* (3), 191-199.
58. (a) Devipriya, S. P.; Yesodharan, S., Photocatalytic degradation of phenol in water using TiO2 and ZnO. *J Environ Biol* **2010,** *31* (3), 247-249; (b) Akbal, F.; Onar, A. N., Photocatalytic degradation of phenol. *Environ Monit Assess* **2003,** *83* (3), 295-302.
59. Li, Y. F.; Liu, Z. M.; Liu, Y. L.; Yang, Y. H.; Shen, G. L.; Yu, R. Q., A mediator-free phenol biosensor based on immobilizing tyrosinase to ZnO nanoparticles. *Anal Biochem* **2006,** *349* (1), 33-40.
60. Kim, G. Y.; Shim, J.; Kang, M. S.; Moon, S. H., Preparation of a highly sensitive enzyme electrode using gold nanoparticles for measurement of pesticides at the ppt level. *J Environ Monitor* **2008,** *10* (5), 632-637.
61. Barlow, S.; Kavlock, R. J.; Moore, J. A.; Schantz, S. L.; Sheehan, D. M.; Shuey, D. L.; Lary, J. M., Teratology society public affairs committee position paper: Developmental toxicity of endocrine disruptors to humans. *Teratology* **1999,** *60* (6), 365-375.
62. Sanz, V. C.; Mena, M. L.; Gonzalez-Cortes, A.; Yanez-Sedeno, P.; Pingarron, J. M., Development of a tyrosinase biosensor based on gold nanoparticles-modified glassy carbon electrodes - Application to the measurement of a bioelectrochemical polyphenols index in wines. *Anal Chim Acta* **2005,** *528* (1), 1-8.
63. Borgmann, S., *Advances in Electrochemical Science and Engineering: Bioelectrochemistry. Chapter 1- Amperometric Biosensors* 2011.
64. (a) IUPAC, Compendium of Chemical Terminology, 2nd ed. (the "Gold Book").Compiled by A. D. McNaught and A. Wilkinson. Blackwell Scientific Publications, Oxford: 1997. XML on-line corrected version: http://goldbook.iupac.org (2006-) created by M. Nic, J. Jirat, B. Kosata; updates compiled by A. Jenkins; (b) Namiesnik, J., Trace analysis - Challenges and problems. *Critical Reviews in Analytical Chemistry* **2002,** *32* (4), 271-300.
65. (a) EPA Method 604, Phenols, Part VIII, 40 CFR Part 136. Environmental Protection Agency: Washington, DC, 1984; p 58; (b) EPA Method 625, Base/Neutrals and Acids, Part VIII, 40 CFR Part 136. Environmental Protection Agency: Washington, DC, 1984; p 153; (c) EPA Method 8041, Phenols by Gas Chromatography: Capillary Column Technique. Environmental Protection Agency: Washington, DC, 1995; Vol. 26, p 1.
66. (a) Registry, A. f. T. S. a. D., *Toxicological Profile for Cresols- Chapter 7*. 2008; (b) Vermeulen, A.; Welvaert, K.; Vercammen, J., Evaluation of a dedicated gas chromatography-mass spectrometry method for the analysis of phenols in water. *J Chromatogr A* **2005,** *1071* (1-2), 41-46.
67. Kovacs, A.; Mortl, M.; Kende, A., Development and optimization of a method for the analysis of phenols and chlorophenols from aqueous samples by gas chromatography-mass spectrometry, after solid-phase extraction and trimethylsilylation. *Microchem J* **2011,** *99* (1), 125-131.

68. Chen, Y. L., *Preparation and Characterization of Water-Soluble Chitosan Gel for Skin Hydration*.
69. Augusto, A. L. P. V. F., Microextração por Fase Sólida. *Química Nova* **2000,** *23* (4), 523-530.
70. Nomenclature Committee of the International Union of Biochemistry (NC-IUB) - Units of Enzyme -Activity - Recommendations 1978. *Eur J Biochem* **1979,** *97* (2), 319-320.
71. Payne, G. F.; Sun, W. Q., Tyrosinase Reaction and Subsequent Chitosan Adsorption for Selective Removal of a Contaminant From a Fermentation Recycle Stream. *Appl Environ Microb* **1994,** *60* (2), 397-401.
72. Cao, Z.; Gilbert, R. J.; He, W., Simple Agarose-Chitosan Gel Composite System for Enhanced Neuronal Growth in Three Dimensions. *Biomacromolecules* **2009,** *10* (10), 2954-2959.

6-Appendixes

1.10- Appendix I- Protein quantification and activity

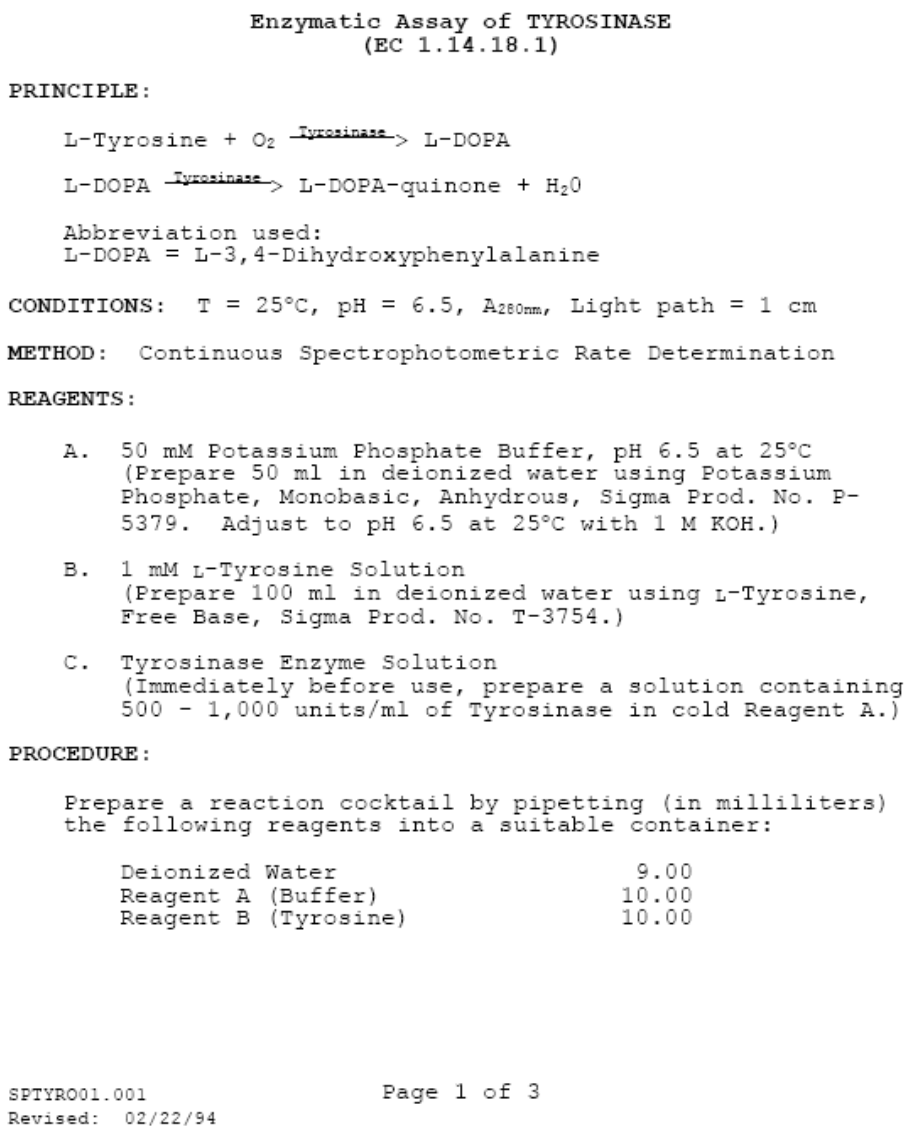

Enzymatic Assay of TYROSINASE
(EC 1.14.18.1)

PRINCIPLE:

L-Tyrosine + O_2 —Tyrosinase→ L-DOPA

L-DOPA —Tyrosinase→ L-DOPA-quinone + H_2O

Abbreviation used:
L-DOPA = L-3,4-Dihydroxyphenylalanine

CONDITIONS: T = 25°C, pH = 6.5, A_{280nm}, Light path = 1 cm

METHOD: Continuous Spectrophotometric Rate Determination

REAGENTS:

A. 50 mM Potassium Phosphate Buffer, pH 6.5 at 25°C
(Prepare 50 ml in deionized water using Potassium Phosphate, Monobasic, Anhydrous, Sigma Prod. No. P-5379. Adjust to pH 6.5 at 25°C with 1 M KOH.)

B. 1 mM L-Tyrosine Solution
(Prepare 100 ml in deionized water using L-Tyrosine, Free Base, Sigma Prod. No. T-3754.)

C. Tyrosinase Enzyme Solution
(Immediately before use, prepare a solution containing 500 - 1,000 units/ml of Tyrosinase in cold Reagent A.)

PROCEDURE:

Prepare a reaction cocktail by pipetting (in milliliters) the following reagents into a suitable container:

Deionized Water	9.00
Reagent A (Buffer)	10.00
Reagent B (Tyrosine)	10.00

SPTYRO01.001 Page 1 of 3
Revised: 02/22/94

Figure 59– Sigma AbT activity protocol. (Page 1/3)

Enzymatic Assay of TYROSINASE
(EC 1.14.18.1)

PROCEDURE: (continued)

Mix and adjust to pH 6.5 at 25°C with 1 M HCl or 1 M NaOH, if necessary. Immediately before use, oxygenate by bubbling 99.9% pure O_2 through the reaction cocktail for 3 to 5 minutes. Pipette (in milliliters) into suitable quartz cuvettes:[1]

	Test	Blank
Reaction Cocktail	2.90	2.90

Equilibrate to 25°C. Monitor the A_{280nm} until constant, using a suitably thermostatted spectrophotometer. Then add:

Reagent A (Buffer)	------	0.10
Reagent C (Enzyme Solution)	0.10	------

Immediately mix by inversion and record the increase in A_{280nm} for approximately 10 minutes. Obtain the ΔA_{280nm}/minute using the maximum linear rate for both the Test and Blank.

CALCULATIONS:

$$\text{Units/ml enzyme} = \frac{(\Delta A_{280nm}/\text{min Test} - \Delta A_{280nm}/\text{min Blank})\ (df)}{(0.001)\ (0.1)}$$

df = Dilution factor
0.001 = The change in A_{280nm}/minute per unit of Tyrosinase at pH 6.5 at 25°C in a 3 ml reaction mix
0.1 = Volume (in milliliters) of enzyme used

$$\text{Units/mg solid} = \frac{\text{units/ml enzyme}}{\text{mg solid/ml enzyme}}$$

$$\text{Units/mg protein} = \frac{\text{units/ml enzyme}}{\text{mg protein/ml enzyme}}$$

UNIT DEFINITION:

One unit will cause an increase in A_{280nm} of 0.001 per minute at pH 6.5 at 25°C in a 3 ml reaction mix containing

Figure 60– Sigma AbT activity protocol. (Page 2/3)

L-tyrosine.

Figure 61– Sigma AbT activity protocol. (Page 3/3)

1.10- Appendix II- Protein concentration – BCA Assays

BCA assay results over the three most representative AbT commercial lots (Sigma-Aldrich) used during this dissertation were tested.

BCA Assay- AbT aliquots (1 mg solid extract/1 mL phosphate buffer pH 7 10 mM) test

Lot1- (total protein samples diluted by a factor of 34.33)

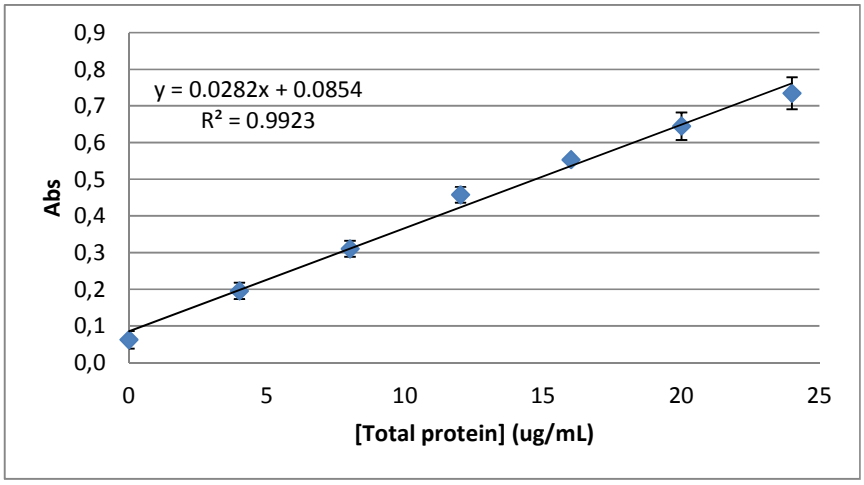

Figure 62– BCA calibration curve for Lot1.

Mean Abs_{Lot1}= 0.615±0.004 => 621 µg/mL total protein => 0.621 mg protein/1 mg extract

Lot2- (total protein samples diluted by a factor of 34.33)

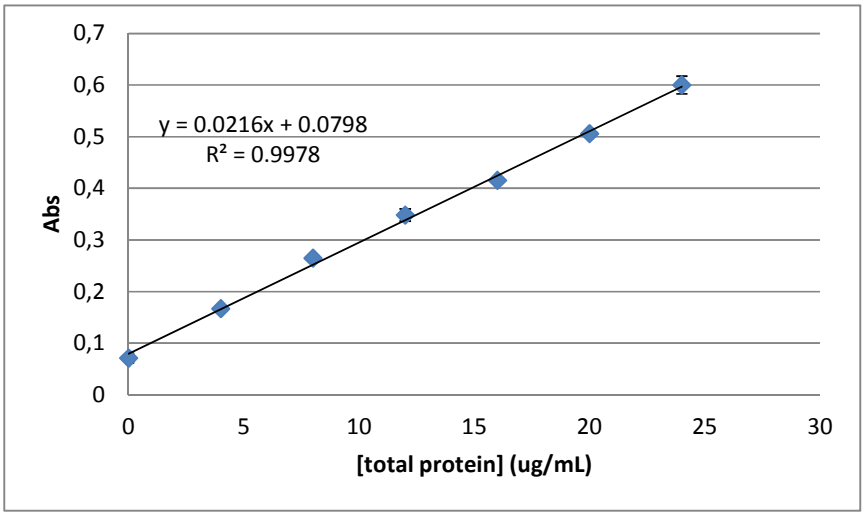

Figure 63– BCA calibration curve for Lot2.

Mean Abs_{Lot2}= 0.445±0.002 => 576 µg/mL total protein => 0.576 mg protein/ 1 mg extract

Lot3-(total protein samples diluted by a factor of 34.33)

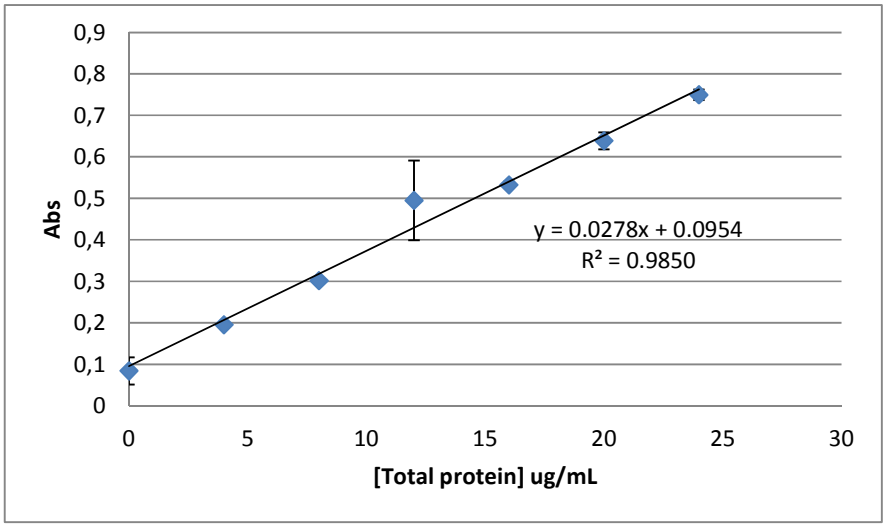

Figure 64– BCA calibration curve for Lot3.

Mean Abs_{Lot3}= 0.643±0.006 => 661 µg/mL total protein => 0.661 mg protein/1mg extract

BCA Assay- TrT aliquot (as purchased from VVT, Finland) test

(total protein samples diluted by a factor of 101)

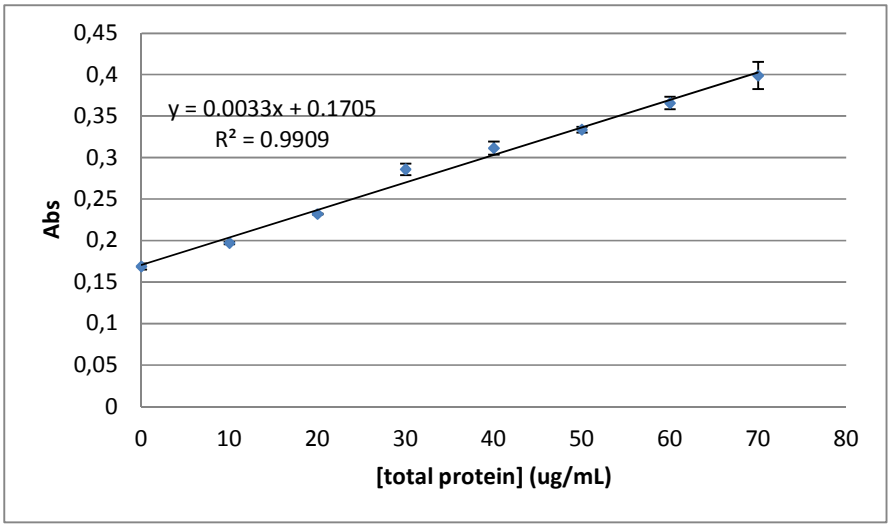

Figure 65– BCA calibration curve for TrT.

Mean Abs_{Lot}= 0.353±0.027 => 5530 µg/mL total protein (-7.8% than labeled 6000 µg/mL)

1.10- Appendix III- Protein concentration – Activity determination

Sigma activity assay (Appendix I) results over the three most representative AbT commercial lots (Sigma-Aldrich) used during this dissertation were tested.

Sigma Assay- AbT aliquots (1 mg extract/1 mL phosphate buffer pH 7 10 mM)

Lot1-(aliquots diluted by a factor of 4.276)

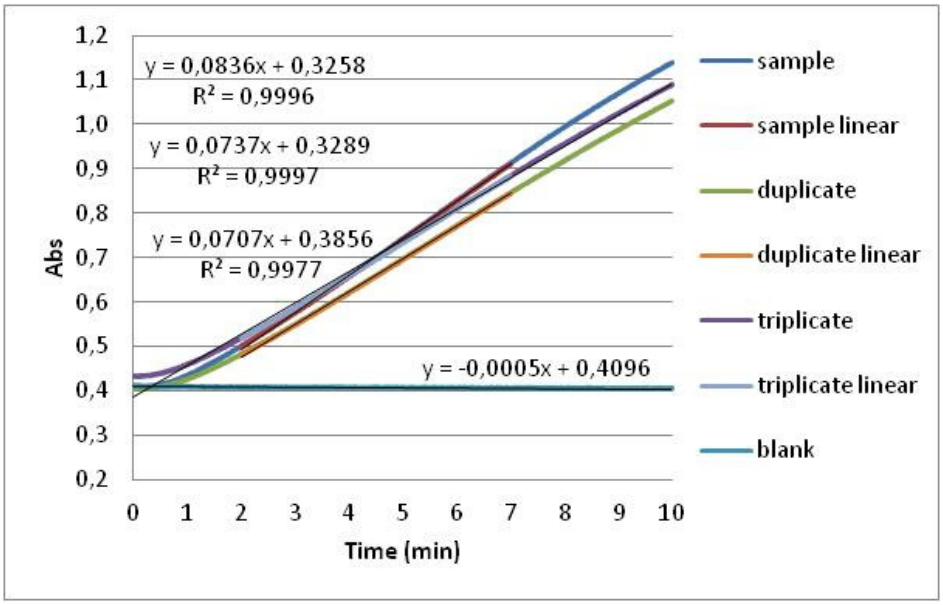

Figure 66– Sigma assay for Lot1.

Mean $Slope_{Lot1}$= 0.077±0.006 Abs/min => 2346 U/ 234 µg extract => 10033 U/mL (+134% than labeled 4276 U/mg total protein)

Lot2-(aliquotes diluted by a factor of 4.276)

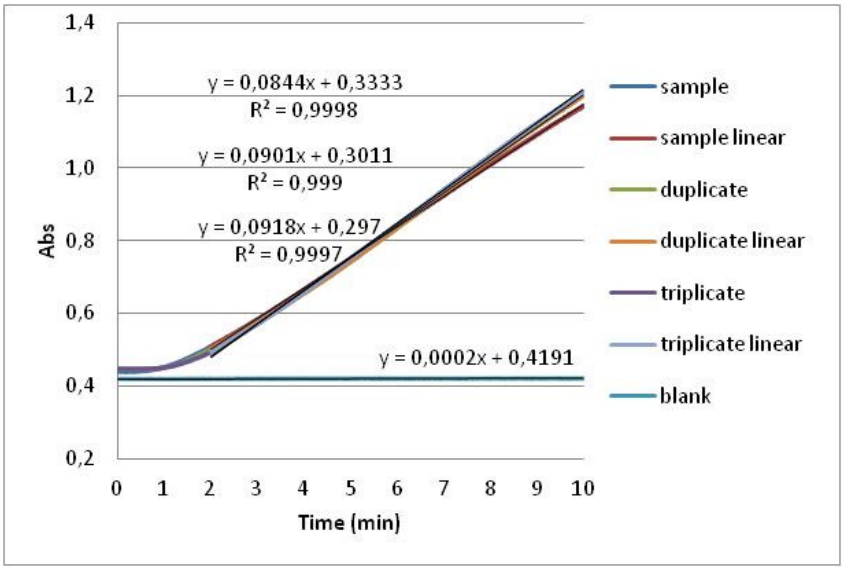

Figure 67– Sigma assay for Lot2.

Mean $Slope_{Lot2}$= 0.089±0.004 Abs/min => 3787 U/ 234 µg extract => 16193 U/mL (+278% than labeled 4276 U/mg total protein)

Lot3-(aliquotes diluted by a factor of 10)

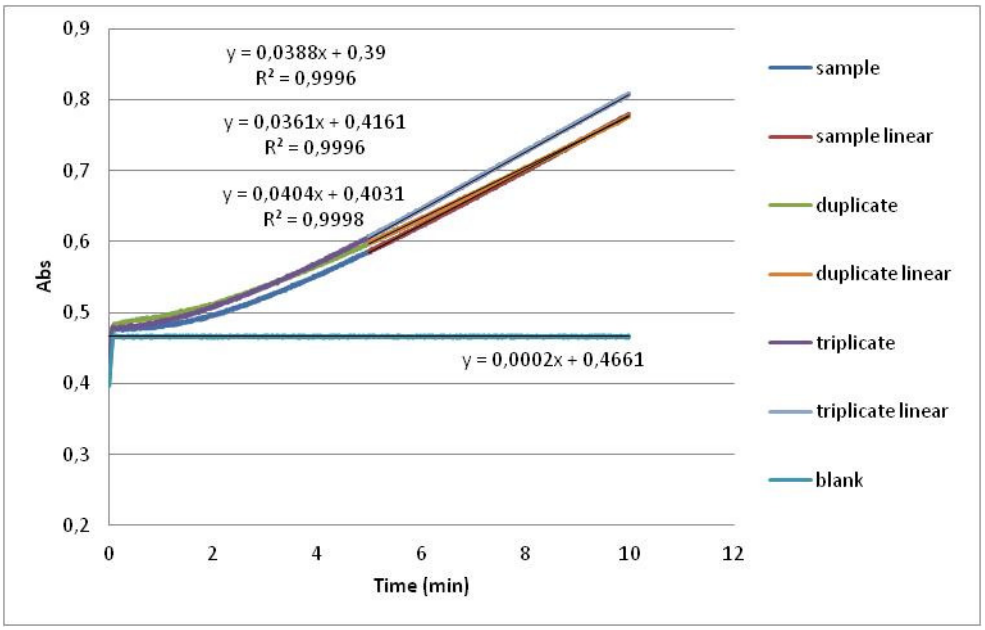

Figure 68– Sigma assay for Lot3.

Mean $Slope_{Lot3}$= 0.384±0.002 Abs/min => 382 U/ 23 µg => 3820 U/mL (+5.8% than labeled 3610 U/mg)

Activity Assay- TrT aliquot (as purchased) testing

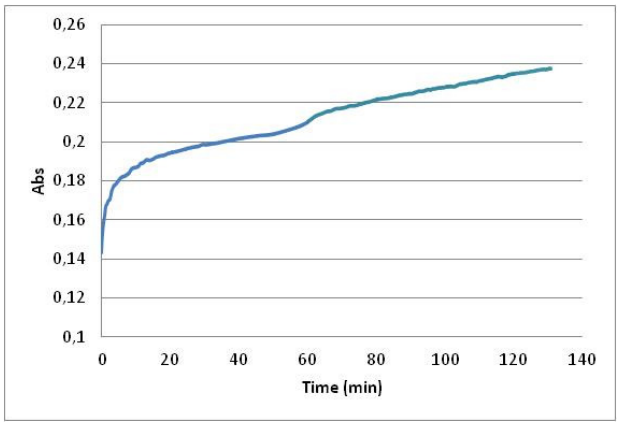

Figure 69– Activity assay for TrT.

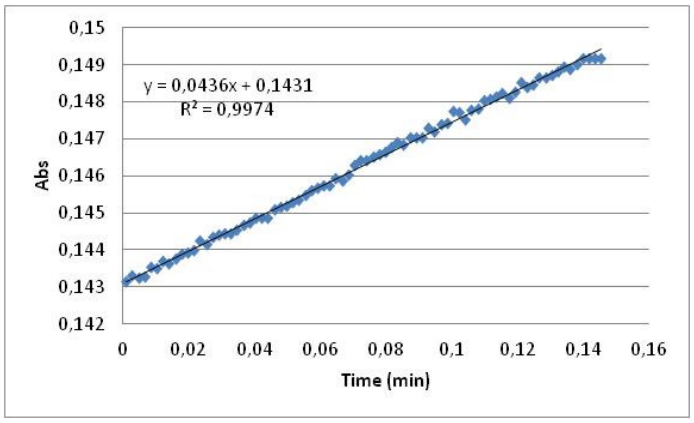

Figure 70– Maximum activity rate zone for TrT. Magnification of Figure 69.

Slope= 0.044 Abs/min => 1330 U/mL (by Sigma criteria)

or

$\varepsilon_{dopachrome280}$=3400 $M^{-1}cm^{-1}$=> 128.2 M/(min.mol_{TrT}) => (for 15 mM L-DOPA equivalent) 1164 mol/(min.mol_{TrT}) =2693 nkatal (-10.1% than the provided 2996 nktal)

1.10- Appendix IV- Ultrafiltration

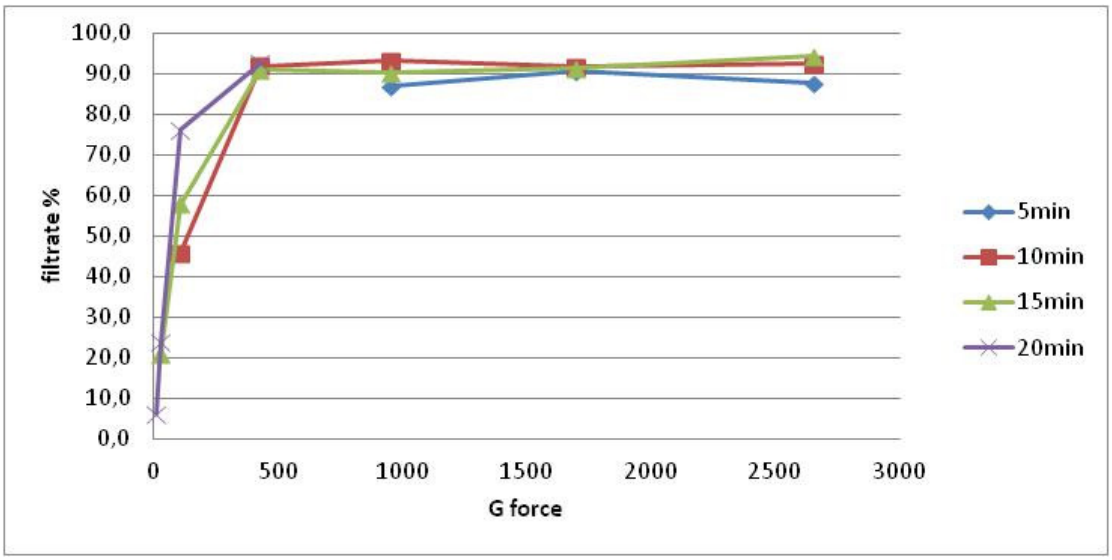

Figure 71– Distilled water filtrated volume as G force centrifugation function, using a Amicon Ultra-4 centrifugal unit 100 kDa cut-off(Millipore).

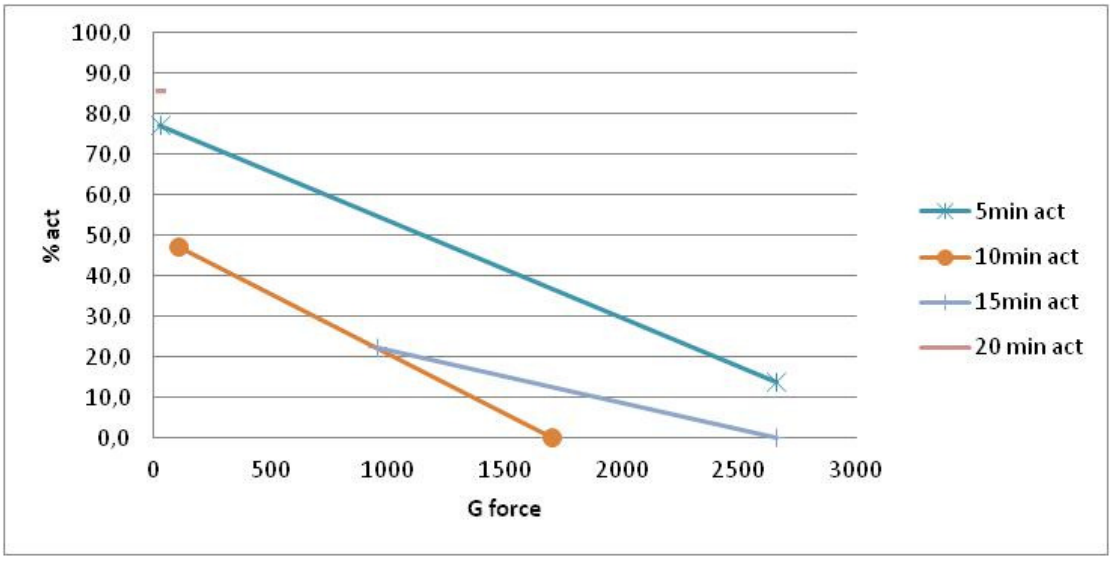

Figure 72– Percentage of activity retained by BNC-AbT after a single centrifugation [Amicon Ultra-4 centrifugal unit 100 kDa cut-off (Millipore)] at different velocities. Sigma activity protocol used to test the activity. 100% activity= BNC-AbT before centrifugation.

1.10- Appendix V- GC Chromatograms

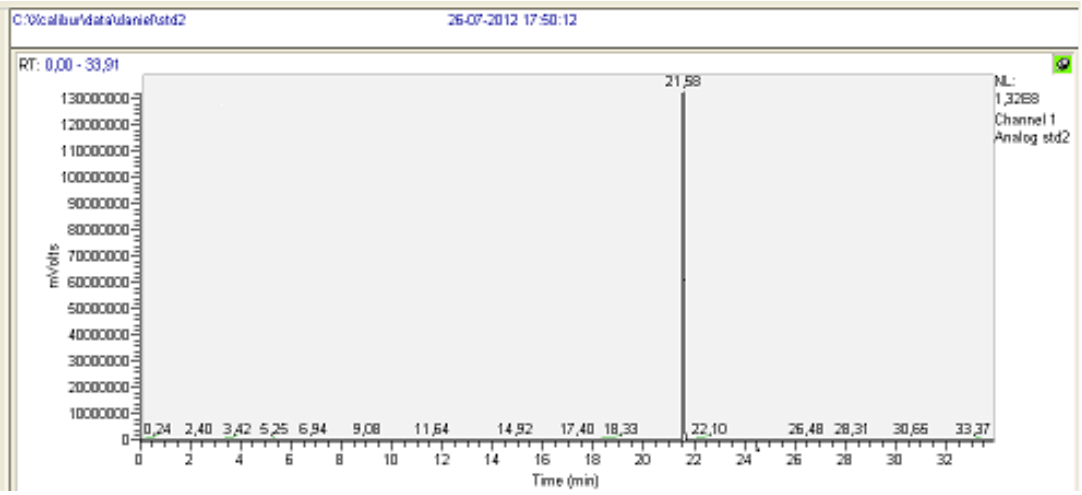

Figure 73– Pure phenol chromatogram, retention time: 21.58 minutes.